Spring 2011

Towards Wiener system identification with minimum a priori information

John M. Reyland
University of Iowa

TOWARDS WIENER SYSTEM IDENTIFICATION WITH MINIMUM A-PRIORI INFORMATION

by

John M Reyland, Jr

An Abstract

Of a thesis submitted in partial fulfillment of the
requirements for the Doctor of Philosophy
degree in Electrical and Computer Engineering
in the Graduate College of
The University of Iowa

May 2011

Thesis Supervisor: Professor Er-Wei Bai

ABSTRACT

The ability to construct accurate mathematical models of real systems is an important part of control systems design. A block oriented systems identification approach models the unknown system as interconnected linear and nonlinear blocks. The subject of this thesis is a particular configuration of these blocks referred to as a Wiener model. The Wiener model studied here is a cascade of an input linear block followed by a nonlinear block which then provides one output. We assume that the intermediate signal between the linear and nonlinear block is unknown, only the Wiener model input and output can be sampled.

The difficulty of Wiener model identification is the interaction of the linear and nonlinear blocks. If one of the blocks is known then the intermediate signal can be produced and identification becomes much easier. Thus this thesis focuses on identification of the linear transfer function in a Wiener model. The question examined throughout the thesis is: given some "small" amount of a priori information on the nonlinear part, what can we determine about the linear part? Examples of minimal a priori information are knowledge of only one point on the nonlinear characteristic, or the sign of the output or simply that the transfer characteristic is monotonic over a certain range. Nonlinear blocks with and without memory are discussed.

The contributions of this thesis are several algorithms for identifying the linear transfer function of a block oriented Wiener system. These are presented and analyzed in detail. These methods can be applied to either finite or infinite impulse response (i.e. FIR or IIR) linear blocks. Each algorithm has a carefully defined set of a priori information on the nonlinearity. Also, each approach has a set of assumptions on the input excitation.

Abstract Approved: _____
Thesis Supervisor

_____
Title and Department

_____
Date

TOWARDS WIENER SYSTEM IDENTIFICATION WITH MINIMUM A-PRIORI INFORMATION

by

John M Reyland, Jr

A thesis submitted in partial fulfillment
of the requirements for the Doctor of
Philosophy degree in Electrical and Computer Engineering
in the Graduate College of
The University of Iowa

May 2011

Thesis Supervisor: Professor Er-Wei Bai

Graduate College
The University of Iowa
Iowa City, Iowa

CERTIFICATE OF APPROVAL

_____

PH.D. THESIS

_____

This is to certify that the Ph.D. thesis of

John M Reyland, Jr

has been approved by the Examining Committee
for the thesis requirement for the Doctor of Philosophy
degree in Electrical and Computer Engineering at the May 2011 graduation.

Thesis Committee: _____
Er-Wei Bai, Thesis Supervisor

_____
Soura Dasgupta

_____
Yangbo Ye

_____
Mark S. Andersland

_____
Raghuraman Mudumbai

To my family and especially my wife Diane

ACKNOWLEDGMENTS

I gratefully acknowledge the confidence that my advisor, Professor Bai, showed in me throughout this process. Thanks are also due to the four faculty members who graciously volunteered to evaluate my thesis. Finally, I wish to thank my employer, Rockwell Collins, Inc. of Cedar Rapids, Iowa for their financial support of this endeavor.

ABSTRACT

The ability to construct accurate mathematical models of real systems is an important part of control systems design. A block oriented systems identification approach models the unknown system as interconnected linear and nonlinear blocks. The subject of this thesis is a particular configuration of these blocks referred to as a Wiener model. The Wiener model studied here is a cascade of an input linear block followed by a nonlinear block which then provides one output. We assume that the intermediate signal between the linear and nonlinear block is unknown, only the Wiener model input and output can be sampled.

The difficulty of Wiener model identification is the interaction of the linear and nonlinear blocks. If one of the blocks is known then the intermediate signal can be produced and identification becomes much easier. Thus this thesis focuses on identification of the linear transfer function in a Wiener model. The question examined throughout the thesis is: given some "small" amount of a priori information on the nonlinear part, what can we determine about the linear part? Examples of minimal a priori information are knowledge of only one point on the nonlinear characteristic, or the sign of the output or simply that the transfer characteristic is monotonic over a certain range. Nonlinear blocks with and without memory are discussed.

The contributions of this thesis are several algorithms for identifying the linear transfer function of a block oriented Wiener system. These are presented and analyzed in detail. These methods can be applied to either finite or infinite impulse response (i.e. FIR or IIR) linear blocks. Each algorithm has a carefully defined set of a priori information on the nonlinearity. Also, each approach has a set of assumptions on the input excitation.

TABLE OF CONTENTS

LIST OF TABLES

LIST OF FIGURES

CHAPTER 1
INTRODUCTION

This thesis studies the construction of mathematical models that predict the output of real systems. Input and output samples from a real system are collected and then used to infer a mathematical model. The mathematical model can then be used to predict the response of the real system to other inputs. To illustrate the many benefits obtainable from this approach, consider model predictive control of the pH of a chemical mixing process [18]. In real time, a mathematical model accepts flow rate measurements of various chemicals entering a large unwieldily mixing system. The control algorithm predicts and applies changes to the various flow rates to regulate the effluent pH to a desired setpoint. Errors between actual and desired pH can be averaged over time and used to adjust the model. The model that the control engineers started with probably came from a system identification procedure.

For a given real world process, there are many different models that could be applied. A block oriented model consists of a number of interconnected blocks each having a carefully defined system function and various numbers of inputs and outputs. These blocks are sometimes refered to as “black-boxes”. As described in [32], the system function of a black-box is very flexible and has been proven useful for describing many natural phenomena. Each block is classified as linear or nonlinear. The dynamics of linear blocks are usually characterized by a set of transfer function parameters. The nonlinear blocks are usually characterized by a nonparametric set of input output points, although other representations are possible, for example piecewise linear described by only a few parameters [3]. In this thesis the focus is on a particular block oriented

technique called Wiener system modeling.

A Wiener system consists of a linear dynamic system followed by a static nonlinearity, see Figure 1. The input $u(k)$ is filtered by linear system $G(z)$. The output $x(k)$ then goes to static nonlinearity $f(x(k))$. Note that all these signals are represented by discrete time indexed samples. Finally, the output of $f(x(k))$ is disturbed by noise $v(k)$ to produce final output $y(k)$. Throughout this thesis output noise $v(k)$ is uncorrelated with $y(k)$.

Linear system $G(z)$ and nonlinearity $f(x(k))$ can take many forms. For example $G(z)$ can have a finite or infinite impulse response (FIR or IIR). Also $f(x(k))$ can be a simple memory-less input to output mapping or a more complicated memory based system where the output depends on previous inputs. These blocks can have one input and one output (SISO) or multiple inputs and outputs (MIMO). In this thesis we study only SISO linear systems with either FIR or IIR system functions. We consider nonlinearities with and without memory.

Wiener system structure

The Wiener nonlinear system is named after Norbert Wiener and was probably first described in [38]. The block diagram of the discrete time Wiener model considered throughout this proposal is shown in Figure 1. The system identification task is challenging because usually the intermediate signal, $x(k)$, is not available. Thus identification has to rely only on observations of input $u(k)$ and output $y(k)$.

There are a wide range of applications of block oriented Wiener models. They have been applied to both natural phenomena, such as the pH control process described

above [18], and man made devices, such as valves [31] and power amplifiers [6, 25]. The Wiener model blocks are assigned to model the behavior of specific parts of the real world system. For example, in the pH control system discusses above the Wiener model linear subsystem represents the mixing dynamics of the input reagent streams and the nonlinear subsystem represents the nonlinear titration curve (pH as a function of the chemical components).

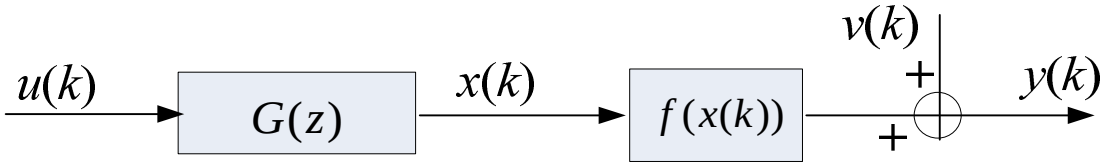

Figure 1: Wiener system block diagram

Identification of Wiener systems has been an active research area for many years and there exist several identification algorithms in the literature. Most of these algorithms rely on the following assumptions about the input and/or output and/or system structure:

1. Gaussian random input, see [7, 19 or 22]
2. The unknown nonlinearity is invertible and/or monotonic, and represented by some known basis functions, see [2, 19 or 41]
3. The unknown nonlinearity is a piecewise linear function, see [36]

In the first case, identification of the linear system is possible without knowing additional facts about the nonlinearity. This is due to the Bussgang theorem ([12], Theorem 1) which says that for a Gaussian distributed input signal the cross correlation between input and output of a nonlinearity is a scaled version of the input auto correlation, independent

of nonlinear distortion. The second and third cases use some a priori information about the Wiener model to allow identification without a Gaussian distributed input.

In this thesis we ask the following question about Wiener models: what is the least amount of a priori information on the unknown system so that identification of the linear block is possible with a non-Gaussian input? In Chapters 2 and 3, a starting point to answering this question is to consider what constitutes the least amount of a priori information on the nonlinearity so that the linear part can be identified without the Gaussian assumption on the input. In Chapter 4, we identify a linear block that is followed by a memory nonlinearity. A minimal a prori information set is defined for this more complicated nonlinearity.

Clearly, if the linear part can be reliably identified and the internal signal $x(k)$ recovered then identification of the nonlinearity is relatively easy. However, quantifying what exactly is meant by "The least amount of a priori information on the nonlinearity" is very difficult.

Some efforts have been made to answer this question in an indirect way, i.e. to develop identification algorithms using as little a priori information as possible. To this end, some work has been reported in the literature [41] that a monotonicty assumption on the unknown nonlinearity ensures a (not necessarily unique) solution for an FIR linear system. This was the first time an identification algorithm was developed in a non-Gaussian case by only assuming monotonicity of an unknown, possibly non-parametric, nonlinearity. Part of the research presented here extends and enhances the work of [41] in several directions.

The purpose of this research is to develop identifiability proofs and associated

algorithms that approach the minimal amount of a priori information needed on the Wiener system nonlinearity to allow linear system identification. To be specific, this research is concerned with parametric identification of the first block in Figure 1, the linear system, under one of the following sets of a priori information on the second block, the nonlinearity:

1. Only the nonlinearity output sign is known, i.e. one bit quantization.
2. Only a single point on the memoryless nonlinear characteristic is known.
3. The nonlinearity is known to be monotonic over an output range.
4. The X-axis intersection points of a memory nonlinearity are known.

In the following chapters, the above conditions are used to develop identifiability proofs and algorithms for both FIR and IIR linear systems.

System identification procedure summary

The following steps are common to all the block oriented nonlinear system identification algorithms developed in this thesis.

Input stimulus choice

For the purpose of this thesis, we will have to assume that all input identification signals are independent and identically distributed (i.i.d.). The requirements on the probability density of each sample are very minimal.

Data collection

The next step is to collect input and output data records, $u(k)$ and $y(k)$ for $k = 1, 2, \ldots, N$ from the system to be identified. As will be discussed, N should be as large as possible for better estimation performance.

Model selection

Past experience with the real system to be identified, or some other insight, may lead to the conclusion that a Wiener model is a good starting point. If so, decide what prior information can be assumed. Examples are, what is the maximum order of the linear block or can we assume that the nonlinearity goes through the origin and is monotonic. See [26, 32] for an indepth discussion of this step.

Model estimation

The Wiener system linear and nonlinear blocks must be parameterized to fit the real data collected in the second step. The linear system is assumed of be of known order. The nonlinear subsystem could have a structure that can be described by a small set of parameters. Sometimes this is not possible and the nonlinearity has a nonparametric characterization. In this case the nonlinear function is represented by a set of estimated input/output points.

For the linear part, the estimation procedure adjusts the linear parameters to minimize the error between the output of the unknown system and the estimated system. More precisely, we minimize a cost function such as $J_N = \frac{1}{N}\sum_{k=1}^{N}\left(e(k)^2\right)$ where $e(k) = \left(y(k) + v(k)\right) - \hat{y}(k)$ and $y(k)$ is the true system output, $\hat{y}(k)$ is the estimated system output that we can control and $v(k)$ models the noise. There are various gradient based search techniques to minimize J_N. There is also a set of highly organized iterative seach techniques called Genetic Algorithms [16].

Model validation

This is the final test to determine if the model produced by the above steps is useful. A fresh set of input and output data records, $u(k)$ and $y(k)$ for $k = 1, 2, \ldots, N$ is collected from the system to be identified. The new input samples are processed through the estimated model. The model output is compared with the new output samples and the mean squared error cost function is evaluated to determine if a good fit has been achieved.

Thesis outline

Throughout the thesis, discussion centers on the following three sets of Wiener system a priori information on the nonlinear block:

1. Quadrant a priori information
2. Single point a priori information
3. Locally monotonic a priori information

Chapter 2 defines these in detail and then goes on to discuss indentification of an FIR linear block given each one of the above a priori information. Chapter 3 is an extension of the proofs and analysis of Chapter 2 to an IIR linear block. Chapter 4 goes further and applies these techniques to a nonlinear block with memory. Finally, Chapter 5 presents overall conclusions.

CHAPTER 2
FIR LINEAR PART IDENTIFICATION

This chapter shows how the impulse response of the FIR linear part of a Wiener system may be identified using a carefully defined set of minimal a-priori information on the nonlinear part.

Problem statement

The Wiener system of Figure 1 is described by

$$\begin{aligned} x(k) &= \big(u(k), u(k-1), \ldots, u(k-n+1)\big)h = \phi^T(k)h \\ y(k) &= f(x(k)), \quad k = 1, 2, \ldots, N \end{aligned} \tag{2.1}$$

where $u(k)$, $x(k)$ and $y(k)$ are the input, the internal and the output signals, respectively. Parameter vector $h \in \Re^n$ is to be identified. The first non-zero element of *h* is positive and $\|h\| = 1$ (note that throughout this thesis we define $\|x\| = \sqrt{\sum_{i=1}^{n} x_i^2}$).

This condition is necessary and standard in Wiener system identification because the scaling of the linear and nonlinear subsystems cannot be separately identified. The internal variable $x(k)$ is assumed unknown. Both $x(k)$ and $y(k)$ are assumed bounded for all *k*. As stated, not much information is known about nonlinearity $f(x(k))$. Input $u(k)$ is i.i.d. but not necessarily Gaussian. Finally, it is assumed that an upper bound, *n*, on the impulse response of the FIR linear part is known.

We say that the parameter vector *h* is identifiable from the input-output data set $\{\phi(k), y(k)\}_{k=1}^{N}$ if *h* can be uniquely identified from the Wiener system model and the data set, independent of the unknown nonlinearity $f(x(k))$. Equivalently, there does not exist

a different pair $(\bar{h}, \bar{f})$ that would produce an identical input-output data set $\{\phi(k), y(k)\}_{k=1}^{N}$ As previously stated, the pertinent question is: what minimal a priori information on the unknown $f(x(k))$ allows identification of *h*?

Quadrant a priori information

This section considers a case where only quadrant information about the nonlinear subsystem is known a priori. The nonlinearity is strictly in the first and third quadrants so that: $sign(x(k)) = sign(y(k))$ for $k = 1, \ldots, N$. This choice of first and third quadrants is for simplicity only. The results can be extended to other quadrant a priori information cases. The nonlinearity is not assumed to be continuous, monotonic or invertible except with regard to quadrants. For example, the nonlinearity can be discontinuous at the origin. Now we can observe the sign of $x(k)$ by processing the output of the system to be identified, $y(k)$, through the following:

$$sign(y(k)) = \begin{cases} +1 & y(k) > 0 \\ 0 & y(k) = 0 \\ -1 & y(k) < 0 \end{cases} \tag{2.2}$$

Sometimes this is written as $\mathrm{sgn}(x(k))$. Also, some references (for example mathematical authority [42]) define this function with ± 1 outputs only. For this thesis, we must have the definition above.

There is only sparse information in the published literature about system identification using polarity sensing. In the case that the nonlinearity is known, although not necessarily invertible, convergence results were obtained in [39] with a quantized output signal provided that there is signal energy around the switch points. In particular,

global convergence was achieved in [39] for a FIR system with an arbitrary and known output quantizer.

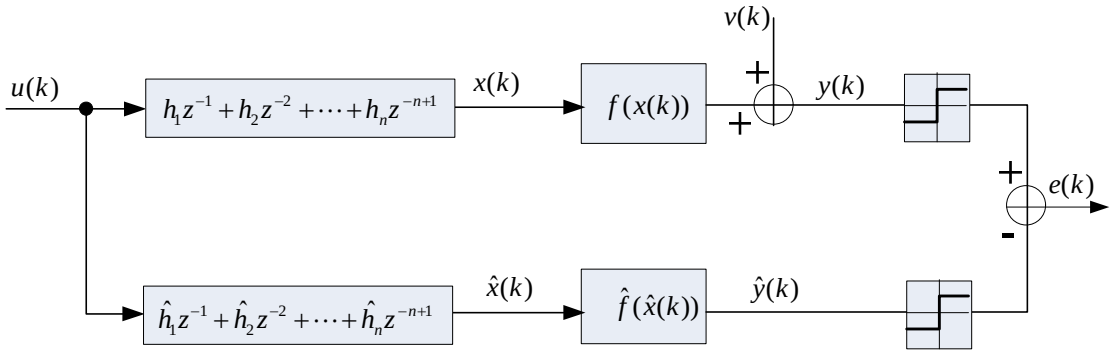

Figure 2: Wiener FIR system identification, quadrant only a priori knowledge

Figure 2 shows the system identification setup, $v(k)$ is arbitrarily distributed noise, uncorrelated with input $u(k)$. The system identification algorithm adjusts coefficient estimate $\hat{h}$ to match unknown coefficients h. The square boxes on the right side implement sign function (2.2). A cost function based on the sign error output, $e(k) = sign\left(y(k) + v(k)\right) - sign\left(\hat{y}(k)\right)$, isused to direct the adjustments of $\hat{h}$. Although $\hat{f}\left(\hat{x}(k)\right)$ is shown, it is not necessary for linear part identification. If included, it must conform to Assumption 2.1, below.

There is an obvious practical advantage to only needing to observe the sign of $y(k)$. The output sensing circuit can be as simple as a zero crossing detector. In addition, the detected polarity can be transferred as just one bit with high noise immunity. The following assumption defines a priori quadrant information.

Assumption 2.1:

The unknown nonlinearity is strictly in the first and third quadrants. In other words, $sign(x(k)) = sign(y(k))$ for $k = 1, ..., N$ *Alternatively, the unknown*

nonlinearity can be in the second and fourth quadrants, where $sign(x(k)) = -sign(y(k))$ for $k = 1,...,N$.

The following assumption defines the allowable inputs for this chapter's analysis.

Assumption 2.2:

Input u(k) is i.i.d. and the input probability density function is positive and continuous in an interval $[-a, a]$ *for some* $a > 0$.

To establish identifiability, we propose the following:

Theorem 2.1:

For any unit vector $\bar{h} \neq h$, *with probability one as* $N \to \infty$, *there exists some* $\phi(k)$, $1 \le k \le N$ *so that* $sign(y(k)) = sign(x(k)) = sign(\phi^T(k)h) \neq sign(\phi^T(k)\bar{h})$

Proof:

The proof has two parts:

1. For any input data vector $\phi(k), 1 \le k \le N$ and unit vectors h and $\bar{h}$, represented in rectangular coordinate space $\Re^n$, there are regions (called sign difference regions) in $\Re^n$ such that $sign(\phi^T(k)h) \neq sign(\phi^T(k)\bar{h})$.
2. Because the positive distribution over interval $[a, -a]$, with probability one some $\phi(k)$ will be in the sign difference regions as $N \to \infty$.

In the first part, we show that for any unit vector $\bar{h} \neq h$, there exists some ϕ so that $sign(\phi^T h) \neq sign(\phi^T \bar{h})$. For any unit vector $\bar{h} \neq h$, there are two cases: $\angle(h, \bar{h}) \ge 90^0$ and $\angle(h, \bar{h}) < 90^0$. For the first case, let ϕ be any non-zero vector such that:

$$90^0 < \angle(\phi, h) < 180^0, \quad 0 < \angle(\phi, \bar{h}) < 90^0 \tag{2.3}$$

This leads to:

$$\begin{aligned}\phi^T h &= \|\phi\|\|h\|\cos\left(\angle(\phi,h)\right) < 0 \\ \phi^T \bar{h} &= \|\phi\|\|\bar{h}\|\cos\left(\angle(\phi,\bar{h})\right) > 0\end{aligned} \tag{2.4}$$

and this in turn implies:

$$sign(\phi^T h) \neq sign(\phi^T \bar{h}) \tag{2.5}$$

For the second case, denote $0 < \theta = \angle(h,\bar{h}) < 90^0$. Let ϕ be a non-zero vector that lies in the plane spanned by h and $\bar{h}$ such that:

$$\angle(\phi,h) = 90^0 + \frac{1}{3}\theta > 90^0, \quad \angle(\phi,\bar{h}) = 90^0 - \frac{2}{3}\theta < 90^0 \tag{2.6}$$

This implies

$$\begin{aligned}\phi^T h &= \|\phi\|\|h\|\cos\left(\angle(\phi,h)\right) < 0 \\ \phi^T \bar{h} &= \|\phi\|\|\bar{h}\|\cos\left(\angle(\phi,\bar{h})\right) > 0\end{aligned} \tag{2.7}$$

and thus

$$sign(\phi^T h) \neq sign(\phi^T \bar{h}) \tag{2.8}$$

From the above discussion, for any unit vector $\bar{h} \neq h$, there exists some non-zero vector ϕ, independent of the magnitude, and $sign(\phi^T h) \neq sign(\phi^T \bar{h})$.

For the second part of the proof, we construct a cone with a small volume around ϕ. As long as the volume is small enough, by the continuity argument, $sign(\phi^T h) \neq sign(\phi^T \bar{h})$ for all ϕ in the cone. Now, by the input probability distribution continuity of Assumption 2.2, with probability one as $N \to \infty$, some $\phi(k)$ will be in the cone. This completes the proof.

For an algorithm based on the above theorem, the quadratic cost function based

on the error $e(k) = sign\big(y(k) + v(k)\big) - sign\big(\hat{x}(k)\big)$ in Figure 2 will be used:

$$J(\hat{h}) = \frac{1}{N}\sum_{k=1}^{N} e(k)^2 = \frac{1}{N}\sum_{k=1}^{N} [sign(y(k) + v(k)) - sign(\hat{y}(k))]^2 \tag{2.9}$$

The following minimization problem is solved to find the estimate $\hat{h}$:

$$\hat{h} = \arg\min_{\|\hat{h}\|=1} \frac{1}{N}\sum_{k=1}^{N} e(k)^2 \tag{2.10}$$

The theorem only establishes that there is a unique global minimum at $\hat{h} = h$ such that if $\hat{h} \neq h$ then the cost function will be greater than zero for large enough *N*. However, it is not clear if there are one or more local minimums that would interfere with a numerical simulation.

To function reliably, the cost function should have no local minimums and be nonzero whenever $\hat{h} \neq h$. To this end, consider the two dimensional case illustrated in Figure 3. First, suppose the input $u(k)$ is distributed such that the probability density of $\phi(k)$ is positive for any direction. Next, consider that the space $\Re^2$ can be divided into the four sectors shown in Figure 3. Clearly, $\phi^T h = \|\phi\|\|h\|\cos\theta$ implies:

$$\begin{aligned}
\phi(k) \in \text{Sector 1} &\Rightarrow \left|sign(\phi^T(k)h) - sign(\phi^T(k)\hat{h})\right| = |e(k)| = 0 \\
\phi(k) \in \text{Sector 2} &\Rightarrow \left|sign(\phi^T(k)h) - sign(\phi^T(k)\hat{h})\right| = |e(k)| = 2 \\
\phi(k) \in \text{Sector 3} &\Rightarrow \left|sign(\phi^T(k)h) - sign(\phi^T(k)\hat{h})\right| = |e(k)| = 0 \\
\phi(k) \in \text{Sector 4} &\Rightarrow \left|sign(\phi^T(k)h) - sign(\phi^T(k)\hat{h})\right| = |e(k)| = 2
\end{aligned} \tag{2.11}$$

Let $F(\theta) \geq 0$ be the probability that $\phi(k)$ lies in sectors 2 or 4. A reasonable observation from Figure 3 is that, given assumptions on the input $u(k)$, a larger θ results in larger sign difference regions which result in a larger cost function in (2.9). To help quantify

this, consider the sum of a series of N squared sign errors:

$$\frac{1}{N}\sum_{k=1}^{N}\left(sign(\phi(k)^T h) - sign(\phi(k)^T \hat{h})\right)^2 = \frac{4w}{N} \tag{2.12}$$

Here, w is the number of samples of $y(k)$ in the series that have different signs. Thus $\frac{4w}{N}$ is the relative frequency probability of landing in sectors 2 or 4.

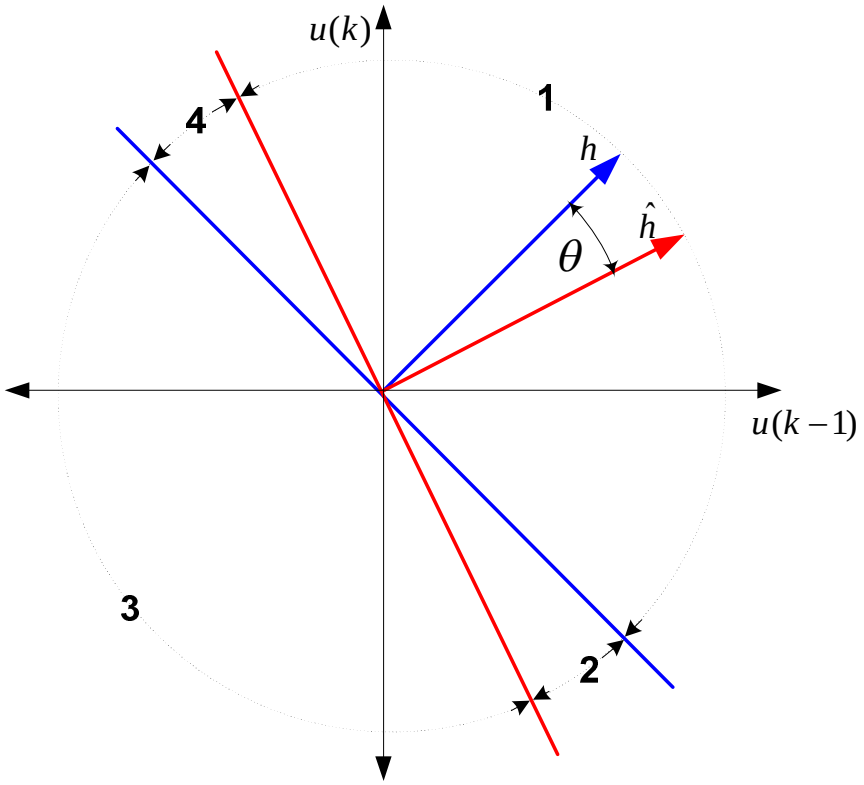

Figure 3: Sign difference regions

We would like the average of the relative frequency probability over N samples to be a direct function of θ:

$$\lim_{N\to\infty}\frac{1}{N}\sum_{k=1}^{N}\left(sign(\phi(k)^T h) - sign(\phi(k)^T \hat{h})\right)^2 = 4F(\theta) \tag{2.13}$$

Properties of $F(\theta)$ are described in more detail below. To show this correspondence we prove the following mean square convergence:

$$E\left\{\frac{1}{N}\sum_{k=1}^{N}\left(sign(\phi(k)^T h)-sign(\phi(k)^T \hat{h})\right)^2-4F(\theta)\right\}^2 \to 0 \quad \text{as} \quad N\to\infty \qquad (2.14)$$

See the Appendix for details of the proof. This implies that, in probability:

$$\lim_{N\to\infty}\frac{1}{N}\sum_{k=1}^{N}\left(sign(\phi(k)^T h)-sign(\phi(k)^T \hat{h})\right)^2 = 4F(\theta) \qquad (2.15)$$

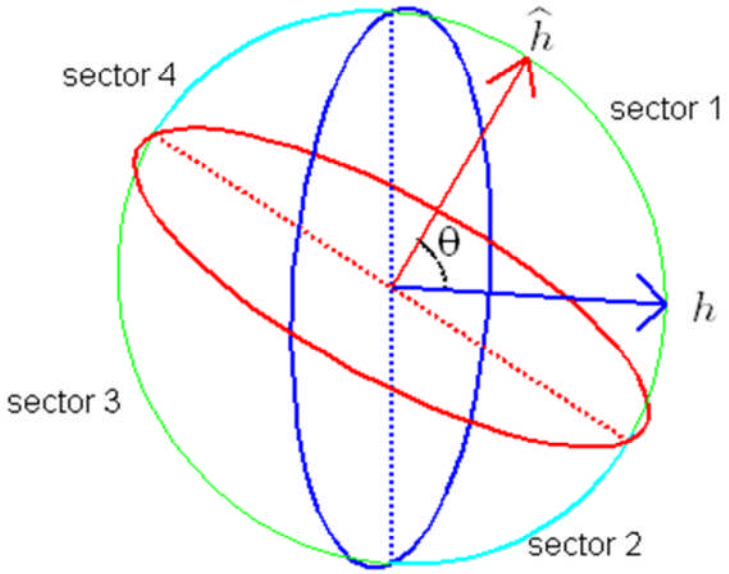

Figure 4: Four sign difference regions in three dimensions

The idea can be easily extended to a higher dimensional case. Let h and $\hat{h}$ be unit vectors in $\Re^n$. Consider that h and $\hat{h}$ span a plane, $S(h,\hat{h})=\left\{\alpha h+\beta\hat{h},\quad \alpha,\beta\in R\right\}$, in a two dimensional subspace of $\Re^n$. Let $r(\eta), -\pi\le\eta\le\pi$ denote the unit circle on the

plane. Further, let $r(0) = h$ and $r(\theta) = \hat{h}$. Without loss of generality, rotate the coordinate reference to line up $S(h, \hat{h})$ and $r(\eta)$ with the first two axes:

$$\begin{aligned} r(\eta) &= \begin{bmatrix} \cos(\eta) & \sin(\eta) & 0 & 0 & \cdots & 0 \end{bmatrix}^T \\ r(\theta) &= \begin{bmatrix} \cos(\theta) & \sin(\theta) & 0 & 0 & \cdots & 0 \end{bmatrix}^T = \hat{h} \\ r(0) &= \begin{bmatrix} 1 & 0 & 0 & 0 & \cdots & 0 \end{bmatrix}^T = h \end{aligned} \tag{2.16}$$

A vector tangent to $r(\eta)$: $\dfrac{dr(\eta)}{d\eta} = \begin{bmatrix} -\sin(\eta) & \cos(\eta) & 0 & 0 & \cdots & 0 \end{bmatrix}^T$ is also a normal vector for plane $Q(\eta)$. $Q(\eta)$ and $S(h, \hat{h})$ are perpendicular and both contain the origin. Their line of intersection is thus collinear with a radius of $r(\eta)$ at angle η. For example, $Q(0)$ lines up with h and $Q(\theta)$ lines up with $\hat{h}$. Two planes, $Q\left(\theta - \dfrac{\pi}{2}\right)$ and $Q\left(\dfrac{\pi}{2}\right)$, divide up $\Re^n$ into the same four sectors seen in the two dimensional case. A three dimensional example is shown in Figure 4.

The following additional theorem helps establish cost function monotonicity:

Theorem 2.2:

For any unit vector $\hat{h}$ *with* $\theta = \angle(h, \hat{h})$ for $-\pi \le \theta \le \pi$ *:*

$\lim_{N\to\infty} \dfrac{1}{N} \sum_{k=1}^{N} \left(sign(\phi(k)^T h) - sign(\phi(k)^T \hat{h}) \right)^2 = 4F(\theta)$ *in probability.* $F(\theta) \ge 0$ *is the probability that* $\phi(k)$ *lies in sectors 2 or 4, further: Thus* $F(\theta)$ *is strictly decreasing for* $-\pi \le \theta \le 0$ *and strictly increasing for* $0 \le \theta \le \pi$ *and* $F(\theta) = 0 \Leftrightarrow \theta = 0$

Proof:

The proof of the above theorem is a direct consequence of the observations.

Consider Assumption 2.2. The continuity on the distribution of input $u(k)$ guarantees that $\phi(k)$ assumes any direction in $\Re^n$ with a positive probability. Hence, the probability $F(\theta)$ that $\phi(k)$ lies in sectors 2 or 4 is monotonic as a function of the (probabilistic) volume of sectors 2 and 4. This leads to the statement that $F(\theta)$ is strictly decreasing for $-\pi \le \theta \le 0$ and strictly increasing for $0 \le \theta \le \pi$. This completes the proof.

The existence of one and only one global minimum is based on infinite *N*. For finite *N*, it may be possible that although $\hat{h} \neq h$, no $\phi(k)$ happen to inhabit either sector 2 or 4 and the cost function will be zero. This would not happen with infinite *N*. As the next section will demonstrate, a large *N* can be chosen to achieve reliable convergence.

Simulation testing

A system identification experiment was set up using the circuit of Figure 2 combined with the cost function of (2.9). The input $u(k)$ for $k = 1, 2, \ldots, N$ is i.i.d. uniformly in $[-1, 1]$ and noise $v(k)$ is Gaussian. For adjusting the estimate $\hat{h}$, based on the cost function, the recently developed Genetic Algorithm (GA) was chosen as the best performer. The GA used here was adapted from [1]. For this simulation, the number of total GA parents is 32. Note that the GA is a zero order carefully organized heuristic search algorithm that could be suboptimal. More GA details are provided in Chapter 3, for example see Figure 22. Also see reference [16].

The unknown FIR transfer function to be identified is:

$$h = \begin{pmatrix} 0.5795 - 0.4745\,z^{-1} + 0.3885\,z^{-2} - 0.318\,z^{-3} + 0.2604\,z^{-4} \\ -0.2132\,z^{-5} + 0.1746\,z^{-6} - 0.1429\,z^{-7} + 0.117\,z^{-8} - 0.09579z^{-9} \end{pmatrix} \qquad (2.17)$$

This linear system was followed by the following discontinuous nonlinearity:

$$y(k) = \begin{cases} 0.8x(k), & x(k) \le 0 \\ 1.4x(k), & 0 < x(k) \le 0.5 \\ 2x(k), & x(k) > 0.5 \end{cases} \tag{2.18}$$

Figure 5 and Figure 6 are plots of the FIR frequency response and the nonlinear transfer function, respectively. The error minimized by the GA is defined as $\text{MSE} = \left\| \hat{h} - h \right\|$. Each point in Table 1 is the result of 500 GA iterations; total GA run time for each point was about 15 minutes. Because the GA can potentially take hours to search a high dimensional space, a reasonable run time is important when considering practicality.

SNR (dB)	5	10	20	40
MSE	0.0529	0.0394	0.0211	0.0044

Table 1: Quadrant information estimation error vs. noise level, *N*=35000

N	5000	15000	25000	35000	50000
MSE	0.0422	0.0358	0.0359	0.0211	0.0175

Table 2: Estimation error vs. *N*, for SNR = 20dB

It should be emphasized that the uniqueness of the unknown parameter vector *h* is achieved as the number of data points $N \to \infty$. For finite *N*, the cost function behaves as a step function and a slight variation in the estimate may not give any change. The use of the sign function in the identification algorithm is dictated by the available information, i.e. Assumptiom 2.1.

Table 2 shows the simulation results for SNR = 20dB and various values of *N*. Recall that the convergence results are derived under the assumption that $N \to \infty$. A large *N* should lead to a small estimation error as supported by the results of Table 2.

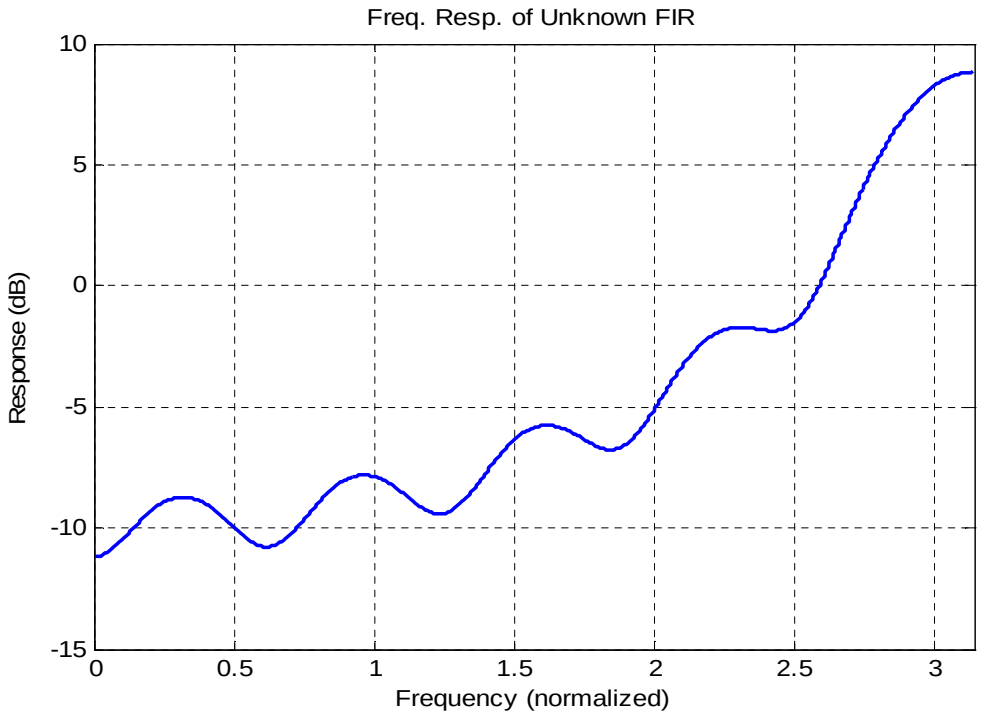

Figure 5: Simulation example, FIR lowpass response

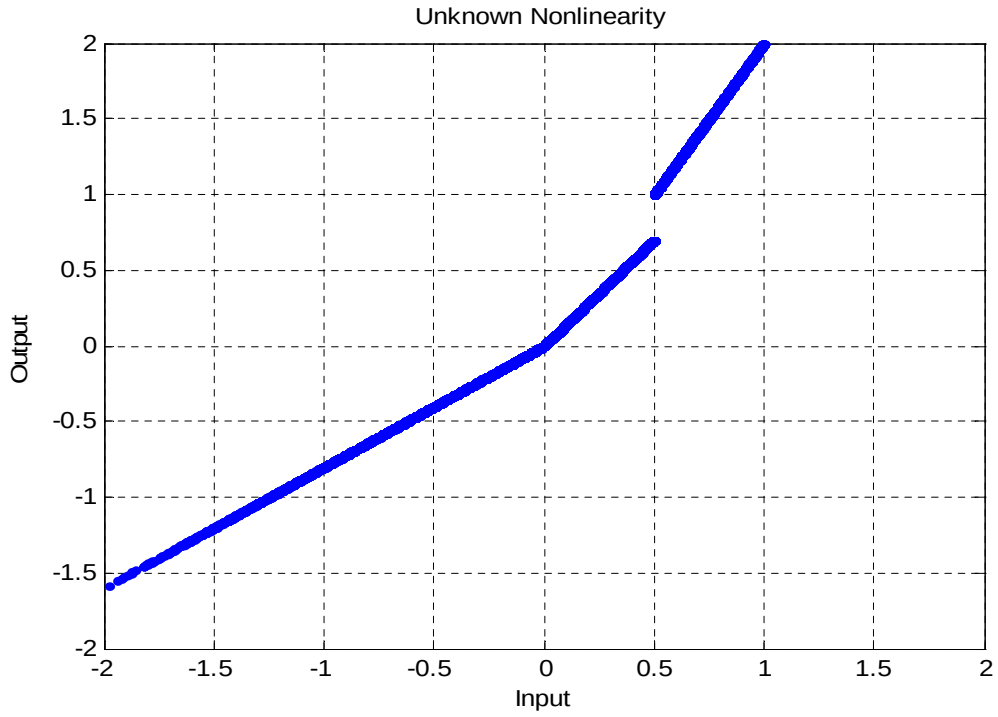

Figure 6: Simulation example, nonlinear block

Single point a priori information

Consider identification of the FIR linear part assuming we know one point on the static nonlinear transfer function such that $f(x_0) = y_0$. Take the point to be at the origin for simplicity. Unlike the a priori quadrant information described above, for identification under single point a priori information we assume continuity on $f\left(x(k)\right)$ in the neighborhood of the origin. For example, the preload nonlinearity of Figure 7 is acceptable for a priori quadrant information but will not work for single point a priori information.

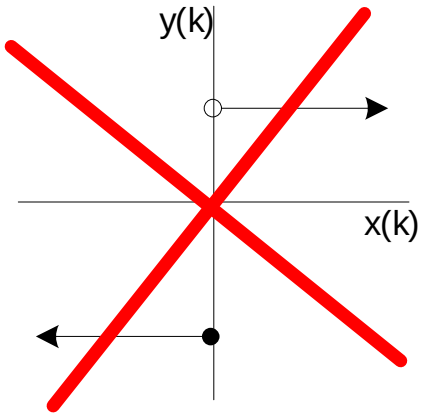

Figure 7: Unacceptable nonlinearity for single point identification

Assumption 2.3:

It is assumed that $f(0) = 0$. *Further,* $f(x) = 0 \Leftrightarrow x = 0$ *and* $f(\cdot)$ *is continuous in the neighborhood of the origin.*

Notice that Assumptions 2.1 and 2.3 are not equivalent. In particular, Assumption 2.1 does not necessarily imply Assumption 2.3 because no continuity on $f(\cdot)$ was assumed in 2.1. As mentioned, the pre-load nonlinearity satisfies Assumption 2.1

because all input/output points are in the first and third quadrant but does not satisfy Assumption 2.3 because $f(0) \neq 0$.

Intermediate signal $x(k)$ is unknown. From Assumption 2.3, only $x(k) = 0$ is known if $y(k) = 0$. Hence, non-zero $y(k)$ does not reveal any information on the unknown $x(k)$ and is not very useful in terms of identification. Identification has to rely on $y(k) = 0$ or $y(k)$ that is close to zero.

The following lemma is fundamental to understanding single point system identification:

Lemma 2.1:

Assume that the PDF of $u(k)$ *has a positive support containing a non-empty interval* $[-a, a]$ *for some* $0 < a < 1$. *Then h is identifiable for a given input-output data set* $\{\phi(i), y(i)\}_{i=1}^{N}$ *if and only if there exists some* $1 \le p_1 < p_2 < \cdots < p_k \le N$ *where the output* $y(p_k)$ *is zero valued (and thus* $x(p_k)$ *is also zero valued) and the corresponding matrix* $\Phi(p_1 \quad p_2 \quad \cdots \quad p_k)$ *satisfies:*

$$rank\ \Phi(p_1 \quad p_2 \quad \cdots \quad p_k) = rank \begin{pmatrix} \phi^T(p_1) \\ \phi^T(p_2) \\ \vdots \\ \phi^T(p_k) \end{pmatrix} = (n-1) \tag{2.19}$$

Proof:

First we prove sufficiency. That is, the existence of $1 \le p_1 < p_2 < \cdots < p_k \le N$ where $x(p_k)$ and output $y(p_k)$ are zero valued and rank $\Phi(p_1 \quad p_2 \quad \cdots \quad p_k) = (n-1)$ implies unique identifiability. If rank $\Phi(p_1 \quad p_2 \quad \cdots \quad p_k) = (n-1)$ then any non-zero

solution *h* of:

$$\begin{pmatrix} \phi^T(p_1) \\ \phi^T(p_2) \\ \vdots \\ \phi^T(p_k) \end{pmatrix} h = \begin{pmatrix} x(p_1) \\ x(p_2) \\ \vdots \\ x(p_k) \end{pmatrix} = \begin{pmatrix} y(p_1) \\ y(p_2) \\ \vdots \\ y(p_k) \end{pmatrix} = \begin{pmatrix} 0 \\ 0 \\ \vdots \\ 0 \end{pmatrix} \tag{2.20}$$

lies in the one dimensional null subspace of $\Phi(p_1 \quad p_2 \quad \cdots \quad p_k)$. Each solution has the form αh. So the solution is unique by normalization. End of sufficiency proof.

Second, we prove necessity. That is, unique identifiability implies the existence of $1 \le p_1 < p_2 < \cdots < p_k \le N$ where $x(p_k)$ and output $y(p_k)$ are zero valued and rank $\Phi(p_1 \quad p_2 \quad \cdots \quad p_k) = (n-1)$. This proof makes use of logically equivalent contrapositives. That is, instead of proving from Lemma 2.1 that *h* is identifiable if and only if there exists some $1 \le p_1 < p_2 < \cdots < p_k \le N$ where the output $y(p_k)$ is zero valued and the corresponding matrix rank $\Phi(p_1 \quad p_2 \quad \cdots \quad p_k) = (n-1)$, we prove:

1. If rank $\Phi(p_1 \quad p_2 \quad \cdots \quad p_k) \ne (n-1)$ then *h* is not identifiable.
2. If rank $\Phi(p_1 \quad p_2 \quad \cdots \quad p_k) = (n-1)$ and $y(p_i) \ne 0$ for $i = 1, \ldots, k$ then *h* is not identifiable.

We start by proving that identifiability implies rank $\Phi(p_1 \quad p_2 \quad \cdots \quad p_k) = (n-1)$ for some $1 \le p_1 < p_2 < \cdots < p_k \le N$ (item 1 above). First, we look at identifiability when rank $\Phi(1, ..., N) < (n-1)$. Let $\bar{h}$ be a vector, independent of *h*, in the null space of $\Phi(1, ..., N)$. It follows that:

$$\Phi(1,...,N)(h+\bar{h}) = \Phi(1,...,N)h = \begin{pmatrix} x(1) \\ x(2) \\ \vdots \\ x(N) \end{pmatrix} \tag{2.21}$$

This contradicts the uniqueness of *h*. Therefore if the null space has dimension two or higher then *h* cannot be uniquely identifiable. Second, we look at identifiability when rank $\Phi(1,...,N) = n$. Since $h \neq 0$, we have:

$$\begin{pmatrix} \phi^T(1) \\ \vdots \\ \phi^T(k) \\ \phi^T(k+1) \\ \vdots \\ \phi^T(N) \end{pmatrix} h = \begin{pmatrix} 0 \\ \vdots \\ 0 \\ x(k+1) \\ \vdots \\ x(N) \end{pmatrix} \tag{2.22}$$

for some *k* so that $x(k+1) \neq 0,...,x(N) \neq 0$ up to a row permutation. Here $k < N$ can have any value as long as the linear system output is zero for the first *k* rows. The entire matrix has null space dimension zero. Although the rank of $\Phi(k+1,...,N) = n$, consider a sub-matrix made up of only the first *k* rows:

$$\begin{pmatrix} \phi^T(1) \\ \vdots \\ \phi^T(k) \end{pmatrix} h = \begin{pmatrix} 0 \\ \vdots \\ 0 \end{pmatrix} \tag{2.23}$$

The given hypothesis is that rank $\Phi(p_1 \quad p_2 \quad \cdots \quad p_k) \neq (n-1)$. On the other hand, $h \neq 0$ implies that rank $\Phi(1,...,k) < n$. The only other possibility is that rank $\Phi(1,...,k) \leq (n-2)$. Thus there exists a non-zero $\bar{h}$, independent of *h*, in the null space of $\Phi(1,...,k)$ and a small α so that:

$$\begin{pmatrix} \phi^T(1) \\ \vdots \\ \phi^T(k) \\ \phi^T(k+1) \\ \vdots \\ \phi^T(N) \end{pmatrix} (h+\alpha\bar{h}) = \begin{pmatrix} 0 \\ \vdots \\ 0 \\ \bar{x}(k+1) \\ \vdots \\ \bar{x}(N) \end{pmatrix} \qquad (2.24)$$

$$\bar{x}(k+1) \neq 0, ..., \bar{x}(N) \neq 0$$

Thus *h* is not identifiable using the first *k* rows. Remove these and we have:

$$\begin{pmatrix} \phi^T(k+1) \\ \vdots \\ \phi^T(N) \end{pmatrix} (h+\alpha\bar{h}) = \begin{pmatrix} \bar{x}(k+1) \\ \vdots \\ \bar{x}(N) \end{pmatrix} \qquad (2.25)$$

$$\bar{x}(k+1) \neq 0, ..., \bar{x}(N) \neq 0$$

Note that rank $\Phi(k+1, ..., N) = n$. Recall the nonlinear transfer function one point a priori knowledge is limited to $f(0) = 0$.

Since any function can have the same output value for two different input values, and because we have no knowledge of the nonlinear function except at the origin, we can not identify *h* on the basis of non-zero $x(.)$ and $\bar{x}(.)$. For example, let $\bar{f}(.)$ be an arbitrarily defined nonlinearity except at:

$$\begin{aligned} &\bar{f}(0) = 0 \\ &\bar{f}(\bar{x}(k+1)) = f(x(k+1)) = y(k+1) \\ &... \\ &\bar{f}(\bar{x}(N)) = f(x(N)) = y(N) \end{aligned} \qquad (2.26)$$

This implies that the pairs (h, f) and $(h+\alpha\bar{h}, \bar{f})$ produce identical input-output data sets and h is not identifiable. Thus we have shown that (2.22) cannot be used to identify *h*. We conclude that $\Phi(p_1 \quad p_2 \quad \cdots \quad p_k) = (n-1)$ for some $1 \leq p_1 < p_2 < \cdots < p_k \leq N$ is a necessary condition.

For necessity we must prove that identifiability implies *both* rank $\Phi(p_1 \quad p_2 \quad \cdots \quad p_k) = (n-1)$ for some $1 \le p_1 < p_2 < \cdots < p_k \le N$ *and* $x(p_k)$ is zero valued. So far we have proven that identifiability implies rank $\Phi(p_1 \quad p_2 \quad \cdots \quad p_k) = (n-1)$ for some $1 \le p_1 < p_2 < \cdots < p_k \le N$. To prove that given rank $\Phi(p_1 \quad p_2 \quad \cdots \quad p_k) = (n-1)$ for some $1 \le p_1 < p_2 < \cdots < p_k \le N$ identifiability also implies $x(p_k)$ is zero valued, we use the contrapositive approach in item two, above.

If rank $\Phi(p_1 \quad p_2 \quad \cdots \quad p_k) = (n-1)$ for some $1 \le p_1 < p_2 < \cdots < p_k \le N$ and $x(p_k)$ is not zero valued for all p_k then h is not identifiable. If rank $\Phi(p_1 \quad p_2 \quad \cdots \quad p_k) = (n-1)$ then the null space is one dimensional, i.e. a line. Any h on this line is unique to within a scaling factor. For h to span the null space, outputs $x(p_k)$ corresponding to rows of $\Phi(p_1 \quad p_2 \quad \cdots \quad p_k)$ must all be zero due to the definition of a null space. Say, for example, δ below, is non-zero. Then, as described above, the situation could exist where the nonlinear function $f(x(p_1)) = \delta$ as well as $f(\overline{x}(p_1)) = \delta$. This would make h not identifiable.

$$\begin{pmatrix} \phi^T(p_1) \\ \phi^T(p_2) \\ \vdots \\ \phi^T(p_k) \end{pmatrix} h = \begin{pmatrix} y(p_1) \\ y(p_2) \\ \vdots \\ y(p_k) \end{pmatrix} = \begin{pmatrix} \delta \\ 0 \\ \vdots \\ 0 \end{pmatrix} \tag{2.27}$$

Thus identifiability implies *both* rank $\Phi(p_1 \quad p_2 \quad \cdots \quad p_k) = (n-1)$ for some $1 \le p_1 < p_2 < \cdots < p_k \le N$ *and* $x(p_k)$ is zero valued.

From the above results, it is obvious that to identify h, output samples have to be collected when $y(p_k) = 0$. Exact values of $y(p_k) = 0$ are unlikely in practice. Practical

system identification will have to rely on samples collected when $y(p_k) \approx 0$. In the following, we show that these will work if a small identification error is allowed. To this end we need some preliminary analysis.

Let $e_1, e_2, \ldots, e_n$ be an orthonormal basis of $\Re^n$ with $e_n = h$. Recall that $\|h\| = 1$ Given any small $\varepsilon_1 > 0$, construct a cone C_i around e_i for $i = 1, 2, \ldots, n$. For $i = 1, 2, \ldots, (n-1)$:

$$\phi \in C_i(\varepsilon_1) \Leftrightarrow \cos\left(\angle(\phi, e_i)\right) \geq (1 - \varepsilon_1) \tag{2.28}$$

In Figure 8, the bottom of these cones appears truncated due to the constraint $a \leq \|\phi\| \leq 1$, where *a* is defined in Lemma 2.1. For $i = n$:

$$\phi \in C_n(\varepsilon_1) \Leftrightarrow \cos\left(\angle(\phi, e_n)\right) \geq 1 - \varepsilon_1 \tag{2.29}$$

And also $0 < \|\phi\| \leq \varepsilon$. See Figure 8 for a three dimensional illustration.

Under the conditions of Lemma 2.1, for any $\varepsilon > 0$ and $0 < a < 1$, there exists a small $\bar{\varepsilon} = f(\varepsilon, a) > 0$ so that for all $\varepsilon_1 \leq \bar{\varepsilon}$, we have:

$$\begin{aligned} &\phi(i) \in C_i, \phi(l) \in C_l \\ &\left|\cos(\angle(\phi(i), \phi(l))\right| \leq \varepsilon \\ &\left|\phi(i)^T \phi(l)\right| = \|\phi(i)\| \|\phi(l)\| \left|\cos(\angle(\phi(i), \phi(l))\right| \leq \varepsilon \end{aligned} \tag{2.30}$$

$$rank \begin{bmatrix} \phi^T(i_1) \\ \phi^T(i_2) \\ \ldots \\ \phi^T(i_n) \end{bmatrix} = n \tag{2.31}$$

if $\phi(i_1) \in C_1, \ldots, \phi(i_2) \in C_2, \phi(n) \in C_n$. Now consider a sample matrix with $(n-1)$ rows. Let $\phi(i) \in C_i$ for $i = 1, 2, \ldots, (n-1)$. We can write:

$$\phi(i) = \beta_{i,1}e_1 + \beta_{i,2}e_2 + \ldots + \beta_{i,n-1}e_{n-1} + \beta_{i,n}h \tag{2.32}$$

Where $\beta_{i,j}$ for $i = 1,2, \ldots, n-1$ and $j = 1,2, \ldots, n$ are the projection coefficients of $\phi(i)$ into the orthonormal basis (e_1, e_2 … e_n) = (e_1, e_2 … h). Since all the $\phi(i)$ for $i = 1,2,\ldots,(n-1)$ have a constraint $a \le \|\phi\| \le 1$, the projection coefficient matrix is strictly diagonally dominant, for sufficient small ε: $|\beta_{i,i}| > \sum_{\substack{j=1 \\ j \ne i}}^{n} |\beta_{i,j}| \quad i = 1,2,...,n-1$

$$\begin{bmatrix} \phi(1) \\ \vdots \\ \phi(n-2) \\ \phi(n-1) \end{bmatrix} = \begin{bmatrix} \beta_{1,1} & \beta_{1,2} & \cdots & \beta_{1,n} \\ \vdots & \vdots & \vdots & \vdots \\ \beta_{n-2,1} & \beta_{n-2,2} & \cdots & \beta_{n-2,n} \\ \beta_{n-1,1} & \beta_{n-1,1} & \cdots & \beta_{n-1,n} \end{bmatrix} \begin{bmatrix} e_1^T \\ \vdots \\ e_{n-1}^T \\ h^T \end{bmatrix} \tag{2.33}$$

The last column is very small since it is the projection of the first $(n-1)$ cone vectors onto true coefficient vector *h*.

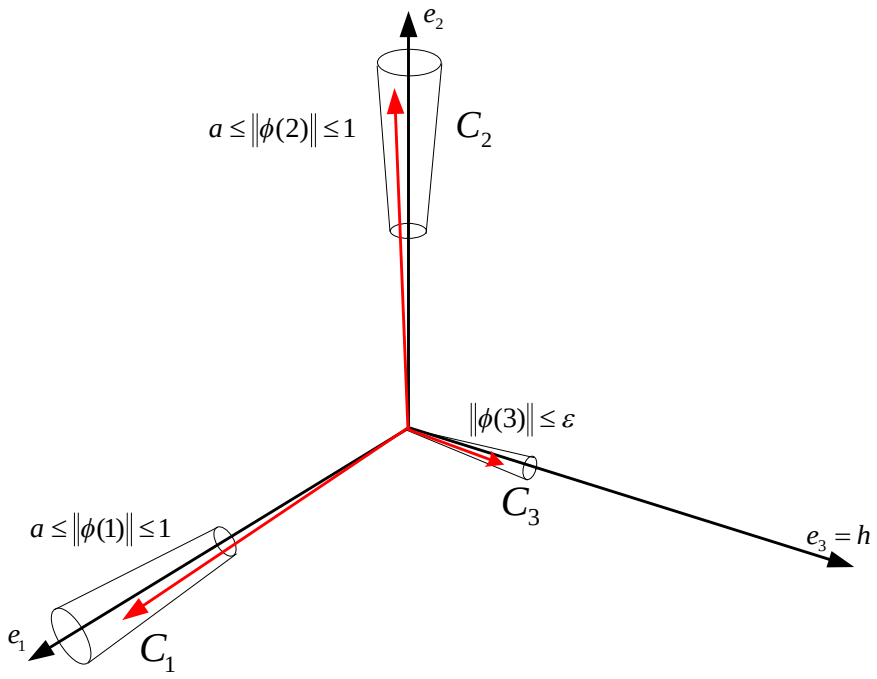

Figure 8: Cone construction for three dimensions

The following theorem helps explain why single point system identification is possible when, instead of being equal to zero, outputs are only close to zero. This result shows the practicality of the single point a priori information system identification approach.

Theorem 2.3:

From Assumption 2.3, we have nonlinearity a priori point information, $f(x) = 0 \Leftrightarrow x = 0$, *and* $f(\cdot)$ *is continuous in a neighborhood of the origin. Also assume that the PDF of* $u(\cdot)$ *has a positive support containing a non-empty interval* $[-a, a]$ *for some* $0 < a < 1$.

1. *Given any small* $\varepsilon > 0$, *with probability one as* $N \to \infty$ *there exists a sequence* $\phi(i_l)$ *for l=1,2,…,n such that* $|x(i_l)| = |\Phi(i_l)h| \le \varepsilon$ *and rank* $\Phi(i_1, i_2 \ldots, i_n) = n$.
2. *The matrix* $\Phi(i_1, i_2 \ldots, i_n)$ *can be written as:* $\Phi(i_1, i_2 \ldots, i_n) = Q + E(\varepsilon)$. *For some Q and* $E(\varepsilon)$, *where rank Q = n-1, independent of* ε, *and* $E(\varepsilon) \to 0$ *as* $\varepsilon \to 0$. *Further, let the singular value decomposition (SVD) of* Φ be $\Phi(i_1, i_2 \ldots, i_n) = U(\varepsilon)\Sigma(\varepsilon)[v_1(\varepsilon), v_2(\varepsilon) \ldots v_n(e)]^T$. *Then,* $\|v_n(\varepsilon) - h\| \to 0$ *as* $\varepsilon \to 0$ *(modulo* $\pm$ *signs).*

Proof:

To prove part 1 of Theorem 2.3, consider a set of input sample indexes that select a matrix of non-overlapping input sample vectors, $\Phi(p_1, p_2, \ldots, p_n)$, that inhabit the cones described previously. To make the proof simpler, the input sample vectors are

statistically independent and non-overlapping[1].

Consider a set of indexes $p_1 < p_2 < \cdots < p_k \le p_n$ where p_1 is in the range $\left[0, N - n^2\right]$ and $p_l = n + p_{l-1}$. For any $\varepsilon > 0$, there is probability $\alpha > 0$ for each set of indexes such that:

$$\begin{aligned} &\phi(p_1) \in C_1 \\ &\cdots \\ &\phi(p_{n-1}) \in C_{n-1} \\ &\phi(p_n) \in C_n \end{aligned} \tag{2.34}$$

In other words there is non-zero probability α that $\left|x(p_i)\right| = \left|\phi^T(p_i)h\right| \le \varepsilon$ for *i=1,2, …n* and at the same time:

$$rank\begin{bmatrix} \phi^T(p_1) \\ \vdots \\ \phi^T(p_{n-1}) \\ \phi^T(p_n) \end{bmatrix} = n \tag{2.35}$$

Note that:

1. $\left|\phi^T(p_i)h\right| \le \varepsilon$ for $i = 1, 2, \ldots, n-1$ because $h = e_n$ and $\phi(p_i) \in C_i$.
2. $\left|\phi^T(p_n)h\right| \le \varepsilon$ because $0 < \left\|\phi(p_n)\right\| \le \varepsilon$ and $\|h\| = 1$.

For each set of indexes $p_1 < p_2 < \cdots < p_k \le p_n$ starting at some randomly chosen p_1, define the event: A_{p_1} = {at least one $\phi(p_i) \notin C_i$ for $i = 1, 2, \ldots, n$} and also $P\left(\bar{A}_{p_1}\right) = \alpha$. If m is the number of such index sets then, due to the Assumption 2.2 and the independence of $\phi(p_n)$, we obtain: $P\left\{A_{p_1} \cap A_{p_2} \cap \ldots \cap A_{p_m}\right\} = (1-\alpha)^m \to 0$ as

[1] In the simulation we will let the sample vectors overlap. Even though the sample vectors may not be independent they can still be at right angles to each other.

$m \to \infty$. This says that the probability is zero of sample vectors not lining up in orthogonal cones for any value of m as $m \to \infty$. Furthermore, because $\sum_{m=1}^{\infty}(1-\alpha)^m < \infty$, the Borel Lemma ([27], page 240) tells us that the convergence in probability is changed to convergence with probability one as $N \to \infty$. Thus (2.34) is true with probability one for some set of indexes $p_1 < p_2 < \cdots < p_k \le p_n$ as $N \to \infty$. This completes the proof of part 1 of Theorem 2.3.

For part 2 of the proof we note that from (2.32) and the above proof: $\phi(i_j) = \sum_{k=1}^{n} \beta_{i_j,k} e_k$ for $j = 1, 2 \ldots, \mathrm{n}$. Note that $\phi(i_n) \in C_n \Rightarrow \|\phi(i_n)\| \le \varepsilon \Rightarrow \left|\beta_{i_n,k}\right| \le \varepsilon$. If we assume that $e_n = h$, on a rectangular axis and the other basis vectors are at right angles then the requirement $\left|\phi^T(p_i)h\right| \le \varepsilon$ for $i = 1, 2, \ldots, n$ implies a diagonal dominance, in the first $(n-1)$ rows. In the construction below, h is a null space basis for Q

$$\Phi(i_1, \ldots, i_{n-1}, i_n) = \begin{bmatrix} \varphi^T(i_1) \\ \\ \varphi^T(i_{n-1}) \\ \varphi^T(i_n) \end{bmatrix} = \begin{bmatrix} \beta_{i_1,1} & \beta_{i_1,2} & \ldots & \beta_{i_1,n} \\ \ldots & \ldots & \ldots & \ldots \\ \beta_{i_{n-1},1} & \beta_{i_{n-1},2} & \ldots & \beta_{i_{n-1},n} \\ \beta_{i_n,1} & \beta_{i_n,2} & \ldots & \beta_{i_n,n} \end{bmatrix} \begin{bmatrix} e_1^T \\ \ldots \\ e_{n-1}^T \\ h_n^T \end{bmatrix}$$
$$= \begin{bmatrix} \beta_{i_1,1} & \beta_{i_1,2} & \ldots & \beta_{i_1,n-1} \\ \ldots & \ldots & \ldots & \ldots \\ \beta_{i_{n-1},1} & \beta_{i_{n-1},2} & \ldots & \beta_{i_{n-1},n-1} \\ \beta_{i_n,1} & \beta_{i_n,2} & \ldots & \beta_{i_n,n-1} \end{bmatrix} \begin{bmatrix} e_1^T \\ \ldots \\ e_{n-2}^T \\ e_{n-1}^T \end{bmatrix} + \begin{bmatrix} \beta_{i_1,n} \\ \ldots \\ \beta_{i_{n-1},n} \\ \beta_{i_n,n} \end{bmatrix} h^T \tag{2.36}$$

Define:

$$Q = \begin{bmatrix} \beta_{i_1,1} & \beta_{i_1,2} & \ldots & \beta_{i_1,n-1} \\ \ldots & \ldots & \ldots & \ldots \\ \beta_{i_{n-1},1} & \beta_{i_{n-1},2} & \ldots & \beta_{i_{n-1},n-1} \\ \beta_{i_n,1} & \beta_{i_n,2} & \ldots & \beta_{i_n,n-1} \end{bmatrix} \begin{bmatrix} e_1^T \\ \ldots \\ e_{n-2}^T \\ e_{n-1}^T \end{bmatrix}, \quad E(\varepsilon) = \begin{bmatrix} \beta_{i_1,n} \\ \ldots \\ \beta_{i_{n-1},n} \\ \beta_{i_n,n} \end{bmatrix} h^T \tag{2.37}$$

Since $\|h\| = 1$ and $h = e_n$ is orthogonal to e_i for $i = 1,2,\ldots,n-1$:

$$\Phi(i_1,i_2,\ldots,i_n)h = Qh + E(\varepsilon)h = \begin{bmatrix} \beta_{i_1,1} & \beta_{i_1,2} & \ldots & \beta_{i_1,n-1} \\ \ldots & \ldots & \ldots & \ldots \\ \beta_{i_{n-1},1} & \beta_{i_{n-1},2} & \ldots & \beta_{i_{n-1},n-1} \\ \beta_{i_n,1} & \beta_{i_n,2} & \ldots & \beta_{i_n,n-1} \end{bmatrix} \begin{bmatrix} e_1^T \\ \ldots \\ e_{n-2}^T \\ e_{n-1}^T \end{bmatrix} h + \begin{bmatrix} \beta_{i_1,n} \\ \ldots \\ \beta_{i_{n-1},n} \\ \beta_{i_n,n} \end{bmatrix} h^T h = \begin{bmatrix} \beta_{i_1,n} \\ \ldots \\ \beta_{i_{n-1},n} \\ \beta_{i_n,n} \end{bmatrix} = \begin{bmatrix} x(i_1) \\ \ldots \\ x(i_{n-1}) \\ x(i_n) \end{bmatrix} \tag{2.38}$$

Thus $|x(i_j)| = |\beta_{i_j,n}| \le \varepsilon \to 0$ and $E(\varepsilon) \to 0$ as $\varepsilon \to 0$

Moreover, rank $\Phi(i_1,i_2,\ldots,i_n) = n$ and rank of $E(\varepsilon) \le 1$ implies rank Q is $(n-1)$ and $Qh = 0$. In addition, considering the hypothesized vector basis, the matrix:

$$\begin{bmatrix} \beta_{i_1,1} & \beta_{i_1,2} & \ldots & \beta_{i_1,n-1} \\ \ldots & \ldots & \ldots & \ldots \\ \beta_{i_{n-1},1} & \beta_{i_{n-1},2} & \ldots & \beta_{i_{n-1},n-1} \\ \beta_{i_n,1} & \beta_{i_n,2} & \ldots & \beta_{i_n,n-1} \end{bmatrix} \tag{2.39}$$

is strictly diagonally dominant and $|\beta_{i_n,k}| < \varepsilon \to 0$ as $\varepsilon \to 0$. This implies rank Q is $(n-1)$, independent of ε by the Gerschgorin Circle Theorem (see [17], page 320). From [23], each of the $(n-1)$ singular values of Q is in a ball centered at $\beta_{i,i}$ with radii defined by: $r_i = \frac{1}{2}\left(\sum_{\substack{j=1 \\ j \ne i}}^{n-1} |\beta_{i,j}| + \sum_{\substack{j=1 \\ j \ne i}}^{n} |\beta_{j,i}| \right)$

The diagonal dominance and the Gerschgorin Circle Theorem insure that the singular values and singular vectors corresponding to the first $(n-1)$ rows of $Q + E(\varepsilon)$ remain there and the last singular value and singular vector remains associated with h_n. Now write $Q = U_Q \Sigma_Q (V_{Q1},\ldots V_{Qn})^T \Rightarrow h = V_{Qn}$ (modulo $\pm$ sign). Clearly:

$$\Phi(i_1, i_2, \ldots, i_n) = U(\varepsilon)\Sigma(\varepsilon)\left[V_1(\varepsilon), V_2(\varepsilon)...V_n(\varepsilon)\right]^T = Q + E(\varepsilon) \tag{2.40}$$

and by the Wielant-Hoffman Theorem [17]: $\left\|V_{Qn} - V_n(\varepsilon)\right\| \to 0$ as $\varepsilon \to 0$ Therefore, as $\varepsilon \to 0$:

$$\left\|V_n(\varepsilon) - h\right\| = \left\|V_n(\varepsilon) - V_{Qn} + V_{Qn} - h\right\| \to 0 \tag{2.41}$$

Thus as $\varepsilon \to 0$, the last singular value of the SVD of Φ is close to zero. As described above, the corresponding singular vector becomes close to *h*. (see [8]). Thus, Φ starts to exhibit rank deficiency as $\varepsilon \to 0$. This completes the proof. Based on the theorem, we introduce the identification algorithm.

Simulation testing

Using the same Wiener model as in the previous simulation (see Figure 5 and Figure 6) the following algorithm was simulated:

1. Collect a set of $y(k)$ and corresponding $\phi(k)$ for $k = 1, 2, \ldots, N$
2. Construct matrix $\Phi(i_1, i_2, \ldots, i_M)$ of $\phi(k)$ for $k = 1, 2, \ldots, M$ corresponding to $|y(k)| \le \varepsilon$. Note that $M \le N$.
3. Calculate SVD of $\Phi(i_1, i_2, \ldots, i_M) = U(\varepsilon)\Sigma(\varepsilon)\left[V_1(\varepsilon), V_2(\varepsilon), \ldots, V_n(\varepsilon)\right]^T$
4. Define $\hat{h} = \pm V_n$ so that the first non-zero element of $\hat{h}$ is positive.

Results of an average of 10 Monte Carlo runs of the algorithm are shown in Table 3. The estimation error is defined as MSE = $\| h - \hat{h} \|$. Note that at the top of each column the variable ε is chosen differently for each SNR. A simulation that varied ε and monitored MSE was run to determine the best ε for a fixed *N* and SNR. The ε that resulted in the

lowest MSE was simply read for the graph in Figure 9.

There is a practical concern with the size of *M*, the number of rows in $\Phi(i_1, i_2, \ldots, i_M)$. As *M* gets larger and larger, computer hardware configurations can run out of memory and/or take an excessively long time. To alleviate this problem, ε should be as small as possible consistent with low MSE, as demonstrated in Figure 9. Note that for some of the entries in Table 3, *M* is limited to 900 to avoid a memory overrun problem.

The idea behind this algorithm is to use local data near $y(k) = 0$ to identify the linear part without interference from the unknown nonlinearity. In fact, measurements corresponding to $|y(k)| > \varepsilon$ are not used. From the theorem, $\hat{h} \approx h$ if ε is small and further $\hat{h} \to h$ as $\varepsilon \to 0$ at least in the absence of noise. A caution should be noted. The algorithm throws away all data observed with magnitudes larger than ε. For small ε, fewer data is retained to construct the estimate. Therefore, it takes a much longer time to collect the same number of data useful for construction of the estimate for a small ε than a large ε. Observe from Table 3 that for the smallest $\varepsilon = 0.016$, *N* = 20000 is required to collect M = 421 rows at SNR = 40dB. Thus considerable data is discarded.

N	SNR = 5dB $\varepsilon = 0.1$		SNR = 10dB $\varepsilon = 0.046$		SNR = 20dB $\varepsilon = 0.041$		SNR = 40 dB $\varepsilon = 0.016$	
	MSE	M	MSE	M	MSE	M	MSE	M
5000	0.1237	501	0.092	272	0.028	266	0.0068	106
10000	0.0952	900	0.066	549	0.021	536	0.0046	211
20000	0.0946	900	0.054	900	0.016	900	0.0034	421

Table 3: FIR single point simulation results

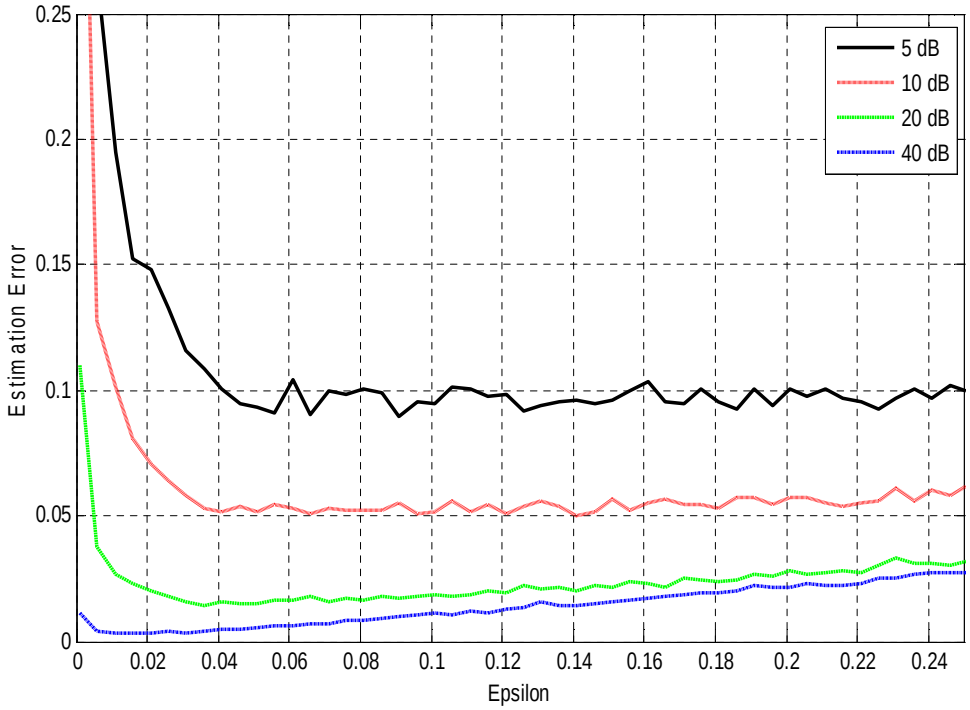

Figure 9: Variation of estimation error with ε, N=20000

The choice of ε is reminiscent of the choice of the bandwidth in kernel identification [13, page 20]. Kernel estimation attempts to estimate the output of an unknown function for a given single input point. Output values are weighted by the distance between their corresponding inputs and the given input. The output points that correspond to inputs very close to the given input are given the highest weight. Thus a neighborhood of inputs and corresponding outputs averaged is formed. The size of the neighborhood is controlled by the kernel "bandwidth". A large bandwidth results in a large neighborhood of output points averaged and a small variance. However, because the set of points in the output average is more likely to be distributed asymmetric with respect to the true output, a larger bandwidth can result in a larger bias.

In this situation, larger ε results in many more sample vectors in $\Phi(i_1, i_2, \ldots, i_M)$. However, because the shape of the unknown nonlinearity does not have to be symmetric around the origin, there is a possibility of introducing bias in the estimate. The SVD produces the best estimate of null space basis vector $h \to V_n(\varepsilon)$ when the sample vectors landing inside the cones in Figure 8 are symmetrically distributed around the center axis of each cone. A larger ε leading to a larger cone solid angle increases the possibility of asymmetry and bias.

Thus increasing ε tends to reduce the variance but at the same time to increase the bias. The best choice is to balance between the bias and the variance.

Locally monotonic nonlinearities

For quadrant a priori information, Assumption 2.1 defined quadrant conditions on the nonlinearity. For single point a priori information, Assumption 2.3 replaced quadrant conditions with a requirement for continuity around a single known point. In this section, the requirement is local monotonicity of the nonlinearity.

Assumption 2.4:

Assume there exists an interval $\underline{f} < \overline{f} \le M$ *and within the interval* $f(x) \in \left[\underline{f}, \overline{f}\right]$, $f(.)$ *is continuous and* $f(x_1) = f(x_2) \Leftrightarrow x_1 = x_2$.

Clearly, $f(\cdot)$ is monotonic if $y = f(x) \in \left[\underline{f}, \overline{f}\right]$.

Now define:

$$\begin{aligned} \psi(i, j) &= \phi(i) - \phi(j) \\ z(i, j) &= y(i) - y(j) = f(x(i)) - f(x(j)) \end{aligned} \tag{2.42}$$

Note that because of linearity, $\psi(i, j) = \phi(i) - \phi(j)$ can be considered an input to

the linear system and $z(i, j)$ can be considered the corresponding valid output. Notice that if $z(i, j) = y(i) - y(j) = f(x(i)) - f(x(j)) = 0$ and $f(x(i)) \in \left[\underline{f}, \overline{f}\right]$, $f(x(j)) \in \left[\underline{f}, \overline{f}\right]$ then we have $x(i) - x(j) = 0$. By collecting pairs of input vectors $\phi(i), \phi(j)$ that correspond to outputs whose difference is zero, we can cast identification of *h* under the locally monotonic prior information into identification under point prior information. Consider that ψ in (2.42) can be considered equivalent to ϕ in Lemma 2.1. Thus, we can identify *h* by selecting pairs of $\phi(i), \phi(j)$ whose difference makes the output difference close to zero. Previously derived results can be used to show that our modified input sample difference matrix and output difference vector can uniquely identify *h*. The following theorem helps explain why locally monotonic system identification is possible.

Theorem 2.4:

Consider Assumption 2.4. Further assume that the input samples $u(k)$ *are i.i.d. (not necessarily Gaussian) and the probability density dunction of* $y = f(x)$ *is positive in an interval* $f(x) \in \left[\underline{f}, \overline{f}\right]$. *Then:*

The first claim is that unknown coefficient vector h is identifiable if and only if there exists index sequences $1 \le i_m \le N$ *and* $1 \le j_m \le N$ *for* $m = 1, 2, \ldots, k$ *so that* $y(i_l), y(j_l) \in \left[\underline{f}, \overline{f}\right]$ *and* $z(i_l, j_l) = y(i_l) - y(j_l) = 0$ *for* $l = 1, \ldots, k$ *In addition, the corresponding matrix* $\Psi(1, 2, \ldots, k)$ *satisfies:*

$$rank\ \Psi(1, 2, \ldots, k) = rank \begin{pmatrix} \phi^T(i_1) - \phi^T(j_1) \\ \phi^T(i_2) - \phi^T(j_2) \\ \vdots \\ \phi^T(i_k) - \phi^T(j_k) \end{pmatrix} = (n - 1)$$

Secondly, for any small $\varepsilon > 0$, *with probability one as* $N \to \infty$, *there exists two subsequences:* $\phi(i_l)$ *and* $\phi(j_l)$, *for* $l = 1, \ldots, n$ *such that* $f(x(i_l)),\ f(x(j_l)) \in \left[\underline{f}, \overline{f}\right]$ *and* $\left| f(x(i_l)) - f(x(j_l)) \right| \le \varepsilon$ *and:*

$$rank\ \Psi(1,2,\ldots,n) = rank \begin{pmatrix} \phi^T(i_1) - \phi^T(j_1) \\ \phi^T(i_2) - \phi^T(j_2) \\ \vdots \\ \phi^T(i_n) - \phi^T(j_n) \end{pmatrix} = n$$

Finally, the matrix $\Psi(1,2,\ldots,n)$ *can be written as* $\Psi(1,2,\ldots,n) = Q + E(\varepsilon)$ *for some* Q *and* $E(\varepsilon)$ *where rank* $Q = (n-1)$, *independent of* ε *and* $E(\varepsilon) \to 0$ *as* $\varepsilon \to 0$. *Further, let the SVD of* $\Psi(1,2,\ldots,n)$ *be:* $\Psi(1,2,...,n) = U(\varepsilon)\Sigma(\varepsilon)\left[V_1(\varepsilon), V_2(\varepsilon)...V_n(\varepsilon)\right]^T = Q + E(\varepsilon)$ *Then, modulo* $\pm$ *sign:* $\left\| V_n(\varepsilon) - h \right\| \to 0$ *as* $\varepsilon \to 0$.

Proof:

The proof is a straightforward externsion of the results derived for single point a priori information. In the proof of Theorem 2.3 replace Φ by Ψ, $x(k)$ by $x(i_l) - x(j_l)$ and $y(k)$ by $z(i_l, j_l) = y(i_l) - y(j_l)$. As in the previous section, the result is that as $N \to \infty$, there are guaranteed to exist *n* rows of Ψ such that $\left| f(x(i_l)) - f(x(j_l)) \right| \le \varepsilon$ and at the same time rank Ψ is $(n-1)$.

Indexes i_m and j_m have no particular order, however they index pairs of input sample vectors that correspond to zero difference outputs:

$$\Psi(1,2,\ldots,k)h=\begin{pmatrix}\psi^T(1)\\ \psi^T(2)\\ \vdots\\ \psi^T(k)\end{pmatrix}h=\begin{pmatrix}\phi^T(i_1)-\phi^T(j_1)\\ \phi^T(i_2)-\phi^T(j_2)\\ \vdots\\ \phi^T(i_k)-\phi^T(j_k)\end{pmatrix}h=\begin{pmatrix}x(i_1)-x(j_1)\\ x(i_2)-x(j_2)\\ \vdots\\ x(i_k)-x(j_k)\end{pmatrix}=\begin{pmatrix}y(i_1)-y(j_1)\\ y(i_2)-y(j_2)\\ \vdots\\ y(i_k)-y(j_k)\end{pmatrix}=\begin{pmatrix}0\\ 0\\ \vdots\\ 0\end{pmatrix}$$

Figure 10 shows a simple illustration of this algorithm. The top graph, $y(k)$, is a small record of output samples. The center graph, $y_s(k)$, is the same record sorted lowest to highest in magnitude. Note how the sample indexes get mixed up. Finally the bottom graph, $y_{sd}(k)$, is the result of two-point differencing $y_s(k)$. In the bottom graph four differenced samples are less than ε. The corresponding input sample vectors are:

$$\Psi(1,2,3,4)h=\begin{pmatrix}\psi^T(1)\\ \psi^T(2)\\ \psi^T(3)\\ \psi^T(4)\end{pmatrix}h=\begin{pmatrix}\phi^T(i_9)-\phi^T(j_8)\\ \phi^T(i_2)-\phi^T(j_5)\\ \phi^T(i_{10})-\phi^T(j_0)\\ \phi^T(i_4)-\phi^T(j_7)\end{pmatrix}h=\begin{pmatrix}x(i_9)-x(j_8)\\ x(i_2)-x(j_5)\\ x(i_{10})-x(j_0)\\ x(i_4)-x(j_7)\end{pmatrix}=\begin{pmatrix}y(i_9)-y(j_8)\\ y(i_2)-y(j_5)\\ y(i_{10})-y(j_0)\\ y(i_4)-y(j_7)\end{pmatrix}\le\begin{pmatrix}\varepsilon\\ \varepsilon\\ \varepsilon\\ \varepsilon\end{pmatrix}$$

Assume that $n=4$. If ε is small enough and rank $\Psi(1,2,3,4)$ is 3 or 4, then the SVD can be used to identify *h*.

Based on the above theorem, we can define the identification algorithm to be used for locally monotonic a priori information on the nonlinearity. The next section presents simulation results. An important simulation observation is that the locally monotonic a priori information seems to perform better than the single point a priori information algorithm. A reasonable explanation is that the locally monotonic algorithm makes use of data in the entire monotonic output range whereas the single point algorithm uses data as close as possible to zero. If, for example, the entire nonlinearity is known a priori to be monotonic then outputs $y(k)$ and corresponding input sample vectors range over the entire nonlinearit as long as their respective difference is zero. Contrast this with the single point algorithm where only outputs near the origin are useful.

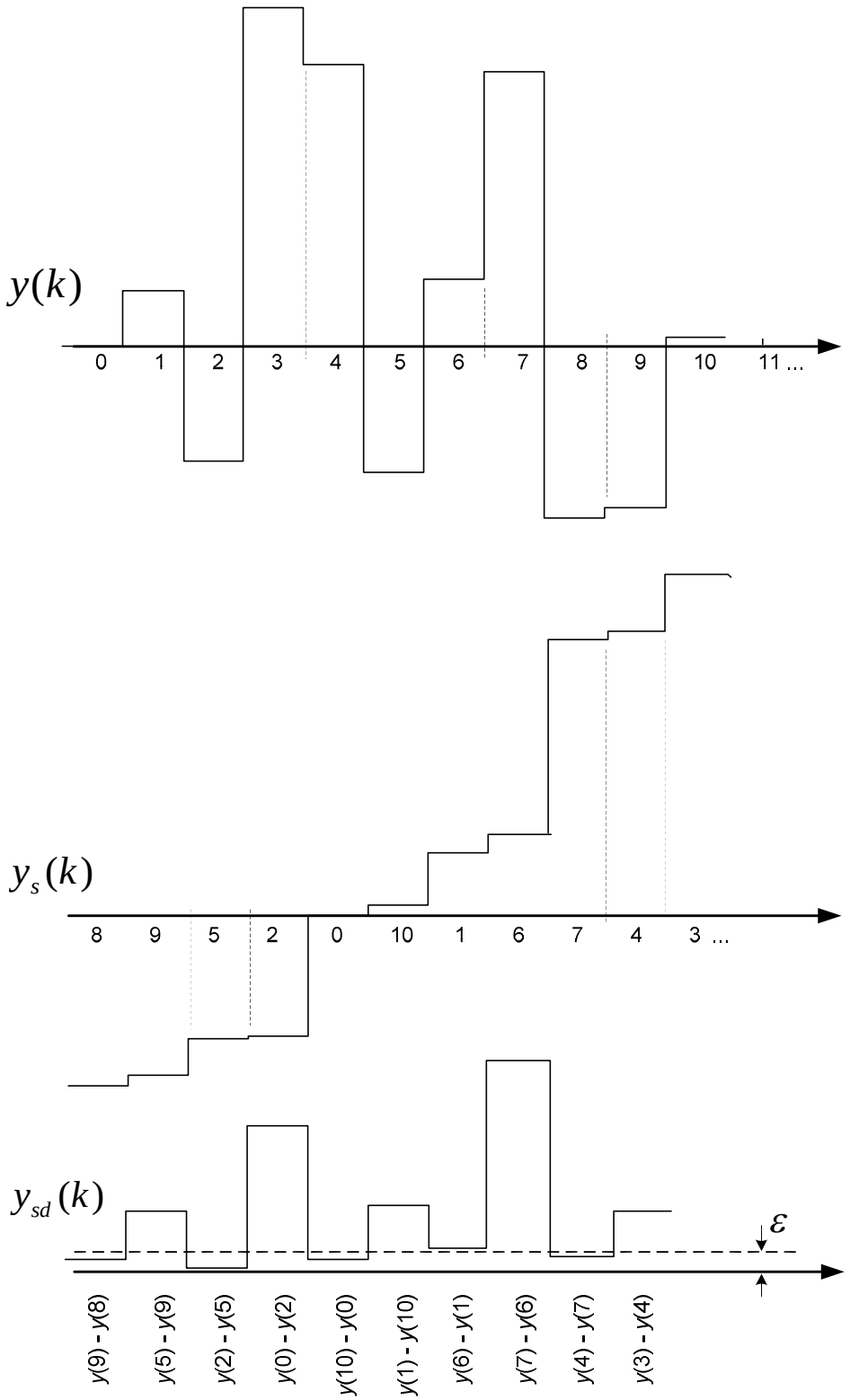

.

Figure 10: Example of sample collection for locally monotonic algorithm

Simulation testing

Using the same Wiener model as in the previous simulation (see Figure 5 and Figure 6), the following simulation steps were implemented:

1. Collect a set of $y(k)$ and corresponding $\phi(k)$ for $k = 1, 2, \ldots, N$
2. Sort the $y(k)$ from least to greatest, result is $y_s(k)$.
3. Construct $\Phi_s(i_1, i_2, \ldots, i_N)$ corresponding to $y_s(k)$.
4. Construct $y_{sd}(k)$ by differencing adjacent points of $y_s(k)$.
5. Construct $\Phi_{sd}(i_1, i_2, \ldots, i_{N-1})$ by differencing rows of $\Phi_s(i_1, i_2, \ldots, i_N)$.
6. Construct $\bar{\Phi}_{sd}(i_1, i_2, \ldots, i_M)$ corresponding to $|y_{sd}(k)| \le \varepsilon$
7. Calculate SVD $\bar{\Phi}_{sd}(i_1, i_2, \ldots, i_M) = U(\varepsilon)\Sigma(\varepsilon)\left[V_1(\varepsilon), V_2(\varepsilon), \ldots, V_n(\varepsilon)\right]^T$
8. Define $\hat{h} = \pm V_n$ so that the first non-zero element of $\hat{h}$ is positive.

Results of an average of 10 Monte Carlo runs of the algorithm are shown in Table 4. The estimation error is defined as MSE = $\| h - \hat{h} \|$. Note that at the top of each column the variable ε is chosen differently for each SNR. A simulation that varied ε and monitored MSE was run to determine the best ε for a fixed *N* and SNR. The ε that resulted in the lowest MSE was simply read for the graph in Figure 11.

As previously discussed for the the single point algorithm simulation, as *M* gets larger and larger, computer hardware configurations can run out of memory and/or take an excessively long time. To alleviate this problem, ε should be as small as possible consistent with low MSE, as demonstrated in Figure 11. Note that for some of the entries in Table 4, *M* is limited to 900 to avoid a memory overrun problem.

N	SNR = 5dB $\varepsilon = 0.096$		SNR = 10dB $\varepsilon = 0.046$		SNR = 20dB $\varepsilon = 0.041$		SNR = 40 dB $\varepsilon = 0.041$	
	MSE	M	MSE	M	MSE	M	MSE	M
5000	0.1372	425	0.089	242	0.030	235	0.0032	240
10000	0.0094	842	0.065	484	0.021	473	0.0019	503
20000	0.0765	900	0.047	900	0.014	899	0.0016	900

Table 4: FIR locally monotonic simulation results

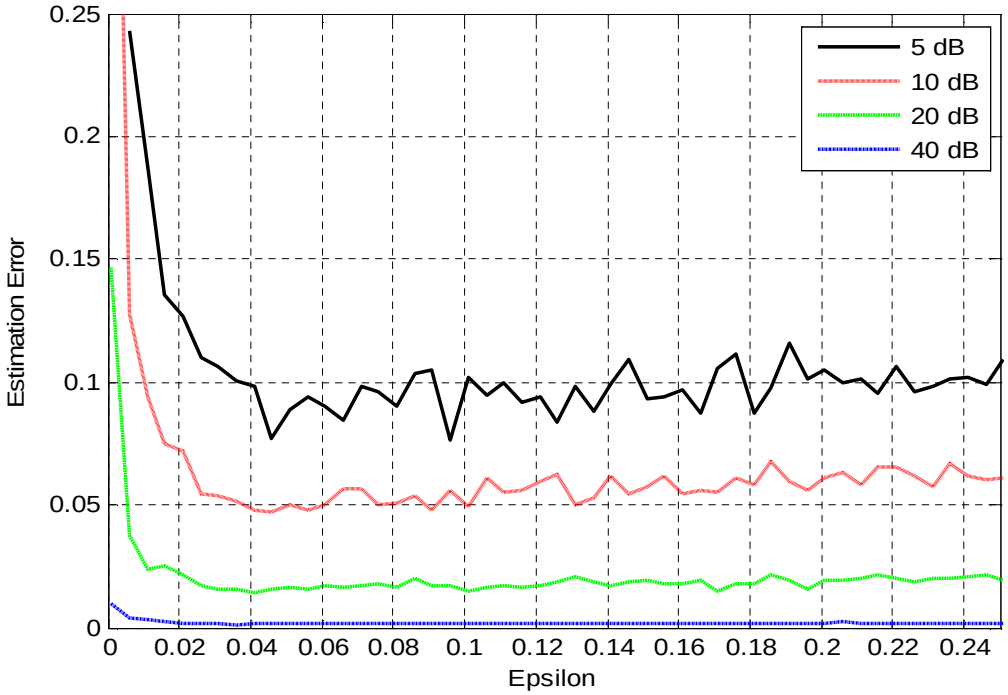

Figure 11: Variation of estimation error with ε, *N*=20000

This algorithm seems to perform better. One explanation is that this algorithm utilizes the data $y \in [-0.5, 0.5]$ and the previous one only uses the data y close to zero. Simply put, more data is allowed for this algorithm than the previous one and thus the effect of noises is averaged out more for a better estimate.

CHAPTER 3
IIR LINEAR PART IDENTIFICATION

This chapter shows how the impulse response of the IIR linear part of a Wiener system may be identified using a carefully defined set of minimal a-priori information on the nonlinear part.

Problem statement

For the IIR case, the Wiener system linear and nonlinear parts are described by

$$\begin{aligned} G(z) &= \sum_{i=0}^{\infty} h(i) z^{-i} \\ y(k) &= f(x(k)), \quad k = 1, 2, \ldots, N \end{aligned} \tag{3.1}$$

respectively. The problem discussed in this chapter is to estimate the unknown transfer function $G(z)$ based on the input $u(k)$ and the output $y(k)$.

The linear part $G(z)$ is assumed to be stable so that $|h(i)| \leq M\lambda^i$ for some $M < \infty$ and $0 < \lambda < 1$. No order information on $G(z)$ is available, unless otherwise specified. The input, internal signal and output at time $k = 0, 1, \ldots, N$ are represented by $u(k)$, $x(k)$ and $y(k)$ respectively. The internal signal $x(k)$ is unavailable for identification. The nonlinearity is unknown but bounded for bounded inputs. No structural a priori information on $f(\cdot)$ is assumed.

Because of embedded scaling ambiguity in Wiener systems, either the linear part or the nonlinear part has to be normalized for identification purpose. It is assumed in this chapter that:

$$\|h\|^2 = \sum_{i=0}^{\infty} h^2(i) = 1 \tag{3.2}$$

Where $h = (h(0), h(1), \ldots)^T$ is an infinite dimensional vector representing the impulse response of the linear part. Further, it is assumed that the first non-zero entry of *h* is positive. All these assumptions are standard to guarantee identifiability. Throughout the paper, it is also assumed that the input $u(k)$ is a bounded independent identically distributed (i.i.d.) random sequence and its probability density function is positive over an interval $[-a, a]$ for some $0 < a < 1$. No specific distribution on the input is needed and the actual distribution could be unknown. Clearly, all the signals $u(k)$, $x(k)$ and $y(k)$ are bounded because of the stability and boundedness of the input.

The goal of identification is to determine an estimate $\hat{G}(z) = \sum_{i=0}^{\infty} \hat{h}(i) z^{-i}$ of $G(z)$, based on the input-output data up to time *N* with little a priori information on the unknown nonlinearity $f(\cdot)$, specified later in subsequent sections, so that:

$$\frac{1}{2\pi} \int_{-\pi}^{\pi} |G(e^{j\omega}) - \hat{G}(e^{j\omega})|^2 \, d\omega \to 0 \tag{3.3}$$

as $N \to \infty$ in some probability sense, preferably convergence with probability one. Note again that no order information on $G(z)$ is available. Now, observe that if the estimate $\hat{G}(z)$ is stable, then:

$$\left\| h - \hat{h} \right\|^2 = \sum_{i=0}^{\infty} \left| h(i) - \hat{h}(i) \right|^2 = \frac{1}{2\pi} \int_{-\pi}^{\pi} \left| G\left(e^{j\omega}\right) - \hat{G}\left(e^{j\omega}\right) \right|^2 d\omega \tag{3.4}$$

where $\hat{h} = (\hat{h}(0), \hat{h}(1), \ldots)^T$ is the impulse response vector of the estimate $\hat{G}(z)$. Thus, the identification problem is equivalent to finding $\hat{h}$ of *h* so that $\hat{h} \to h$. Now, given a positive integer *n*, define:

$$h_n = (h(0), h(1), \ldots, h(n-1))^T$$
$$\hat{h}_n = (\hat{h}(0), \hat{h}(1), \ldots, \hat{h}(n-1))^T \tag{3.5}$$

Because of the stability assumption, $\sum_{i=0}^{\infty} h(i)^2 \to 1$, we have $\sum_{i=n}^{\infty} h(i)^2 \to 0$ as $n \to \infty$.

Thus $\hat{h} \to h$ if and only if $\hat{h}_n \to h_n$ as $n \to \infty$. Further, $\| h_n \| \to 1$ implies:

$$\left\| \hat{h}_n - h_n \right\| = \left\| \hat{h}_n - \frac{h_n}{\|h_n\|} + \frac{h_n}{\|h_n\|} - h_n \right\| \le \left\| \hat{h}_n - \frac{h_n}{\|h_n\|} \right\| + \left\| \frac{h_n}{\|h_n\|} - h_n \right\| \tag{3.6}$$

The second term goes to zero as $n \to \infty$ and therefore, as $n \to \infty$:

$$\left\| \hat{h} - h \right\| \to 0 \Leftrightarrow \left\| \hat{h}_n - h_n \right\| \to 0 \Leftrightarrow \left\| \hat{h}_n - \frac{h_n}{\|h_n\|} \right\| \to 0 \tag{3.7}$$

What we have to do is to identify the normalized first *n* taps of the impulse response of the unknown linear part. In short, to overcome the problem of unknown order, we find the impulse response.

Single point a priori information

In this section we consider identification of the linear part with a priori information $f(x_0) = y_0$ on the unknown nonlinearity for some x_0 and y_0. For simplicity, x_0 and y_0 are assumed to be at the origin.

Assumption 3.1:

$f(x) = 0 \Leftrightarrow x = 0$ *and* $f(\cdot)$ *is continuous in the neighborhood of the origin.*

The condition is based on the local information $f(0) = 0$ however it is stronger than the local point condition $f(0) = 0$. Note that $f(x) = 0 \Rightarrow x = 0$ provides some global information on the nonlinearity since no other values of *x* could lead to $f(x) = 0$.

Because no other a priori information on the unknown $f(\cdot)$ is available, all the observed outputs $y(k) \neq 0$ do not reveal anything about their corresponding inputs $x(k)$ or $f(\cdot)$. In other words, theoretically only the outputs $y(k) = 0$ together with corresponding inputs $u(k)$ are useful for identification. Practically, however, $y(k) = 0$ is unlikely to occur, especially in the presence of noise. A practical identification algorithm is based on the hope that, by the continuity of $f(\cdot)$ in the neighborhood of the origin, all the data $y(k) \approx 0$ imply $x(k) \approx 0$ and these data result in an estimate $\hat{h}_n$ close to $h_n / \|h_n\|$. Thus the analysis contains two parts. The first part is to show that $h_n / \|h_n\|$ can be identified if there are enough data available under the constraint $y(k) = 0$. Then we will show that with the data set $|y(k)| < \varepsilon$ for some small $\varepsilon > 0$, the obtained estimate is a continuous function of ε and converges to $h_n / \|h_n\|$ as $\varepsilon \to 0$.

For each *n*, consider a fictitious FIR system:

$$x(k) = \frac{1}{\|h_n\|}(h(0), h(1), \cdots, h(n-1)) \underbrace{\begin{pmatrix} u(k) \\ u(k-1) \\ \vdots \\ u(k-n+1) \end{pmatrix}}_{\phi_n(k)} \tag{3.8}$$

where $h_n = (h(0), h(1), \cdots, h(n-1))^T \neq 0$ is automatically satisfied for large *n* because $\|h_n\| \to \|h\| = 1$. Given input-output data set $\{\phi_n(k), y(k)\}_1^N$ Chapter Two showed that $h_n / \|h_n\|$ is identifiable for this fictitious FIR linear system based on the point a priori information $f(0) = 0$ if and only if there exist some $1 \leq p_1 < p_2 < \cdots < p_k \leq N$ so that

$x(p_1) = x(p_2) = \cdots = x(p_k) = 0$ (or equivalently $y(p_1) = y(p_2) = \cdots = y(p_k) = 0$ and the corresponding matrix $\phi(p_1, p_1, \ldots, p_k)$ satisfies:

$$\text{rank} \underbrace{\begin{pmatrix} \phi_n^T(p_1) \\ \phi_n^T(p_2) \\ \vdots \\ \phi_n^T(p_k) \end{pmatrix}}_{\Phi(p_1, p_2 \ldots, p_k)} = n - 1. \tag{3.9}$$

This is because $\Phi(p_1, p_1, \ldots, p_k)$ satisfying (3.9) has a one dimensional null space spanned by any scaled versioned of h_n. Chapter Two showed that if:

$$\Phi(p_1, p_1, \ldots, p_k) = U\Sigma(V_1, V_2, \ldots, V_n)^T \tag{3.10}$$

is the singular value decomposition (SVD) of $\Phi(p_1, p_1, \ldots, p_k)$ then it follows that $V_n = h_n / \|h_n\|$ modulus $\pm$ sign. Therefore, $h_n / \|h_n\|$ is identifiable from the SVD of $\Phi(p_1, p_1, \ldots, p_k)$ for data $y(p_1) = y(p_2) = \cdots = y(p_k) = 0$.

Now we are going beyond the FIR identification of Chapter Two and attempting to identify an IIR linear part of a Wiener system. Write the IIR system as

$$x(k) - \sum_{i=n}^{\infty} h(i)u(k-i) = h_n \phi_n(k) \tag{3.11}$$

and also define:

$$z(k) = [x(k) - \sum_{i=n}^{\infty} h(i)u(k-i)] / \| h_n \| = \phi_n(k) \frac{h_n}{\|h_n\|} \tag{3.12}$$

If $z(p_1) = z(p_2) = \cdots = z(p_k) = 0$, the same conclusion discussed above applies. Making use of the fact that, for a stable linear system, large *n*, $\lambda < 1$ and constant *M* results in:

$$\left|\sum_{i=n}^{\infty} h(i)u(k-i)\right| \le M\lambda^n \to 0 \tag{3.13}$$

we conclude that $y(k) \approx 0$ implies $z(k) \approx 0$ and also $x(k) \approx 0$. The question is if the SVD of $\Phi(p_1, p_1, \ldots, p_k)$ will provide a vector V_n that is close to $\frac{h_n}{\|h_n\|}$ when ε (as defined in the previous chapter) is small but not zero. First, some preliminary work.

Given *n*, define the orthonormal basis functions: $e_1, e_2, \ldots, e_{n-1}$ and $e_n = \frac{h_n}{\|h_n\|}$ in $\Re^n$. As shown for $n = 3$ in Figure 8, construct a truncated cone C_i around each e_i for $i = 1, 2, \ldots, n$ as follows. For $i = 1, 2, \ldots, n-1$ we require:

$$\phi \in C_i \Leftrightarrow 0 < \frac{a}{2} \le \|\phi\| \le 1 \tag{3.14}$$

Given $[-a, a]$ for $0 < a < 1$ is the interval over which the input probability density is positive. Now, if $\angle(\phi, e_j)$ is the angle between ϕ and e_j, in addition to (3.14) we define for each $i = 1, 2, \ldots, n-1$:

$$\left|cos(\angle(\phi, e_j))\right| = \begin{cases} \ge \frac{8}{9} & if \quad j = i \\ \le \frac{a}{9(n-2)} & if \quad j \ne i \end{cases} \tag{3.15}$$

For $i = n$ we require:

$$\phi \in C_n \Leftrightarrow 0 < \|\phi\| \le \varepsilon(n) \tag{3.16}$$

$$\left|cos(\angle(\phi, e_j))\right| = \begin{cases} \ge \frac{8}{9} & if \quad j = n \\ \le \frac{a}{9(n-2)} & if \quad j \ne n \end{cases} \tag{3.17}$$

Where $\sqrt{n}\varepsilon(n) \to 0$ as $n \to \infty$. If $\phi \in C_n$ we have:

$$\left|\left\langle \phi, e_i \right\rangle\right| = \|\phi\|\|e_i\| \cdot |\cos(\angle(\phi, e_i))| = \begin{cases} \leq \varepsilon\left(\dfrac{a}{9(n-2)}\right) & i = 1,2,\ldots,n-1 \\ \leq \varepsilon & i = n \end{cases} \tag{3.18}$$

and similarly for $\phi \in C_i$, $i = 1,2,\ldots,n-1$:

$$\left|\left\langle \phi, e_j \right\rangle\right| = \|\phi\|\|e_j\| \cdot |\cos(\angle(\phi, e_j))| = \begin{cases} \geq \left(\dfrac{a}{2}\right)\left(\dfrac{8}{9}\right) = \dfrac{4}{9}a & j = i \\ \leq \dfrac{a}{9(n-2)} & j \neq i \end{cases} \tag{3.19}$$

Note that for (3.15) to (3.19) we need $n > 2$; a practical case for an FIR filter. Recall the definition $\phi_n(i_j) = (u(i_j), u(i_j - 1), ..., u(i_j - n + 1))^T$. Write each $\phi_n(i_j)$ in terms of orthonormal basis functions e_i:

$$\phi_n(i_j) = \beta_{j1}e_1 + \beta_{j2}e_2 + ... + \beta_{jn}e_n \tag{3.20}$$

β_{ij} is the projection of $\phi_n(i_j)$ on e_i. Now, for some $1 \leq i_1 < i_2 < ... < i_n \leq N$, we have :

$$\begin{pmatrix} x(i_1) \\ \vdots \\ x(i_n) \end{pmatrix} = \begin{pmatrix} \phi_n^T(i_1) \\ \vdots \\ \phi_n^T(i_n) \end{pmatrix} h_n + \underbrace{\begin{pmatrix} \sum_{i=n}^{\infty} h(i)u(i_1 - i) \\ \vdots \\ \sum_{i=n}^{\infty} h(i)u(i_n - i) \end{pmatrix}}_{R(i_1,...,i_n)} = \begin{pmatrix} \beta_{1,1} & \cdots & \beta_{1,n} \\ \vdots & \ddots & \vdots \\ \beta_{n,1} & \cdots & \beta_{n,n} \end{pmatrix} \begin{pmatrix} e_1^T \\ \vdots \\ e_n^T \end{pmatrix} h_n + R(i_1,...,i_n)$$

$$= \left\{ \underbrace{\begin{pmatrix} \beta_{1,1} & \cdots & \beta_{1,n-1} \\ \vdots & \ddots & \vdots \\ \beta_{n-1,1} & \cdots & \beta_{n-1,n-1} \\ \beta_{n,1} & \cdots & \beta_{n,n-1} \end{pmatrix} \begin{pmatrix} e_1^T \\ \vdots \\ e_{n-1}^T \end{pmatrix}}_{Q} + \underbrace{\begin{pmatrix} \beta_{1,n} \\ \vdots \\ \beta_{n-1,n} \\ \beta_{n,n} \end{pmatrix} e_n^T}_{E(\varepsilon)} \right\} h_n + R(i_1,...,i_n) \tag{3.21}$$

Lemma 3.1:

Consider the Wiener system under Assumption 3.1. Then we have:

Firstly, for any given large n *and* $\varepsilon(n)$ *satisfying* $\sqrt{n}\varepsilon(n)\to 0$ as $n\to\infty$, *with probability one as* $N\to\infty$, *there exists a sequence of* $\phi_n(i_j)$ *for* $j=1,2,\ldots,n$ *so that* $|y(i_j)|\le\varepsilon$ *and*:

$$rank\ \Phi(i_1,...,i_n)=rank\begin{pmatrix}\phi_n^T(i_1)\\ \phi_n^T(i_2)\\ \vdots\\ \phi_n^T(i_n)\end{pmatrix}\ge n-1$$

Secondly, the matrix $\Phi(i_1,\ldots,i_n)$ *can be written as* $\Phi(i_1,...,i_n)=Q+E(\varepsilon)$ *for some Q and* $E(\varepsilon)$, *where rank* $Q=n-1$ *independent of* ε *and* $\|E(\varepsilon)\|\to 0$ *as* $\varepsilon\to 0$. *Further, let* $\Phi(i_1,..,i_n)=U(\varepsilon)\Sigma(\varepsilon)(V_1(\varepsilon),V_2(\varepsilon),...,V_n(\varepsilon))^T$ *be the SVD of* $\Phi(i_1,\ldots,i_n)$. *Then, modulo* $\pm$ *signs,* $\left\|V_n(\varepsilon)-\frac{h_n}{\|h_n\|}\right\|\to 0$ *as* $n\to\infty$.

Proof:

The proof of the first part is essentially the same as for the FIR case in Chapter Two by noting $\|R(i_1,...,i_n)\|\to 0$ as $n\to\infty$.

To show the second part, consider a submatrix as in (3.21):

$$\begin{pmatrix}\beta_{1,1} & \cdots & \beta_{1,n-1}\\ \vdots & \ddots & \vdots\\ \beta_{n-1,1} & \cdots & \beta_{n-1,n-1}\end{pmatrix} \tag{3.22}$$

By the construction of the cones C_i for $i=1,2,\ldots,n-1$ and the definition of $\phi_n(i_j)$, it follows from (3.19) that for the submatrix of (3.22):

$$|\beta_{ii}|\ge\frac{4}{9}a,\quad |\beta_{ij}|\le\frac{a}{9(n-2)},\quad i\ne j \tag{3.23}$$

This leads to:

$$\left|\beta_{ii}\right| - \frac{1}{2}\left\{ \sum_{j=1,\, j\neq i}^{n-1} \left|\beta_{ji}\right| + \sum_{j=1,\, j\neq i}^{n-1} \left|\beta_{ij}\right| \right\} \geq \frac{4}{9}a - \frac{1}{2}\left(\frac{2(n-2)a}{9(n-2)} \right) = \frac{4}{9}a - \frac{1}{9}a = \frac{3}{9}a \qquad (3.24)$$

By the Gershgorin Theorem [23] on singular values, the right side of (3.24) is also a lower bound on the smallest singular value of (3.22). Thus the singular values of the above submatrix (3.22) satisfy:

$$\sigma_1 \geq \sigma_2 \geq \ldots \geq \sigma_{n-1} \geq \frac{3}{9}a \qquad (3.25)$$

Independent of *n*. Further, by the usual definition of orthonormal basis vectors we have:

$$\begin{pmatrix} e_1^T \\ e_2^T \\ \vdots \\ e_{n-1}^T \end{pmatrix} (e_1, e_2, \ldots, e_{n-1}) = \begin{pmatrix} 1 & 0 & \cdots & 0 \\ 0 & 1 & \cdots & 0 \\ \vdots & \vdots & \ddots & \vdots \\ 0 & 0 & \cdots & 1 \end{pmatrix} \qquad (3.26)$$

To show that rank $Q = n-1$, we write Q as the sum of the submatrix (3.22) and a perturbation:

$$Q = \begin{pmatrix} \beta_{1,1} & \cdots & \beta_{1,n-1} \\ \vdots & \ddots & \vdots \\ \beta_{n-1,1} & \cdots & \beta_{n-1,n-1} \\ 0 & \cdots & 0 \end{pmatrix} \begin{pmatrix} e_1^T \\ \vdots \\ e_{n-1}^T \end{pmatrix} + \begin{pmatrix} 0 & \cdots & 0 \\ \vdots & \ddots & \vdots \\ 0 & \cdots & 0 \\ \beta_{n,1} & \cdots & \beta_{n,n-1} \end{pmatrix} \begin{pmatrix} e_1^T \\ \vdots \\ e_{n-1}^T \end{pmatrix} \qquad (3.27)$$

Taking note of (3.26) and also:

$$\left|\beta_{n,1}\right| \leq \varepsilon, \ldots, \left|\beta_{n,n-1}\right| \leq \varepsilon \qquad (3.28)$$

We have from the Wielandt-Hoffman Theorem [8] for singular values that, for large *n*, the first $n-1$ singular values of *Q* satisfy:

$$\sigma_1 \geq \sigma_2 \geq \cdots \geq \sigma_{n-1} \geq \frac{3}{9}a - O\left(\sqrt{n}\varepsilon\right) \geq \frac{2}{9}a \qquad (3.29)$$

Observe from (3.27) that $Qh_n = 0$ because $h_n \perp e_i$ for $i = 1, 2, \ldots, n-1$. This implies that the last or smallest singular value $\sigma_n = 0$ and rank $Q = n-1$ for all *n*.

In addition, $|\beta_{n,j}| \leq \varepsilon$ implies $\|E(\varepsilon)\| = O(\sqrt{n}\varepsilon) \to 0$ as $n \to \infty$. Now define $Q = U\Sigma(V_1, ..., V_n)^T$ and:

$$Q + E(\varepsilon) = U(\varepsilon)\Sigma(\varepsilon)(V_1(\varepsilon), ..., V_n(\varepsilon))^T \tag{3.30}$$

It is clear that $h_n / \| h_n \| = \pm V_n$ and what is left to show is that $V_n(\varepsilon) \to V_n$ when *n* gets larger. To this end, again by the Wielandt-Hoffman Theorem for singular values [8], the gap between the smallest singular value and the second smallest singular value of the matrix $\Phi = Q + E(\varepsilon)$ is bounded below by:

$$\sigma_{n-1} - \sigma_n = \sigma_{n-1} \geq \frac{2}{9}a - O(\sqrt{n}\varepsilon) \geq \frac{1}{9}a \tag{3.31}$$

Now, we apply a version of the Wielandt-Hoffman Theorem for singular vectors [8]:

$$sin(\angle(V_n(\varepsilon), V_n)) \leq \frac{O(\sqrt{n}\varepsilon)}{(\sigma_{n-1} - \sigma_n) - O(\sqrt{n}\varepsilon)} \leq \frac{O(\sqrt{n}\varepsilon)}{\frac{1}{9}a - O(\sqrt{n}\varepsilon)} \to 0 \tag{3.32}$$

as $n \to \infty$. Since $\|V_n\| = \|V_n(\varepsilon)\| = 1$, the conclusion $V_n(\varepsilon) \to V_n = \frac{h_n}{\|h_n\|}$ follows. This completes the proof.

Theorem 3.1:

Let $\hat{h}_n = (\hat{h}(0), ..., \hat{h}(n-1))' = \pm V_n(\varepsilon)$ *be the estimate of* $\frac{h_n}{\|h_n\|}$ *so that the first non-zero entry is positive and* $\hat{G}(z) = \sum_{i=0}^{n-1} \hat{h}(i) z^{-i}$. *Then, as* $n \to \infty$,

$$\frac{1}{2\pi}\int_{-\pi}^{\pi}\left|G(e^{j\omega})-\hat{G}(e^{j\omega})\right|^2 d\omega \to 0$$

Proof:

Theorem 3.1 is a direct consequence of the above Lemma 3.1.

Based on the results, we can collect the data set $|y(i_1)|\le\varepsilon, |y(i_2)|\le\varepsilon, ..., |y(i_n)|\le\varepsilon$ so that rank $\Phi(i_1,i_2,...,i_n)\ge n-1$. Then, the SVD of $\Phi(i_1,i_2,...,i_n)$ provides the estimate $\hat{h}_n = V_n(\varepsilon)$ modulus $\pm$ sign. A problem is that only data at time index $i_1,i_2,...,i_n$ are used and all other data is discarded. This is not efficient and in fact is not robust in the presence of noise. An efficient way is to use all the data $|y(k)|\le\varepsilon$ and the corresponding matrix Φ. The analysis as discussed before carries over with no or minimal modifications. However at the same time, since more data is used, the average effect of the noise is reduced making the identification algorithm more robust. We are now in a position to introduce the identification algorithm based on point a priori information.

Simulation testing

Consider the system shown in Figure 16 under Assumption 3.1. The following are the steps of a practical identification algorithm with point a priori information $f(0)=0$:

1. Collect data $u(k)$'s and $y(k)$'s, $k=1,2,...,N$.
2. For each *n*, construct a submatrix $\Phi(i_1,i_2,...,i_l)$ of $\Phi(1,2,...,N)$ by deleting *k*'s row if $|y(k)|>\varepsilon$, where $\sqrt{n}\varepsilon\to 0$ as $n\to\infty$.
3. Calculate SVD $\Phi(i_1,...,i_l)=U(\varepsilon)\Sigma(\varepsilon)(V_1(\varepsilon),...,V_n(\varepsilon))^T$.

4. Define $\hat{h}_n = \pm V_n(\varepsilon)$ so that the first non-zero element of $\hat{h}_n$ is positive.

5. Set $\hat{G}(z) = \sum_{i=0}^{n-1} \hat{h}(i) z^{-i}$.

Then, from the lemma and theorem, for each *n*, $\hat{h}_n \to h_n / \| h_n \|$ as $N \to \infty$. Further, as *n* gets larger and larger, $\hat{h}_n \to h$ and $\hat{G}(e^{j\omega}) \to G(e^{j\omega})$ in the integral least squares sense.

We comment that in the algorithm, the choice of ε is not unique. Small ε discards more data and results in fewer data to construct the estimate. Thus, it takes a longer time to collect the same number of data useful to construct the estimate for a small ε than a large ε. On the other hand, however, a large ε collects larger $y(k)$ which results in $x(k)$ that is further from the neighborhood of zero. Clearly, this tends to increase the bias and, at the same time, to reduce the variance because more and more data can be used. So the choice of ε is to balance the bias and variance which is reminiscent of the choice of the bandwidth in kernel identification [13]. The idea is to use local data near $y(k) = 0$ to identify the linear part without interference from the unknown nonlinearity. Of course, preferably, any choice of ε needs to be tested on a fresh data set for validation purpose.

We now provide a numerical simulation. Let the linear part be an 4th order system

$$G(z) = \frac{0.7616z^2 + 0.6160}{z^4 + 0.223z^2 + 0.41} \tag{3.33}$$

and the nonlinear part be a non-continuous, non-symmetric and non-monotonic nonlinearity shown in Figure 6:

$$y = f(x) = \begin{cases} 0.5x - 0.2 & x \le -0.2 \\ 1.2x & -0.2 < x(k) \le 0.8 \\ 0.3x + 0.5 & x > 0.8 \end{cases} \tag{3.34}$$

The input $u(k)$ is i.i.d. uniformly in $[-1,1]$ and Gaussian noise is added to the output. For this IIR case, the estimate is defined as $\hat{h} = (\hat{h}(0),...,\hat{h}(n-1),0,0,\ldots)^T$.

To demonstrate the performance of the identification, the algorithm has been simulated for a number of SNR levels and various choices of thresholds ε and data length *N*. All the results are the averages of 10 Monte Carlo simulations. Table 5 shows the estimation error MSE $= \left\| \hat{h} - h \right\|$ for various ε, *N* and SNR, with *n* =30. Similar to previous simulations, Figure 12 was used to find good settings for ε.

Figure 13 shows the frequency domain match between $\hat{G}(e^{j\omega})$ and $G(e^{j\omega})$ for the case of *N* = 20000, SNR = 20dB and $\varepsilon = 0.066$. Most of the mismatch is in the stop band null. This is due to the error sensitivity of the singularity associated with the null.

N	SNR = 5dB $\varepsilon = 0.071$		SNR = 10dB $\varepsilon = 0.071$		SNR = 20dB $\varepsilon = 0.066$		SNR = 40 dB $\varepsilon = 0.021$	
	MSE	M	MSE	M	MSE	M	MSE	M
5000	0.3278	351	0.1567	410	0.0481	420	0.0153	131
10000	0.2311	704	0.0997	802	0.0307	818	0.0092	264
20000	0.1898	900	0.1048	900	0.0314	900	0.0064	526

Table 5: IIR single point a priori simulation results

Choosing ε based on Figure 12 is an attempt at optimization. Using Figure 14, this is also done in the next section on locally monotonic a priori information. A comparison of Figure 13 and Figure 15 reveals the performance enhancement obtained by the locally montonic technique.

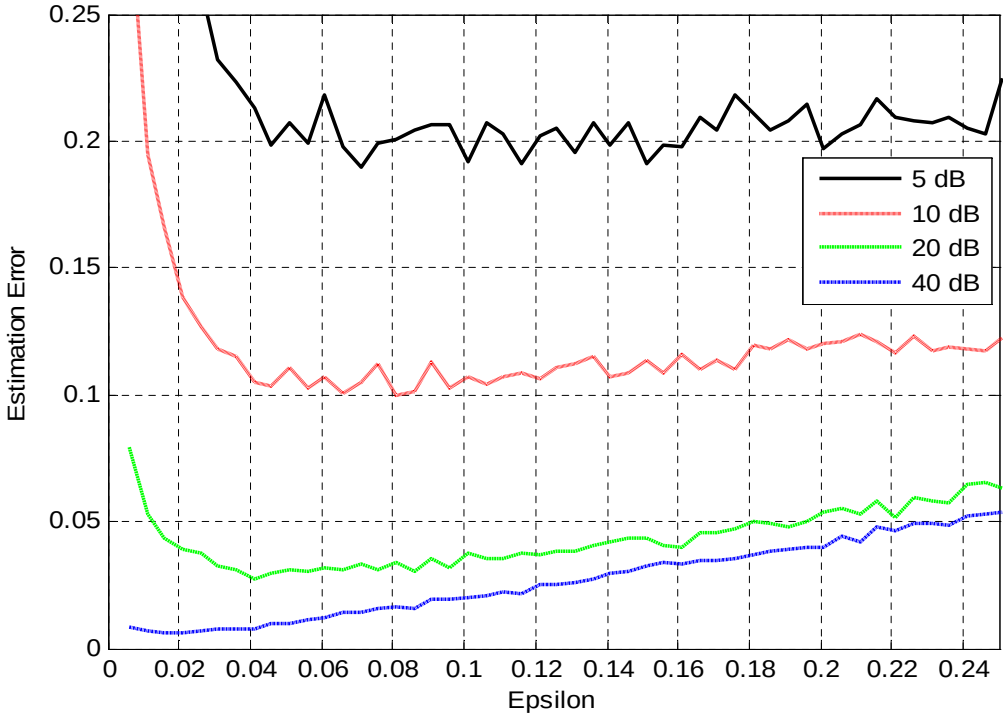

Figure 12: Variation of estimation error with ε, N=20000

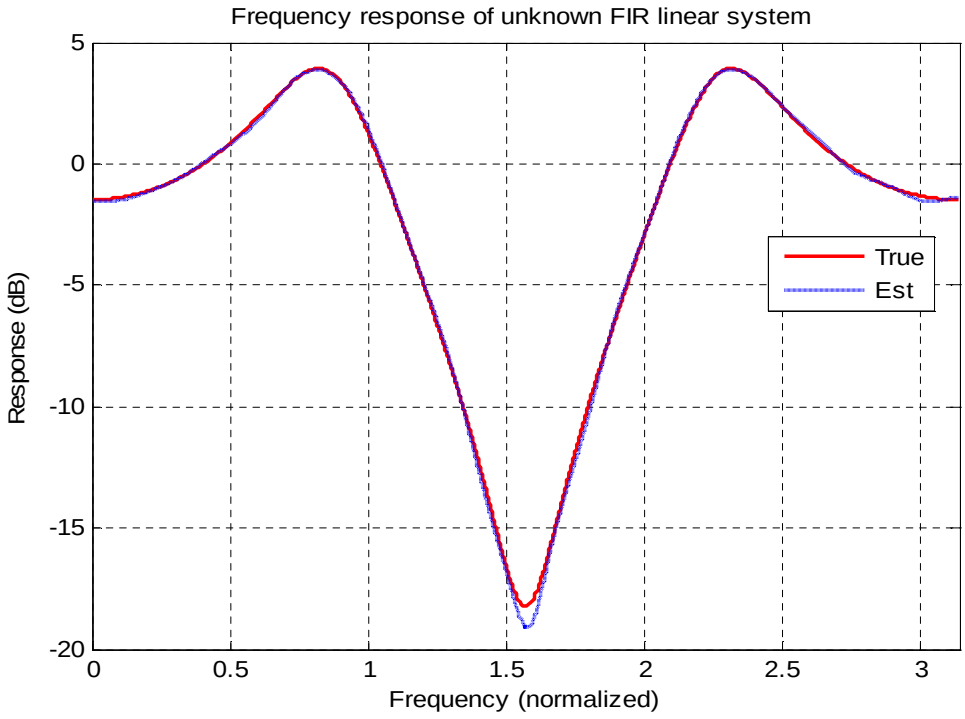

Figure 13: IIR single point simulation result, SNR = 20dB, $\varepsilon = 0.066$

Locally monotonic nonlinearities

The idea of point a priori information is that though there is no other information about the nonlinearity, data in the neighborhood of origin could be used to construct an estimate because the knowledge about the nonlinearity around the origin is known locally. In this section, we extend the idea to a case where no point a priori information is available but the nonlinearity is assumed to be locally monotonic. More precisely, it is assumed that:

Assumption 3.2:

There exists an interval $-\infty < \underline{f} < \overline{f} < \infty$ *and within the interval* $f(x) \in [\underline{f}, \overline{f}]$, $f(\cdot)$ *is continuous and:*

$$f(x_1) = f(x_2) \Leftrightarrow x_1 = x_2 \tag{3.35}$$

Notice that the assumption actually carries some global information on the nonlinearity. Let $f(\underline{x}) = \underline{f}$ and $f(\overline{x}) = \overline{f}$. Then, Assumption 3.2 prevents the nonlinearity from taking any value between $\underline{f}$ and $\overline{f}$ anywhere outside of the range $(\underline{x}, \overline{x})$. Clearly, $f(\cdot)$ is monotonic if $y = f(x) \in [\underline{f}, \overline{f}]$.

Now, define:

$$\begin{aligned} z(i, j) &= x(i) - x(j) \\ \psi_n(i, j) &= \phi_n(i) - \phi_n(j) \end{aligned} \tag{3.36}$$

It is easily verified that:

$$z(i, j) = h_n^T \psi_n(i, j) + \sum_{l=n}^{\infty} h(l)(u(i-l) - u(j-l)) \tag{3.37}$$

This equation is reminiscent of (3.12) and is a key for identification based on point a priori information. Note from the monotonic assumption:

$$y(i)-y(j)=f(x(i))-f(x(j))=0 \Leftrightarrow x(i)=x(j) \Leftrightarrow z(i,j)=0 \tag{3.38}$$

And also:

$$|f(x(i))-f(x(j))| \leq \varepsilon \Leftrightarrow |x(i)-x(j)| \leq \varepsilon_1 \tag{3.39}$$

for small ε_1 thanks to the continuity of *f*, if ε is small enough. Therefore, by identifying $z(i,j)$ as $x(i)$ and $\psi_n(i,j)$ as $\phi_n(i)$, everything developed for point a priori information in the previous section can be carried over here.

Theorem 3.2:

Consider the system shown in Figure 16 under Assumption 3.4. Assume that the probability density function of $y=f(x)$ *is positive in the interval* $[\underline{f}, \overline{f}]$. *Then,*

Firstly, for any n and $\varepsilon>0$ *so that* $\sqrt{n}\varepsilon \to 0$ *as* $n \to \infty$, *with probability one as* $N \to \infty$, *there exist two sequences* $\psi_n(i_l, j_l)=\phi_n(i_l)-\phi_n(j_l)$ *and* $|z(i_l, j_l)|=|y(i_l)-y(j_l)| \leq \varepsilon$ *and:*

$$\text{rank } \Psi(i_1, j_1, \ldots i_n, j_n) = \text{rank} \begin{pmatrix} \phi_n^T(i_1)-\phi_n^T(j_1) \\ \vdots \\ \phi_n^T(i_n)-\phi_n^T(j_n) \end{pmatrix} \geq n-1.$$

Secondly, the matrix $\Psi(i_1, j_1, \ldots i_n, j_n)$ *can be written as* $\Psi(i_1, j_1, \ldots i_n, j_n)=Q+E(\varepsilon)$ *for some* Q *and* $E(\varepsilon)$, *where rank* $Q=n-1$ *independent of n and* $\|E(\varepsilon)\| \to 0$ *as* $n \to 0$. *Further, let the SVD of* Ψ *be* $\Psi(i_1, j_1, \ldots i_n, j_n) .=U(\varepsilon)\Sigma(\varepsilon)(V_1(\varepsilon), V_2(\varepsilon), \ldots, V_n(\varepsilon))^T$. *Then, modulus of* $\pm$ *signs,* $\left\| V_n(\epsilon)-\frac{h_n}{\|h_n\|} \right\| \to 0$ *as* $n \to 0$ *or equivalently* $\frac{1}{2\pi}\int_{-\pi}^{\pi} \left| G(e^{j\omega})-\hat{G}(e^{j\omega}) \right|^2 d\omega \to 0.$

Proof:

Theorem 3.2 is a straightforward extension of Theorem 3.1.

The identification algorithm where the unknown nonlinearity is locally monotonic in $[\underline{f}, \overline{f}]$ is similar to the identification algorithm for single point a priori information.

Simulation testing

Consider the system shown in Figure 16 under Assumption 3.4. The identification algorithm has the following steps:

1. Collect data $u(k)$'s and $y(k)$'s for those $y(k) \in [\underline{f}, \overline{f}]$.
2. Sort out the collected data in a decreasing order: $y(k_1) \geq y(k_2) \geq ... \geq y(k_l)$
3. For each n and ε with $\sqrt{n}\varepsilon \to 0$, construct $z(k_i, k_{i+1}) = y(k_i) - y(k_{i+1})$, $\psi_n(k_i, k_{i+1}) = \phi_n(k_i) - \phi_n(k_{i+1})$. Construct a submatrix $\Psi_n(i_1, j_1, ..., i_l, j_l)$ of Ψ_n by deleting q's row if $|z(q, q+1)| > \varepsilon$.
4. Calculate the SVD $\Psi_n(i_1, j_1, ..., i_l, j_l) = U(\varepsilon)\Sigma(\varepsilon)(V_1(\varepsilon), ..., V_n(\varepsilon))^T$
5. Define $\hat{h}_n = \pm V_n(\varepsilon)$ so that the first non-zero element of $\hat{h}_n$ is positive.
6. Set $\hat{G}(z) = \sum_{i=0}^{n-1} \hat{h}(i) z^{-i}$

We test the algorithm on the same example as in the previous section under the same input but under the assumption that the nonlinearity is monotonic for $|y| \leq 0.7$. As before, all the results are the averages of 10 Monte Carlo simulations. Table 6 shows the estimation error $\text{MSE} = \left\| \hat{h} - h \right\|$ for various N, SNR and ε with $n = 30$. Similar to previous simulations, such as those in Chapter 2 for a priori locally montonic information, Figure 12 was used to find good settings for ε. Finally, Figure 15 shows

the match between $\hat{G}(e^{j\omega})$ and $G(e^{j\omega})$.

This algorithm seems to out perform the one with point a priori information. One explanation is that this algorithm utilizes the data $y \in [-0.7, 0.7]$ and the previous one only uses the data y close to zero.

N	SNR = 5dB $\varepsilon = 0.051$		SNR = 10dB $\varepsilon = 0.041$		SNR = 20dB $\varepsilon = 0.041$		SNR = 40 dB $\varepsilon = 0.036$	
	MSE	M	MSE	M	MSE	M	MSE	M
5000	0.3864	228	0.2074	211	0.0591	244	0.0064	211
10000	0.2678	444	0.1382	437	0.0373	473	0.0043	431
20000	0.1641	899	0.0924	857	0.0291	900	0.0028	853

Table 6: IIR locally monotonic a priori simulation results

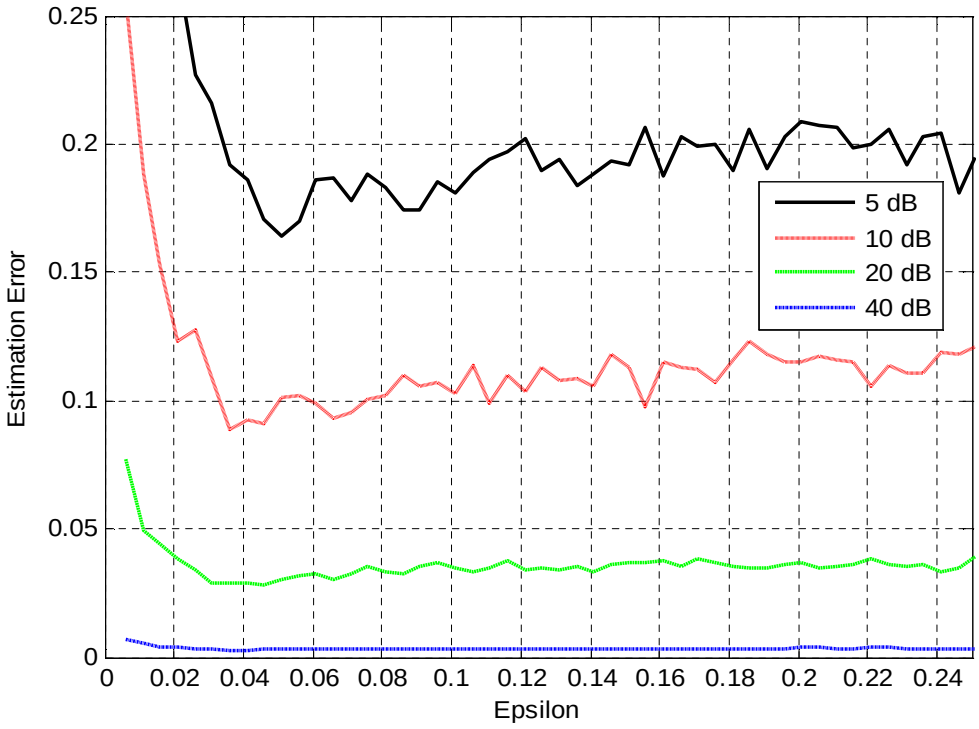

Figure 14: Variation of estimation error with ε, N=20000

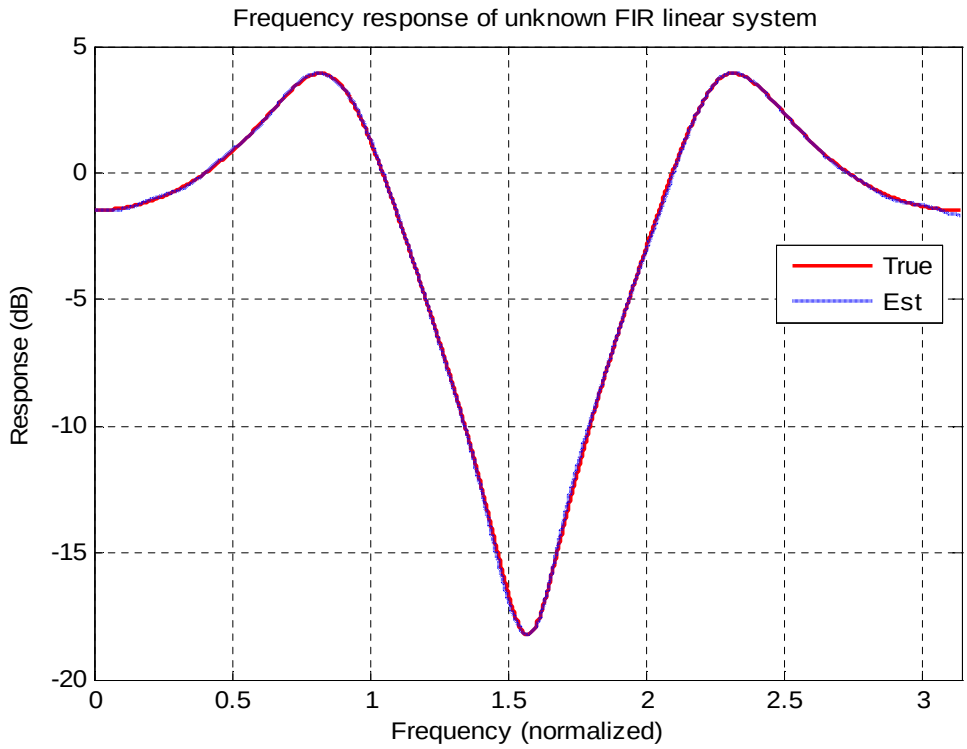

Figure 15: IIR locally monotonic simulation result, SNR = 20dB, $\varepsilon = 0.041$

Quadrant a priori information

This section discusses Wiener system linear IIR identification with quadrant or sign a priori information. Two important assumptions are:

Assumption 3.1:

$$sign(x) = sign(f(x)) = sign(y)$$

Assumption 3.2:

The order m of the linear part is known: $G(z) = \dfrac{\beta_1 z^{m-1} + \beta_2 z^{m-2} + \cdots + \beta_m}{z^m + \alpha_1 z^{m-1} + \cdots + \alpha_m}$

The unknown, $G(z)$, and estimated, $\hat{G}(z)$, linear subsystems are assumed stable

and causal.

The Wiener system output error configuration is shown in Figure 16. The entire system operates on discrete time indexed samples. The top cascade of $G(z)$ and $f\left(x(k)\right)$ is the unknown system to be identified. Only the input $u(k)$ and the output sign difference $e\left(k\right)$ are measurable. All the other signals are unknown but assumed to be bounded. We also require that $v\left(k\right)$ is uncorrelated with $u\left(k\right)$.

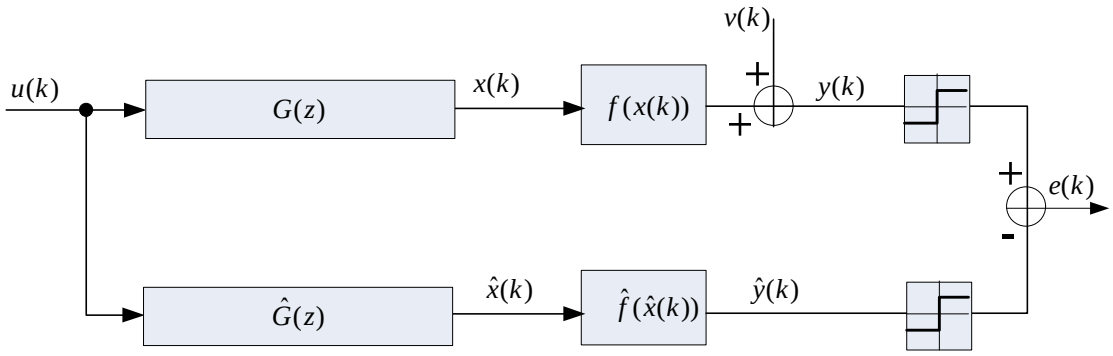

Figure 16: Wiener IIR system identification, quadrant only a priori knowledge

The stability of $G\left(z\right)$ and $\hat{G}(z)$ implies that $x\left(k\right)$ and $\hat{x}(k)$ are uniformly bounded for all k provided that the input is bounded. The corresponding impulse responses are such that, for $a > 0$:

$$x(.) \in \left[-a\sum_{k=1}^{\infty}\left|h(k)\right| \quad a\sum_{k=1}^{\infty}\left|h(k)\right| \right] \tag{3.40}$$

$$\hat{x}(.) \in \left[-a\sum_{k=1}^{\infty}\left|\hat{h}(k)\right| \quad a\sum_{k=1}^{\infty}\left|\hat{h}(k)\right| \right] \tag{3.41}$$

Assumptions on the input $u\left(k\right)$ are exactly the same as for the FIR case. That is,

$u(k)$ is i.d.d. with a distribution continuous over an interval $[-a,a]$ (the symmetry of a is for simplicity and not absolutely necessary).

As shown in Figure 17, the static nonlinearities $f\left(x(k)\right)$ and $\hat{f}(\hat{x}(k))$ are assumed to occupy only quadrants one and three. Quadrants two and four would also work. The idea is that quadrant knowledge gives us the sign of $x(k)$ by observing the sign of $y(k)$. Thus a priori quadrant information about $f\left(x(k)\right)$ and $\hat{f}(\hat{x}(k))$ makes their exact shape irrelevant for this identification technique. Figure 17 shows some acceptable nonlinearities:

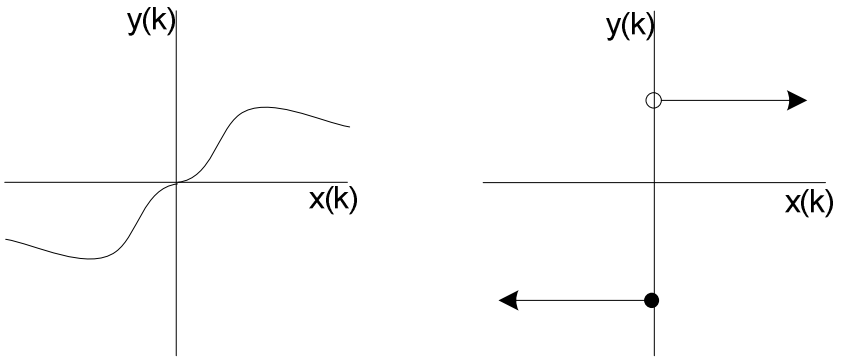

Figure 17: Acceptable nonlinearities for quadrant a priori identification

We define the linear system estimate as the solution to:

$$(\hat{\beta}_1 \cdots \hat{\beta}_m \; \hat{\alpha}_1 \cdots \hat{\alpha}_m) = \arg\min_{Stable\hat{G}(z)} \sum_{k=1}^{N} (sign(y(k)) - sign(\hat{y}(k)))^2 \qquad (3.42)$$

Considering the case where $v(k) = 0$, for any value of N:

$$(\hat{\beta}_1 \cdots \hat{\beta}_m \; \hat{\alpha}_1 \cdots \hat{\alpha}_m) = (\beta_1 \cdots \beta_m \; \alpha_1 \cdots \alpha_m) \Rightarrow \sum_{k=1}^{N} (sign(y(k)) - sign(\hat{y}(k)))^2 = 0 \qquad (3.43)$$

And for at least one value of *N:*

$$(\hat{\beta}_1 \cdots \hat{\beta}_m \; \hat{\alpha}_1 \cdots \hat{\alpha}_m) \neq (\beta_1 \cdots \beta_m \; \alpha_1 \cdots \alpha_m) \Rightarrow \sum_{k=1}^{N} (sign(y(k)) - sign(\hat{y}(k)))^2 \geq 4 \qquad (3.44)$$

Thus, there is one and only one global minimum achieved at the unknown but true *G*(*z*). This implies that solving the minimization gives rise to the transfer function to be identified. The key to proving identifiability is to prove (3.44).

Let $G(z)$ and $\hat{G}(z)$ be represented by their impulses $\{h(k)\}_{k=1}^{\infty}$ and $\{\hat{h}(k)\}_{k=1}^{\infty}$, respectively[2]. Obviously, $G(z) \neq \hat{G}(z)$ or $(\hat{\beta}_1 \cdots \hat{\beta}_n \; \hat{\alpha}_1 \cdots \hat{\alpha}_m) \neq (\beta_1 \cdots \beta_n \; \alpha_1 \cdots \alpha_m)$ if and only if $h(k) \neq \hat{h}(k)$ for some *k*. So what we have to show is that $h(k) \neq \hat{h}(k)$ implies $(sign(x(k)) - sign(\hat{x}(k)))^2 = 4$ for some *k*. Note that for $n > 0$, $x(kn)$ and $\hat{x}(kn)$ can be written as:

$$x(kn) = h_n^T \phi_n(kn) + \sum_{i=n}^{\infty} h(i)u(kn-i) \qquad (3.45)$$

$$\hat{x}(kn) = \hat{h}_n^T \phi_n(kn) + \sum_{i=n}^{\infty} \hat{h}(i)u(kn-i) \qquad (3.46)$$

$$\phi_n(kn) = \begin{bmatrix} u(kn) & u(kn-1) & \cdots & u(kn-n+1) \end{bmatrix}^T \qquad (3.47)$$

$$\begin{aligned} h_n &= \begin{bmatrix} h(0) & h(1) & \cdots & h(n-1) \end{bmatrix}^T \\ \hat{h}_n &= \begin{bmatrix} \hat{h}(0) & \hat{h}(1) & \cdots & \hat{h}(n-1) \end{bmatrix}^T \end{aligned} \qquad (3.48)$$

Thus the linear system output $x(kn)$ is computed every *n* samples as a function of the current block of samples, $\phi_n(kn)$, and the remaining 'tail' of samples

---

[2] Subsequently, $\{h(k)\}_{k=1}^{\infty}$ will be written simply as $\{h(k)\}$ with the understanding that $k \to \infty$ in the IIR linear system impulse response. .

$u(kn-n), u(kn-n-1), \ldots, u(kn-n-\infty)$. Figure 18 shows a set of time indexed samples $\left[u(0)\cdots u(kn)\right]$ with the first n samples of infinite impulse response h convolved with input sample block $\phi_n(kn)$. The samples prior to $\phi_n(kn)$ are convolved with the 'tail' of *h*. For a stable linear system, as $n \to \infty$, the contribution of the 'tail' will be less than the contribution of the initial *n* samples.

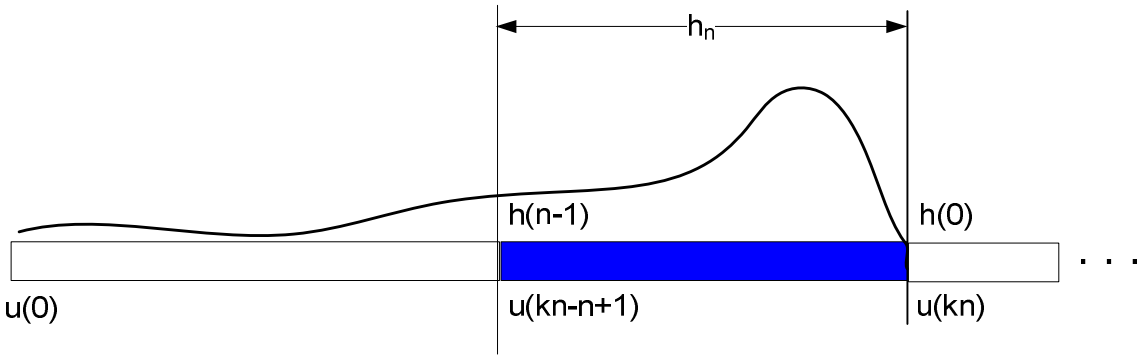

Figure 18: Illustration of block sample processing

Observation 1:

Bocks $\phi_n(kn)$ and $\phi_n(jn)$ are i.i.d. if $j \neq k$. Also, $\phi_n(kn)$ is an *n* dimensional random vector that assumes any direction with a positive probability. Moreover, there is a non-zero probability that $\left\|\phi_n(kn)\right\| \geq a/2$.

Observation 2:

For stable systems $\{h(k)\}$ and $\left\{\hat{h}(k)\right\}$ we require $\sum_{k=1}^{\infty} h(k)^2 = \sum_{k=1}^{\infty} \hat{h}(k)^2 = 1$ Thus for arbitrarily small $\varepsilon > 0$, there is an $n_1 > 0$ such that for all $n > n_1$:

$$1 \geq \sum_{k=0}^{n-1} h(k)^2 \geq 1-\varepsilon \tag{3.49}$$

$$1 \geq \sum_{k=0}^{n-1} \hat{h}(k)^2 \geq 1-\varepsilon \tag{3.50}$$

Observation 3:

For arbitrarily small $\varepsilon > 0$, there is an $n_2 > 0$ such that for all $n \geq n_2$:

$$\left| \sum_{i=n}^{\infty} h(i)u(n-i) \right| \leq \varepsilon \tag{3.51}$$

$$\left| \sum_{i=n}^{\infty} \hat{h}(i)u(n-i) \right| \leq \varepsilon \tag{3.52}$$

We are now in a position to prove identifiability.

Theorem 3.3:

Consider the Wiener system of Figure 16 *under Assumptions 3.1 and 3.2 and the estimate* $\hat{G}(z) = \dfrac{\hat{\beta}_1 z^{m-1} + \hat{\beta}_2 z^{m-2} + \cdots + \hat{\beta}_m}{z^m + \hat{\alpha}_1 z^{m-1} + \cdots + \hat{\alpha}_m}$ *derived from* (3.42). *Then with probability one as* $N \to \infty$: $\sum_{k=1}^{N} (sign(y(k)) - sign(\hat{y}(k)))^2 \geq 4$ *if the coefficient sets are not equal, i.e.* $(\hat{\beta}_1 \cdots \hat{\beta}_n \; \hat{\alpha}_1 \cdots \hat{\alpha}_m) \neq (\beta_1 \cdots \beta_n \; \alpha_1 \cdots \alpha_m)$

Proof:

Proof of the above Theorem is as follows. If for some *k*, $\{h(k)\} \neq \{\hat{h}(k)\}$ then the angle $\theta = \angle(h, \hat{h})$ between the two infinite dimensional vectors h and $\hat{h}$ is greater than zero. There are two cases: $0 < \theta \leq 90^\circ$ and $90^\circ < \theta \leq 180^\circ$. The proofs for the two cases are similar and we only show the first case.

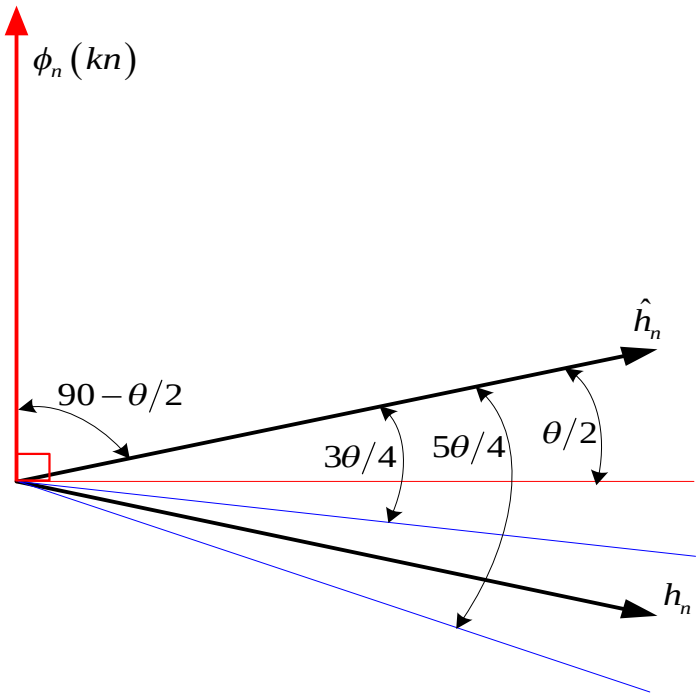

Figure 19: Angles between $h_n, \hat{h}_n, \phi_n(kn)$

Two additional observations are that for $h \neq \hat{h}$ and large enough block size *n*, the impulse response inequality will be manifested in the finite dimensional vector:

$$h \neq \hat{h} \Rightarrow h_n \neq \hat{h}_n \tag{3.53}$$

From the observations, there is a large (possibly unknown) *n* and a small (possibly unknown) $\varepsilon > 0$ such that:

$$\begin{aligned} \|h_n\| > 1-\varepsilon, \quad & \left| \sum_{i=n}^{\infty} h(i)u(kn-i) \right| < \varepsilon \\ \left\|\hat{h}_n\right\| > 1-\varepsilon, \quad & \left| \sum_{i=n}^{\infty} \hat{h}(i)u(kn-i) \right| < \varepsilon \end{aligned} \tag{3.54}$$

Where $\|h\| \to 1$ and $\left\|\hat{h}\right\| \to 1$ as $n \to \infty$. Also if $h_n \to h$ and $\hat{h}_n \to \hat{h}$ as $n \to \infty$ then it follows that at the same time $\angle\left(h_n, \hat{h}_n\right) \to \angle\left(h, \hat{h}\right) = \theta$. Although unknown *h* is fixed, $\hat{h}$

and $\phi_n(kn)$ can exist anywhere in an *n* dimensional vector space. Thus given *h* and $\hat{h}$ there exists a vector $\phi_n(kn)$ as shown in Figure 19 for large enough *n*. We do not know θ exactly because we only have finite vectors h_n and $\hat{h}_n$. However, because we can observe $\phi_n(kn)$ and $\hat{h}_n$, we define $\angle\left(\hat{h}_n, \phi_n(kn)\right) = \left(\frac{\pi}{2} - \frac{\theta}{2}\right)$. Because we cannot observe h_n we make the reasonable assumption that, with some non-zero probability:

$$\left(\frac{\pi}{2} + \frac{\theta}{4}\right) < \angle\left(h_n, \phi_n(kn)\right) < \left(\frac{\pi}{2} + \frac{3\theta}{4}\right) \tag{3.55}$$

Given the preceding assumptions, we can chose $\varepsilon > 0$ such that the two conditions below are meet:

$$0 < \varepsilon < \frac{a}{2}(1-\varepsilon)\left|\sin\frac{\theta}{2}\right| \tag{3.56}$$

$$-\frac{a}{2}(1-\varepsilon)\left|\sin\frac{\theta}{4}\right| < -\varepsilon < 0 \tag{3.57}$$

In (3.56) the right side goes to a positive value and the middle term goes to zero as $\varepsilon \to 0$. In (3.57) the left side goes to a negative value and the middle term goes to zero as $\varepsilon \to 0$ This leads to the following equations:

$$\begin{aligned}
&\varepsilon < \frac{a}{2}(1-\varepsilon)\left|\sin\frac{\theta}{2}\right| \\
&\cos\left(\frac{\pi}{2} - \frac{\theta}{2}\right) > \frac{2\varepsilon}{a(1-\varepsilon)} \\
&\cos\left(\angle\left(\hat{h}_n, \tilde{\phi}_n(kn)\right)\right) > \frac{2\varepsilon}{a(1-\varepsilon)} \\
&(1-\varepsilon)\left(\frac{a}{2}\right)\cos\left(\angle\left(\hat{h}_n, \tilde{\phi}_n(kn)\right)\right) > \left((1-\varepsilon)\left(\frac{a}{2}\right)\right)\left(\frac{2\varepsilon}{a(1-\varepsilon)}\right) = \varepsilon \\
&\hat{h}_n^T \phi_n(kn) > \varepsilon
\end{aligned} \tag{3.58}$$

In addition we have:

$$\begin{aligned}
&-\frac{a}{2}(1-\varepsilon)\left|\sin\frac{\theta}{4}\right| < -\varepsilon \\
&\cos\left(\frac{\pi}{2}+\frac{\theta}{4}\right) < \frac{-2\varepsilon}{a(1-\varepsilon)} \\
&\cos\left(\angle\left(h_n,\phi_n\left(kn\right)\right)\right) < \frac{-2\varepsilon}{a(1-\varepsilon)} \\
&(1-\varepsilon)\left(\frac{a}{2}\right)\cos\left(\angle\left(h_n,\phi_n\left(kn\right)\right)\right) < \left((1-\varepsilon)\left(\frac{a}{2}\right)\right)\left(\frac{-2\varepsilon}{a(1-\varepsilon)}\right) = -\varepsilon \\
&h_n^T\phi_n\left(kn\right) < -\varepsilon
\end{aligned} \tag{3.59}$$

Now from (3.54) we have:

$$\begin{aligned}
-\varepsilon \le \sum_{i=n}^{\infty} h\left(i\right)u\left(kn-i\right) \le \varepsilon \\
-\varepsilon \le \sum_{i=n}^{\infty} \hat{h}\left(i\right)u\left(kn-i\right) \le \varepsilon
\end{aligned} \tag{3.60}$$

Consider again:

$$\begin{aligned}
x(kn) &= h_n^T\phi_n\left(kn\right) + \sum_{i=n}^{\infty} h(i)u(kn-i) \\
\hat{x}(kn) &= \hat{h}_n^T\phi_n\left(kn\right) + \sum_{i=n}^{\infty} \hat{h}(i)u(kn-i)
\end{aligned} \tag{3.61}$$

Since we showed the non-zero probability of $h_n^T\phi_n\left(kn\right) < -\varepsilon$ and $\hat{h}_n^T\phi_n\left(kn\right) > \varepsilon$, it is easy to see from the above and Figure 20 that $x(kn) < 0$ and $\hat{x}(kn) > 0$. Equivalently:

$$\begin{aligned}
&(sign(x(kn)) - sign(\hat{x}(kn)))^2 = 4 \\
&\Rightarrow (sign(y(kn)) - sign(\hat{y}(kn)))^2 = 4
\end{aligned} \tag{3.62}$$

By a continuity argument, any vector close enough to $\phi_n\left(kn\right)$ will result in the same conclusion as (3.62).

Now, from the observations above, the random vectors $\phi_n\left(kn\right)$ are i.i.d. with a

non-zero probability that $\|\phi_n(kn)\| \geq \frac{a}{2}$. They assume any direction with a non-zero probability. Therefore, for each *k*, there is a positive probability that $\phi_n(kn)$ produces (3.62). More precisely, for each *k*, there is probability *p*>0 that $(sign(y(k) - sign(\hat{y}(k)))^2 = 4$ if $(\hat{\beta}_1 \cdots \hat{\beta}_n \; \hat{\alpha}_1 \cdots \hat{\alpha}_n) \neq (\beta_1 \cdots \beta_n \; \alpha_1 \cdots \alpha_n)$. From the Borel lemma, $\sum_{i=1}^{\infty}(1-p)^i < \infty$, we conclude with probability one as $N \to \infty$ there is a *k* such that $(sign(y(k_{j+1})) - sign(\hat{y}(k_{j+1})))^2 = 4$. This completes the identifiability proof.

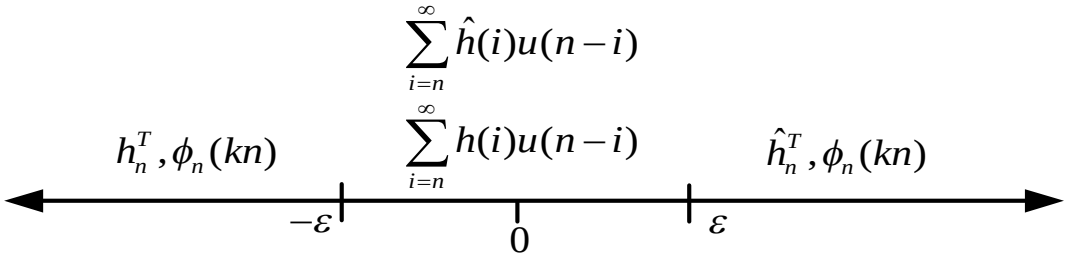

Figure 20: Number line view of IIR identifiability proof

The result presented above is actually weaker than its counterpart for the FIR case in Chapter 2. For FIR identification not only does the minimization have one and only one global minimum but also there are no other local minima. In other words, the objective function is a monotonic function of the angle between the estimate and the true but unknown impulse response.

Simulation testing

Given the system in Figure 16 with the assumptions discussed, the identifiability proof in the previous section tells us that there is only one global minimum at

$(\hat{\beta}_1 \cdots \hat{\beta}_n \; \hat{\alpha}_1 \cdots \hat{\alpha}_m) = (\beta_1 \cdots \beta_n \; \alpha_1 \cdots \alpha_m)$. For large enough block size *n*, any other setting of the estimated parameters results in a non-zero error. Of course proving identifiability is not the same as proving that the cost function used for identification varies monotonically with some measure of the distance between $(\hat{\beta}_1 \cdots \hat{\beta}_n \; \hat{\alpha}_1 \cdots \hat{\alpha}_m)$ and $(\beta_1 \cdots \beta_n \; \alpha_1 \cdots \alpha_m)$. The relationship between impulse response and the transfer function coefficients is highly nonlinear and complicated, even for the simplest one pole filter. Simulation is used to demonstrate (but not prove) that an algorithm can be built around the sign difference cost function.

A system identification experiment for IIR quadrant a priori information was set up using the circuit of Figure 16 combined with the same quadratic cost function used in the quadrant a priori information FIR case, i.e. (2.9). The nonlinearity was also the same as in the FIR case, see Figure 6. The IIR linear system was a notch filter with coefficient values from Table 7.

$$G(z) = \frac{\beta_0 + \beta_1 z^{-1} + \beta_2 z^{-2}}{1 + \alpha_1 z^{-1} + \alpha_2 z^{-2} + \alpha_3 z^{-3} + \alpha_4 z^{-4}} \tag{3.63}$$

The frequency response is shown in the third subplot of Figure 24 and the lattice structure used for implementation is depicted in Figure 21. Although there are several filter structures that could be used for simulation, the IIR lattice was chosen because the reflection coefficient solution is always a point in a hyper-cube with edges in the range $(-1, 1)$. Thus, as the algorithm searches, selected impulse response hypothesis can be easily checked for stability. This is an important feature for an algorithm searching for an IIR system function. Continuous stability checking of direct form coefficients is far more complicated.

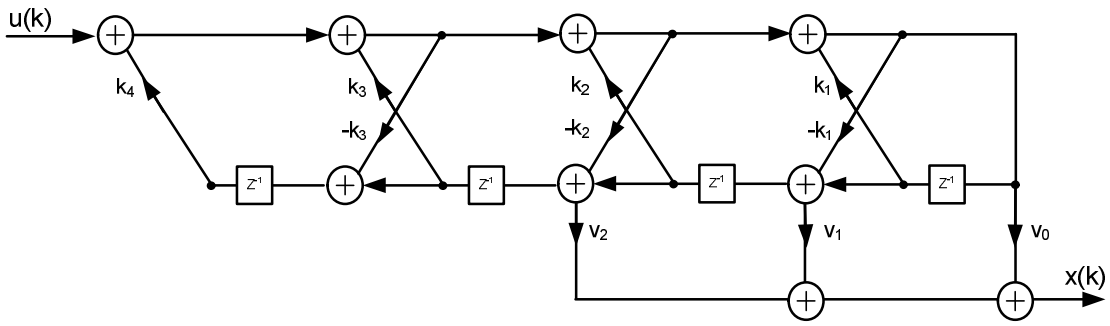

Figure 21: Lattice implementation of IIR notch filter

Direct Form Coefficients				Lattice Coefficients			
Numerator		Denominator		Ladder		Reflection	
β_0	6.800e-1	α_0	1.0	v_0	5.5757e-001		
β_1	-7.495e-17	α_1	0	v_1	-7.495e-17	k_1	-3.269e-17
β_2	5.508e-1	α_2	2.223e-1	v_2	5.508e-1	k_2	1.577e-1
		α_3	-5.551e-17			k_3	6.670e-17
		α_4	4.096e-1			k_4	4.096e-1

Table 7: Simulation example, direct form and lattice coefficients

As described in [21], there is a direct correspondence between direct form coefficients and lattice coefficients. After the minimum average mean squared error is reached, the lattice filter coefficients can be easily translated back into direct form coefficients.

The search procedure makes use of a similar genetic algorithm (GA) as was used for quadrant a priori information simulation in Chapter 2. The GA is a carefully organized zero-order iterative numerical search technique based on "Survival of the fittest".

The GA used here has an initial population of M estimates, $(\hat{\beta}_1 \cdots \hat{\beta}_n \; \hat{\alpha}_1 \cdots \hat{\alpha}_m)$.

These are represented by an equivalent set of M lattice filter coefficients sets $(\hat{v}_1 \cdots \hat{v}_n \ \hat{k}_1 \cdots \hat{k}_m)$, called parents in GA parlance. As shown in Figure 22, the initial population of M parents is chosen from the best of an oversized initial population of $M*r$ parents. The stability required by (3.42) was easy to impose by limiting the magnitude of the reflection coefficients to ± 1.

Some typical GA operating parameters are shown in Table 8. Publications, such as [12] contain guidance on how to use the GA. This, as well as some 'tweaking' was followed to choose the parameters in Table 8

Parameter:	Value used	Description:
M	64	Number of parents
M_{kk}	28	Number of high fitness parents
m	varies	Number of coefficients per parent
r	100	Initial population over sizing factor
N	48000	Number of samples per block
Gain	0.9 to1.0	New parent = best parent + Gain*(Difference between randomly chosen low fitness parents)
M_{ap}	0.4	High fitness reflection coefficients, Prob(mating)
M_{up}	0.4	Low fitness reflection coefficients, Prob(mating)

Table 8: Some GA parameters used for simulation

The simulation results using the GA for system identification and the parameters from Table 8 are summarized in Table 9 below. The run time was 6 minutes in all cases.

N	SNR = 5 dB MSE	SNR = 10 dB MSE	SNR = 20 dB MSE	SNR = 40 dB MSE
5000	0.152	0.101	0.046	0.012
10000	0.092	0.077	0.032	0.0079
20000	0.092	0.042	0.026	0.0086

Table 9: IIR quadrant a priori simulation results

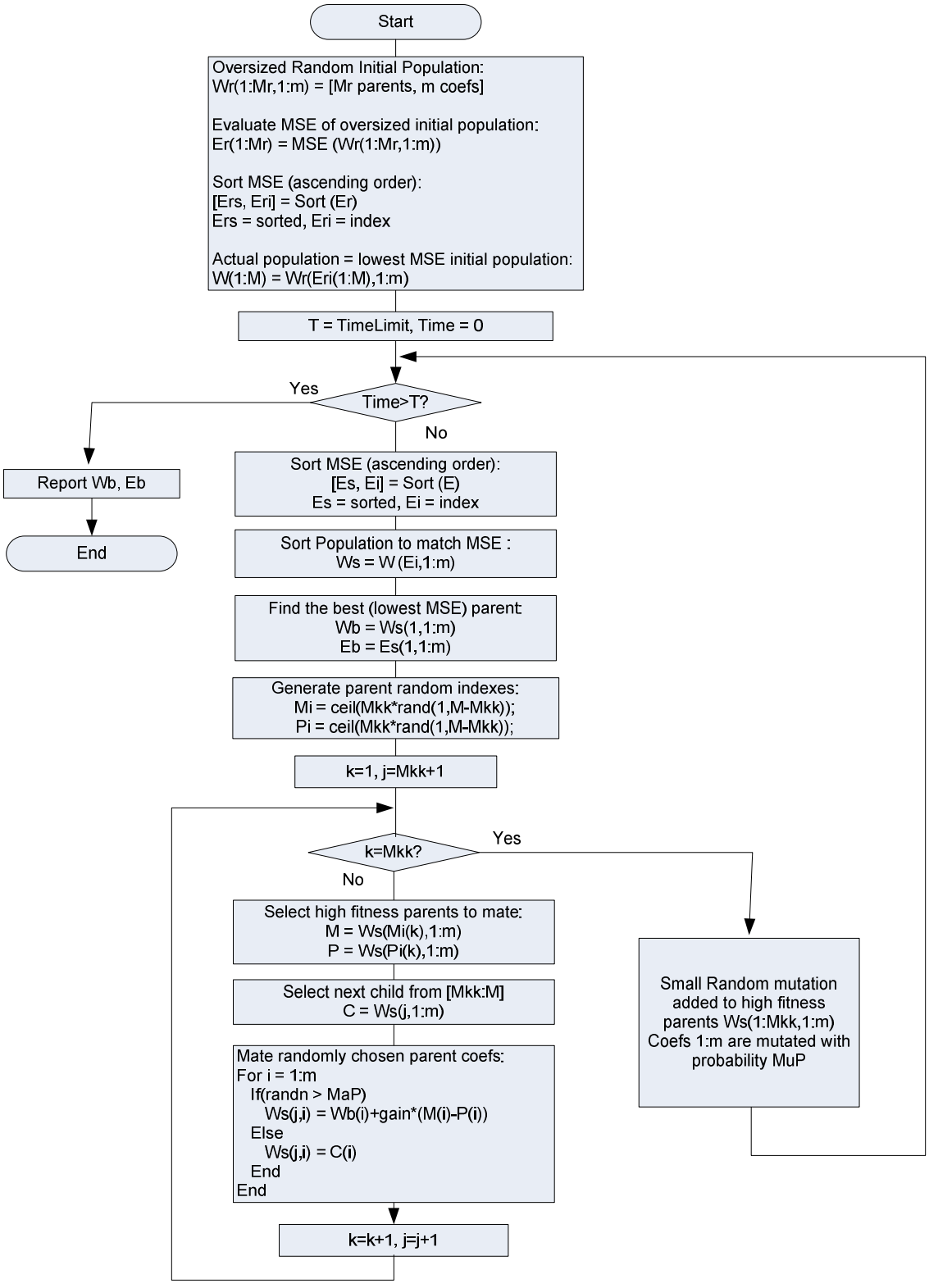

Figure 22: Flowchart of Genetic Algorithm used for simulation

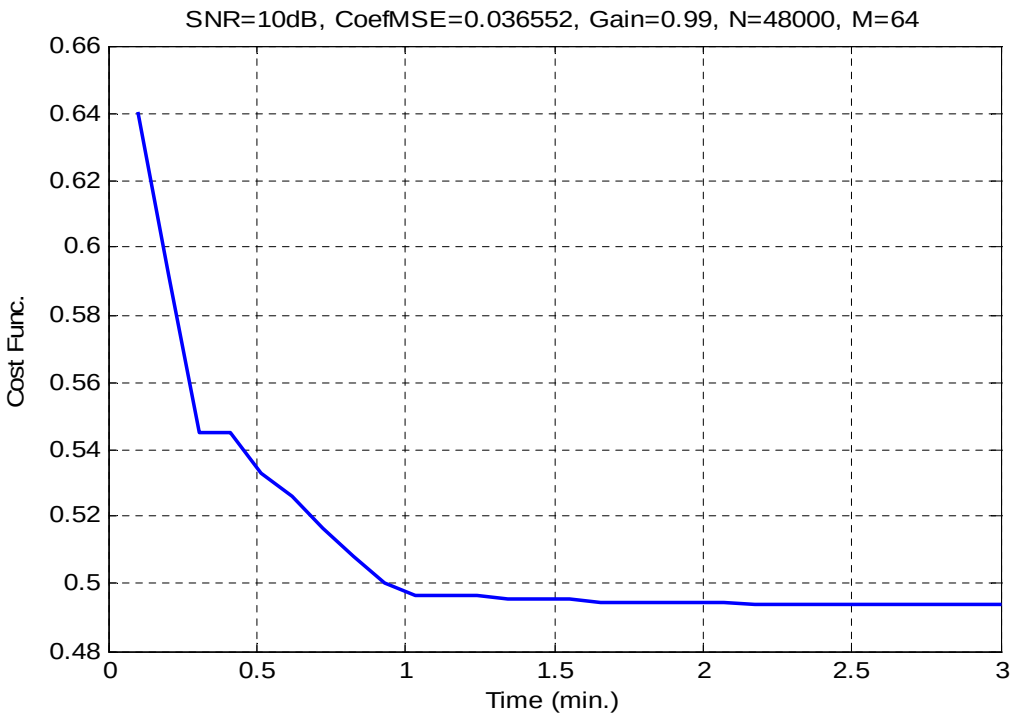

Figure 23: Genetic algorithm cost function reduction vs. time

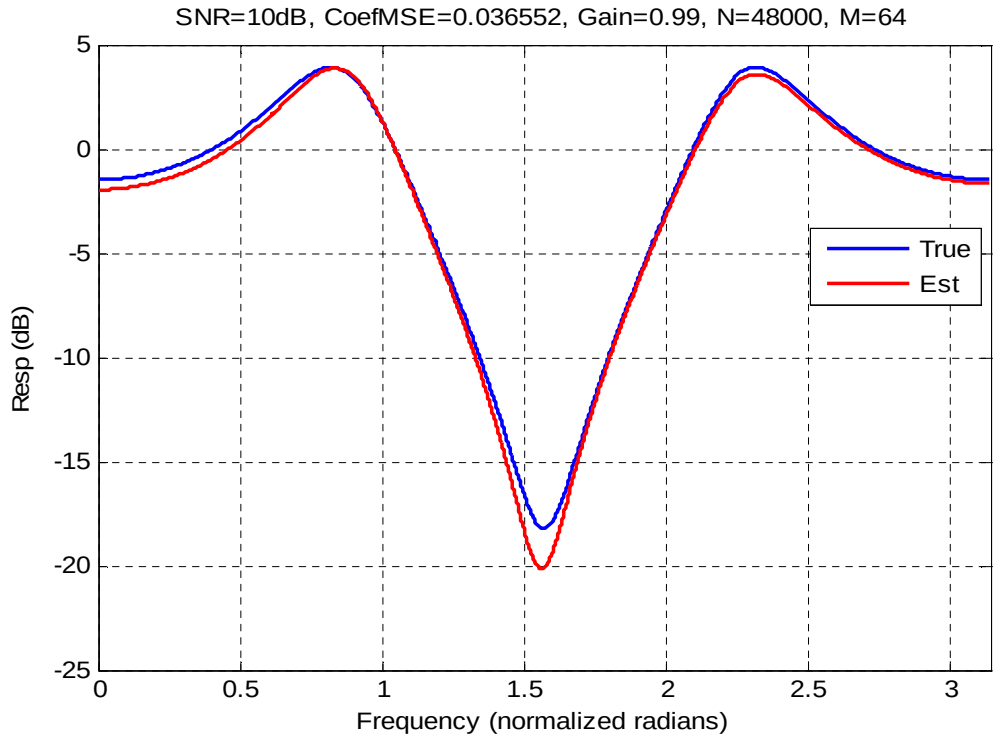

Figure 24: IIR quadrant a priori information simulation results, SNR = 10dB

Although at 100dB SNR the GA gets very close to the exact answer, as the SNR decreases, the noise puts a ‘floor’ on the cost function minimum because the decisions made by the search process are always corrupted by noise and therefore less reliable. Figure 24 is an example of a simulation results graph for SNR = 10dB. From the center subplot in Figure 24, note how the transfer function zero at half the sampling frequency is not as close to the true value as are the two poles. This is because singularities near the unit circle are more sensitive to coefficient estimation errors. The effect on the stop band is clearly evident in the third subplot. In this case, a frequency response plot reveals a lot more than simply listing the mean squared coefficient error. Finally, notice in the top subplot of Figure 24 that most of the GA estimation work is done within 2 minutes. The refinement produced by a long run time may not be needed in a practical situation.

CHAPTER 4
FIR LINEAR PART IDENTIFICATION WITH BACKLASH

This chapter shows how the impulse response of the FIR part of a Wiener system with a backlash nonlinearity may be identified using a carefully defined set of minimal a-priori information on the nonlinear part. Backlash is called a memory nonlinearity because the output depends on the difference between current and previous inputs. Backlash is very similar to valve stiction, discussed in [31]. In general, nonlinear ascending and descending functions result because the output responds differently when the direction of the input changes.

The identification approach of Chapter 1 was to observe the sign of unknown intermediate signal $x(k)$ by processing output $y(k)$ through sign function (2.2). This chapter applies the technique of Chapter 1 to the identification of the FIR coefficients of a Wiener system with a more complicated output nonlinearity.

Several papers have offered identification techniques for Hammerstein systems with backlash nonlinearities. A Hammerstein system has the nonlinearity preceding the linear block, i.e. the blocks are swapped relative to the Wiener system. Both [9] and [10], written by the same authors, require a carefully contrived input signal for identification of input backlash. Although [9] does not require any a priori knowledge of nonlinearity points or structure, [10] requires the nonlinearity to have straight line borders. By contrast, in [6] and [7] the input signal is only required to persistently excite (see [20], page 412) the linear block. However, [6] requires backlash and hysteresis nonlinearities to be described by only one parameter. To accomplish the one parameter description, the nonlinear characteristics are limited to straight lines with slopes of zero, one or infinity.

In [28] the input backlash nonlinearity of a Hammerstien system is described by a four parameter model: $\begin{bmatrix} m_a & m_d & c_a & c_d \end{bmatrix}$. Here c_a and m_a are the ascending function X-axis intersection and slope, respectively. Parameters c_d and m_d are the descending function X-axis intersection and slope, respectively. This description would apply to Figure 25 if $f_a(x)$ and $f_d(x)$ are straight lines. The linear filter numerator and denominator parameters (see (3.1)) are concatenated to produce a parameter vector for the complete system:

$$\Theta = \begin{bmatrix} m_a & m_d & c_a & c_d & \alpha_1 & \cdots & \alpha_m & \beta_1 & \cdots & \beta_n \end{bmatrix} \tag{4.1}$$

The recursive least mean squares algorithm (RLS) is used to compute an estimate for Θ:

$$\hat{\Theta} = \arg\min_{\Theta} \sum_{k=1}^{N} \left(y(k) - \phi^T(k)\Theta \right) \tag{4.2}$$

At each estimation step, data vector $\phi^T(k)$ is updated with the best estimate of intermediate signal $x(k)$. The authors of [11] applied the techniques of [28] to a Wiener system with a four parameter output backlash function. They also added a convergence analysis. An advantage to the approaches of both [11] and [28] is that, unlike [4] and [5], a very general input distribution is used for identification.

One additional paper that analyzes a Wiener system with backlash is [9]. The author starts with the same four parameter description as [28]. In [9], a bounded parameter approach is taken to identify the linear block parameters. A two step procedure is used. The first step uses a multiamplitude square wave input sequence to bound the parameters of the output backlash. The second step uses a pseudo-random binary sequence (PRBS) to estimate bounds on the intermediate signal.

To the author's knowledge, this chapter is the first algorithm for identifying an

output backlash Wiener system by observing only the output polarity. The technique presented in this chapter extends the quadrant a priori information results of Chapter One to the Wiener system with backlash.

Problem statement

In this chapter, the linear system in Chapter 2, Figure 1 is described by:

$$x(k) = \underbrace{[u(k), u(k-1), ..., u(k-n+1)]}_{\phi^T(k)} h, \quad k = 1, 2, ...N \tag{4.3}$$

Note that the length n only needs to be an upper bound if the exact FIR length is unknown. The input $u(k)$ is an independent and identically distributed (i.i.d.) Gaussian random sequence. Parameter vector $h \in \Re^n$ is to be identified. As in Chapter 2 and Chapter 3, the first non-zero element of h is positive and $\|h\| = 1$. The internal variable $x(k)$ is assumed unknown and both $x(k)$ and $y(k)$ are assumed bounded for all k.

We say that the parameter vector h is identifiable from the input-output data set $\{\phi(k), y(k)\}_{k=1}^{N}$ if h can be uniquely identified from the Wiener system model and the data set, independent of the unknown nonlinearity $f(.)$. Equivalently, there does not exist a different pair $(\bar{h}, \bar{f})$ that would produce an identical input-output data set $\{\phi(k), y(k)\}_{k=1}^{N}$ In this chapter we prove identifiability given a set of minimal a priori information on the unknown $f(.)$. A further question is algorithm convergence. In other words, can a cost function be constructed that is monotonic with some measure of the distance between the true and the estimated FIR coefficients? This is discussed in detail but not proven.

An example of a backlash function is shown in Figure 25. Backlash is called a memory nonlinearity because the output characteristic is different for ascending or

descending inputs; the output depends on the current and previous inputs. Backlash is commonly used to describe the transfer of motion across gears. While the driving gear switches direction, the driven gear has a period of non-motion until the driving gear reengages it. Backlash is unavoidable in mechanical systems that must change direction.

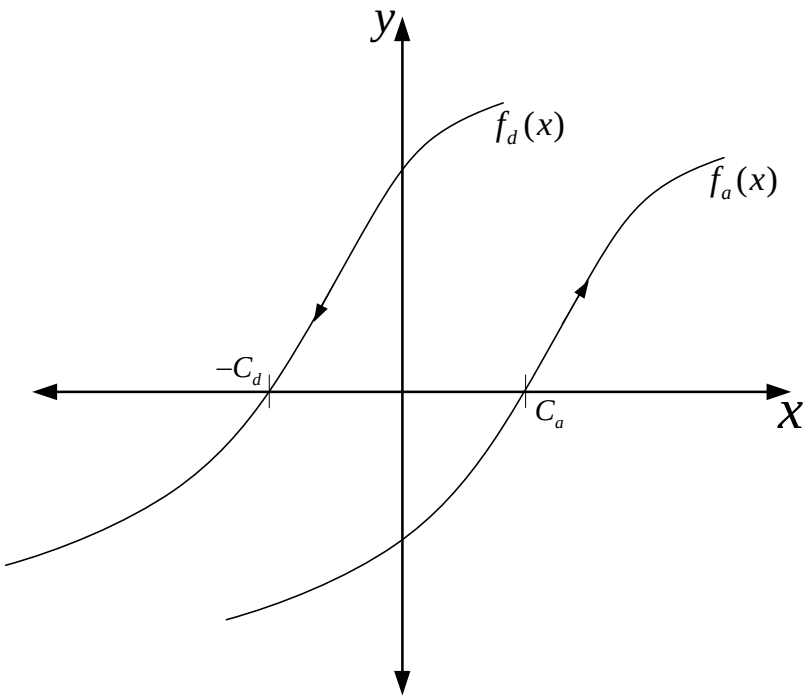

Figure 25: Backlash nonlinearity example

With reference to Figure 25, backlash is based on ascending and descending function $f_a\left(x(k)\right)$ and $f_d\left(x(k)\right)$, respectively. These are unknown and can be different. For $k = 1, 2, \ldots N$ and random input $x(0)$, backlash can be expressed as:

$$y(k) = \begin{cases} f_a(x(k)) & if \quad x(k) > f_a^{-1}(y(k-1)) \\ y(k-1) & if \quad f_d^{-1}(y(k-1)) \le x(k) \le f_a^{-1}(y(k-1)) \\ f_d(x(k)) & if \quad x(k) < f_d^{-1}(y(k-1)) \end{cases} \tag{4.4}$$

We start with the following set of minimum a-priori information:

Assumption 4.1:

1. *The ascending and descending functions are monotonic and have no points in common (i.e. they do not cross over each other).*
2. *The X-axis intersection points C_a and C_d are known.*

For ease of presentation and without loss of generality, we set $C_a = C_d = C > 0$.

Identification approach

Consider the Wiener system inside the dotted box at the top of Figure 26. The nonlinearity $f\left(x(k)\right)$ is the backlash function in Figure 25. Because the output can only increase on the ascending function, $sign(y_d(k)) = sign\left(y(k) - y(k-1)\right) = 1$ indicates an output on the ascending function. Similarly, because the output can only decrease on the descending function, $sign(y_d(k)) = sign\left(y(k) - y(k-1)\right) = -1$ indicates a descending function output:

$$\begin{array}{lllll} sign(y_d(k)) = 1 & \Rightarrow & y_d(k) > 0 & \Rightarrow & y(k) = f_a(x(k)) \\ sign(y_d(k)) = 0 & \Rightarrow & y_d(k) = 0 & & \\ sign(y_d(k)) = -1 & \Rightarrow & y_d(k) < 0 & \Rightarrow & y(k) = f_d(x(k)) \end{array} \tag{4.5}$$

From Figure 26 consider output $y(k)$ and unknown intermediate signal $x(k) = \phi^T(k)h$. For this description, consider that noise $v(k) = 0$ The basis of the identification algorithm is that, for an ascending function output, $sign\left(y(k)\right) = sign\left(x(k) - C\right)$ and for a descending function output $sign\left(y(k)\right) = sign\left(x(k) + C\right)$. Now consider the estimated intermediate signal $\hat{x}(k) = \phi^T(k)\hat{h}$, where $\hat{h}$ is an estimate of h. If $\hat{h} = h$ then, because the FIR linear parts

have the same input, $\hat{x}(k) = x(k)$. In this case for an ascending function output, $sign\big(y(k)\big) = sign\big(\hat{x}(k) - C\big)$ and, for a descending function output, $sign\big(y(k)\big) = sign\big(\hat{x}(k) + C\big)$. Using output $y_d(k)$ from Figure 26 we can detect when $\hat{h} \neq h$ by the following error signal:

$$e(k) = \begin{cases} sign\big(y(k) + v(k)\big) - sign\big(\phi^T(k)\hat{h} - C\big) & y_d(k) > 0 \\ 0 & y_d(k) = 0 \\ sign\big(y(k) + v(k)\big) - sign\big(\phi^T(k)\hat{h} + C\big) & y_d(k) < 0 \end{cases} \tag{4.6}$$

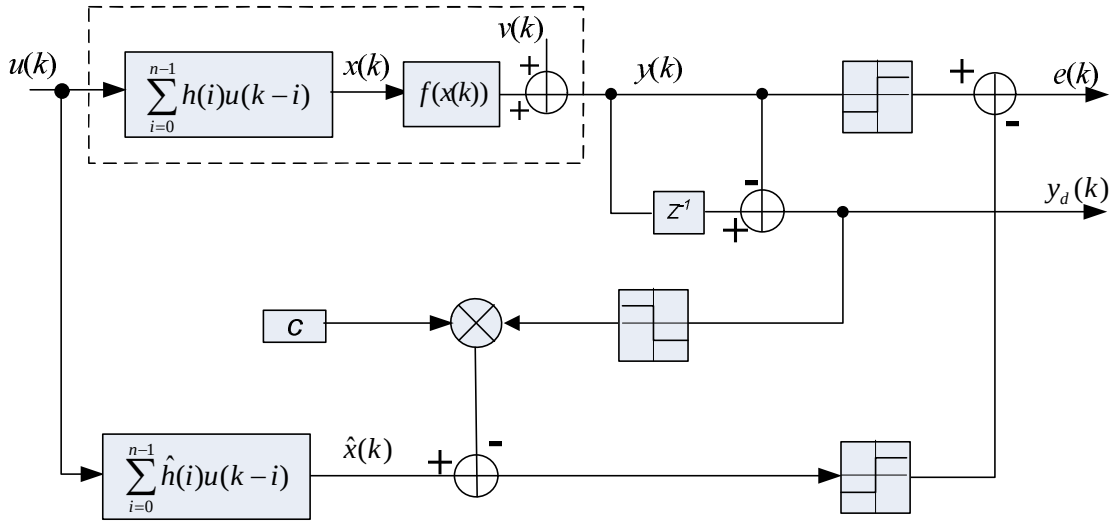

Figure 26: Wiener system identification with backlash

Our goal in this chapter is to show that, for an ascending function output, $sign\big(y(k)\big)$ is equal to $sign\big(x(k) - C\big)$ = $sign\big(\hat{x}(k) - C\big)$ for all k if and only if $\hat{h} = h$ and, for a descending function output, $sign\big(y(k)\big)$ is equal to $sign\big(x(k) + C\big)$ = $sign\big(\hat{x}(k) + C\big)$ for all k if and only if $\hat{h} = h$. Thus the error $e(k)$ is zero for

$k = 1, 2, \ldots N$ if and only if $\hat{h} = h$. A cost function based on these sign differences is referred to throughout the chapter:

$$J_N = \frac{1}{N} \sum_{k=1}^{N} \left(e(k)^2 \right) \tag{4.7}$$

The first question is obviously the identifiability, that is are the above equations based on signs sufficient to determine the unknown *h*? A further question is convergence; is a cost function based on the mean squared error $e(k)^2$ monotonically increasing with $\theta = \angle\left(h, \hat{h}\right)$? The following analysis proves identifiability and discusses convergence in detail. We focus on the ascending function, a similar analysis applies to the descending function.

Identifiability analysis

In addition to Assumption 4.1 we have:

Assumption 4.2:

Random input $u(k)$ *is i.i.d., Gaussian and zero mean.*

A Gaussian input distribution is sufficient for identifiability.

If the output nonlinearity were static, as in Chapters 2 and 3, then with a Gaussian input the results of [7] would apply and there would be nothing new to present. However the Bussgang theorem does not apply to the backlash memory nonlinearity because there is no simple way to calculate the proportionality constant. Although some input distribution generality is lost, we gain the ability to handle a much more complicated output nonlinearity.

Referring to Figure 27 and defining $\theta = \angle\left(h, \hat{h}\right)$, the following development is

easy to see:

$$\begin{aligned} 2\pi &= \theta + \pi + \angle SPW \\ \angle SPW &= \pi - \theta \\ \pi &= \angle SPW + \angle SPZ = \pi - \theta + \angle SPZ \\ \angle SPZ &= \theta \end{aligned} \tag{4.8}$$

And due to vertical angles, $\angle UPW = \angle SPZ = \theta$. Therefore, $\theta > 0 \Leftrightarrow \angle UPW = \angle SPZ > 0$. This will be important to the development below.

Theorem 4.1:

Consider the two dimensional system of Figure 1 under Assumptions 4.1 and 4.2. For any unit vector $\hat{h} = h$, with probability one as $N \to \infty$ there exist some $1 \le k \le N$ so that

$$sign\left(y(k)\right) = sign\left(\phi^T(k)h - C\right) \neq sign\left(\phi^T(k)\hat{h} - C\right)$$

$$sign\left(y(k)\right) = sign\left(\phi^T(k)h + C\right) \neq sign\left(\phi^T(k)\hat{h} + C\right).$$

Proof:

The identifiability proof has three parts. We prove identifiability with respect to the ascending function, the same proof can be applied to the descending function:

1. We show that for any unit vector $\hat{h} \neq h$, represented in a rectangular coordinate space, there exist two regions with non-zero area such that for $\phi(k)$ in either region: $sign\left(\phi^T(k)h - C\right) \neq sign\left(\phi^T(k)\hat{h} - C\right)$. These are called sign difference regions. Sign difference regions were first introduced in Chapter 2.
2. We show that as $N \to \infty$, some $\phi(k)$ will be in one of these regions with a non-decreasing probability greater than zero.

3. Finally we show that when $\phi(k)$ is in one of the sign difference regions there is a non-zero probability that output $y(k)$ will be on the ascending function.

Proof of part 1:

Figure 27 shows h and $\hat{h}$ as well as two tangents to a circle of radius C. Tangent $\overline{SU}$ is normal to h and tangent $\overline{ZW}$ is normal to $\hat{h}$. The equation for $\overline{SU}$ is $\phi^T(k)h = C$ and the equation for $\overline{ZW}$ is $\phi^T(k)\hat{h} = C$. From this we conclude that:

$$\begin{aligned} \phi(k) \in S_1 &\Rightarrow \phi^T(k)h > C \text{ and } \phi^T(k)\hat{h} < C \\ \phi(k) \in S_3 &\Rightarrow \phi^T(k)h < C \text{ and } \phi^T(k)\hat{h} > C \end{aligned} \tag{4.9}$$

Considering the ascending function (descending is similar) we will show that:

$$\begin{aligned} sign\left(y_d(k)\right) = 1 \text{ and } \phi(k) \in S_1 &\Rightarrow sign\left(\phi^T(k)h - C\right) = +1 \text{ and } sign\left(\phi^T(k)\hat{h} - C\right) = -1 \\ sign\left(y_d(k)\right) = 1 \text{ and } \phi(k) \in S_3 &\Rightarrow sign\left(\phi^T(k)h - C\right) = -1 \text{ and } sign\left(\phi^T(k)\hat{h} - C\right) = +1 \end{aligned} \tag{4.10}$$

When $\phi(k)$ is in region S_2, $x(k)$ and $\hat{x}(k)$ are both less than C and for $\phi(k)$ in S_4, $x(k)$ and $\hat{x}(k)$ are both greater than C. Thus, $e(k) = 0$ for $\phi(k)$ in these regions.

Now, Observation 1 established that $\angle UPW = \angle SPZ = \theta$ in Figure 27. Thus for $\hat{h} \neq h$ both regions exist with area greater than zero.

Proof of part 2:

For the two dimensional case considered here, Assumption 4.2 implies that joint probability distribution $f_{\phi(k)}\left(u(k), u(k-1)\right)$ will be continuous and non-zero everywhere inside a circle of radius $r > C$. Because the boundaries of S_1, S_2, S_3 and S_4 are tangent to a circle of radius C, the intersection of a circle of radius $r > C$ with S_1 and S_3 will have probability greater than zero. In addition, due to the continuous input

probability distribution, the angle of $\phi(k)$ will also have some continuous distribution from 0 to 2π. Thus, as $N \to \infty$, some $\phi(k)$ will be in S_1 or S_3 with non-zero probability.

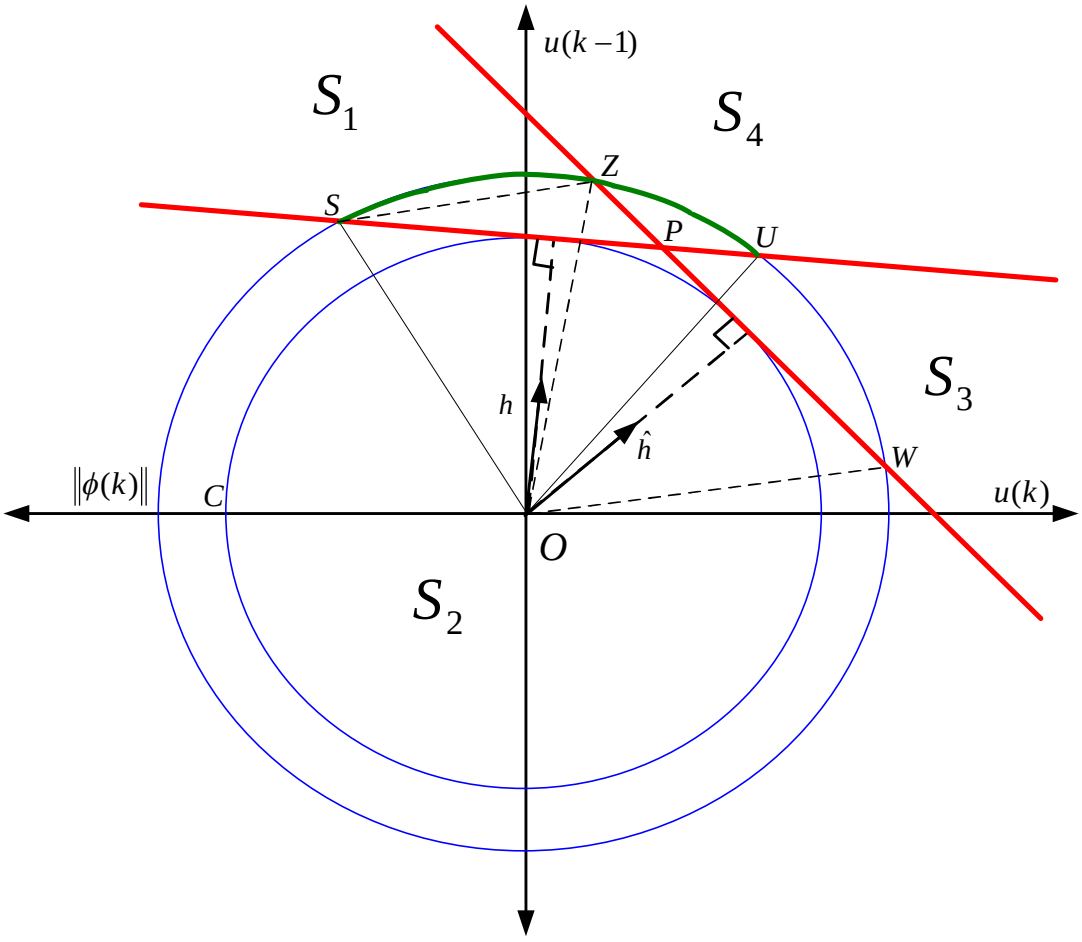

Figure 27: Sign difference regions for backlash

Proof of part 3:

For the ascending function (descending is similar) identifiability is based on the non-zero probability:

$$P\{(\phi(k) \in S_1 \text{ or } \phi(k) \in S_3) \text{ and } (sign(y_d(k)) = 1)\} > 0 \qquad (4.11)$$

This is equivalent to either of the next two equations:

$$P\{(y(k)>0) \text{ and } (\hat{x}(k)<C) \text{ and } (sign(y_d(k))=1)\}>0 \tag{4.12}$$

$$P\{(y(k)<0) \text{ and } (\hat{x}(k)>C) \text{ and } (sign(y_d(k))=1)\}>0 \tag{4.13}$$

For $sign\left(y_d(k)\right)=1$, output $y(k)$ must be a point on the ascending function. To guarantee this for some k, we show the non-zero probability of sequences $\chi(k,L)=\left[x(k-L+1),\ldots,x(k)\right]$, where $0<k<\infty$ and $L<k$, that force $y(k)$ on to the ascending function.

Unknown intermediate signal $x(k)$ results from passing i.i.d. Gaussian signal $u(k)$ thru a linear system. Because $x(k)$ is a stationary random Gaussian process at constant time increments, we can calculate a probability density function for sequence $\chi(k,L)$, for example:

$$f_{(x(k-L+1),\ldots,x(k))}\left(\lambda(k-L+1),\ldots,\lambda(k)\right)=\frac{1}{\sqrt{(2\pi)^{L-1}|\mu|}}e^{-\frac{1}{2}[\lambda(k-L+1),\ldots,\lambda(k)]\mu^{-1}[\lambda(k-L+1),\ldots,\lambda(k)]^T} \tag{4.14}$$

Here, μ is the covariance matrix of $\chi(k,L)$. For a two dimensional $(n=2)$ example:

$$\mu=\begin{bmatrix} 1 & h(0)h(1) & 0 & 0 & \cdots & 0 & 0 & 0 \\ h(1)h(0) & 1 & h(0)h(1) & 0 & \cdots & 0 & 0 & 0 \\ 0 & h(1)h(0) & 1 & h(0)h(1) & \cdots & 0 & 0 & 0 \\ \vdots & \vdots & \vdots & \vdots & & \vdots & \vdots & \vdots \\ 0 & 0 & 0 & 0 & \cdots & 0 & h(1)h(0) & 1 \end{bmatrix} \tag{4.15}$$

We can now analyze the probability in (4.12) or (4.13), above. Because the input and intermediate signals are zero mean and $\|h\|=\|\hat{h}\|=1$, the variance of input $u(k)$ will determine the probability of $x(k)>C \Rightarrow y(k)>0$, see Figure 25. Thus, for a large enough input power, it is reasonable to assume the existence of $\left[x(k),y(k)\right]$ with

$x(k) > C$ and $y(k) > 0$. We want to show the non-zero probability that $y(k)$ is on the ascending function. This is based on the following necessary and sufficient condition:

$$f_a^{-1}\big(y(k-1)\big) < x(k) < \infty \tag{4.16}$$

Note that $y(k-1)$ may already be on the ascending function. If so, the condition (4.16) keeps it there. Due to Assumption 4.2, the above constraint defines a nonzero probability mass starting at $f_a^{-1}\big(y(k-1)\big)$ and extending to infinity. Thus, any output $y(k)$ has a non-zero probability of being on the ascending function. A similar analysis could be carried out for the descending function.

From the first conjunction of (4.1) we have shown that for a selected $y(k) > 0$, there is a non-zero probability that $y(k) - y(k-1) > 0$. We still need to show the nonzero probability that, for the same time index *k*, $\hat{x}(k) < C$.

Referring to the previous discussion about the variance of zero mean stationary input $u(k)$, it is reasonable to expect $\|\phi(k)\| > C$ for some *k*. (note that $\|\phi(k)\| \le C$ is not useful for identification). Also, we expect the angle of $\|\phi(k)\|$ will be continuous distributed between 0 and 2π. The condition $x(k) > C \Rightarrow y(k) > 0$ can be interpreted as:

$$x(k) = \| \phi(k) \| \ \ \| h \| \cos\big(\angle(\phi(k), h)\big) > C \Rightarrow \angle(\phi(k), h) < \cos^{-1}\left(\frac{C}{\| \phi(k) \|}\right) = \alpha \tag{4.17}$$

In Figure 3, $\widehat{SU}$ extends from $\angle h - \alpha$ to $\angle h + \alpha$. As shown above, $\phi(k)$ on $\widehat{SU}$ and within this sector will result in $x(k) > C$, $y(k) > 0$. Because of the continuous distribution of the angle of $\phi(k)$, this $\phi(k)$ will be on $\widehat{SZ}$ with some positive probability and, because it is in S_1, will satisfy $\hat{x}(k) < C$. This concludes the identifiability proof.

The indentifiability proof can be extended to a higher dimensional case. Let h and $\hat{h}$ be unit vectors in $\Re^n$ for $n > 2$. Consider that h and $\hat{h}$ span a plane in a two dimensional subspace of $\Re^n$:

$$S(h,\hat{h}) = [\alpha h + \beta\hat{h} : \alpha, \beta \in R] \tag{4.18}$$

Let $r(\eta), -\pi \le \eta \le \pi$ denote the unit circle on this plane. Further, let $r(0) = h$ and $r(\theta) = \hat{h}$. Without loss of generality, rotate the coordinate reference to line up $S(h,\hat{h})$ and $r(\eta)$ with the first two axis in $\Re^n$. Assume there is a rotation matrix T that performs this transformation such that:

$$\begin{aligned} r(\eta) &= \left[cos(\eta)\ sin(\eta)\ 0\ 0 \cdots 0\right]^T \\ \hat{h}_r &= T\hat{h} = r(\theta) = \left[cos(\theta)\ sin(\theta)\ 0\ 0 \cdots 0\right]^T \\ h_r &= Th = r(0) = \left[1\ 0\ 0 \cdots 0\right]^T \\ \phi_r(k) &= T\phi(k) \end{aligned} \tag{4.19}$$

Note that both $\phi(k)$ and rotated input sample vector $\phi_r(k)$ are vectors of stationary, zero-mean, i.i.d., Gaussian samples. Due to the rotation, $\phi_r(k)$ may be fully represented in the two dimensional subspace spanned by h and $\hat{h}$. However, recall that:

$$\hat{x}(k) = \phi_r^T(k)\hat{h}_r = \left[u_r(k)cos(\theta) \quad u_r(k-1)sin(\theta) \quad 0 \quad \cdots \quad 0\right] \tag{4.20}$$

By making $x(k)$ and $\hat{x}(k)$ dependent on only the first two components of $\phi_r^T(k)$ we force the problem into the two dimensional framework already proven:

$$\begin{aligned} \hat{x}(k) &= \phi^T(k)\hat{h} = \left(T^{-1}\phi_r(k)\right)^T T^{-1}\hat{h}_r = \phi_r^T(k)\hat{h}_r \\ &= \left[u_r(k)cos(\theta) \quad u_r(k-1)sin(\theta) \quad 0 \quad \cdots \quad 0\right] \end{aligned} \tag{4.21}$$

Convergence discussion

We have shown identifiability; that our identification approach has only one global minimum $\hat{h} = h$ as $N \to \infty$. For convergence, the probability of $\phi(k)$ in S_1 or S_3 together with the probability of being on the ascending (or descending) function must be monotonic with $0 \le \theta < 2\pi$. To study this, let us partition the output into the following three events:

$$\begin{aligned} D_p &= \{sign(y_d(k)) = +1\} = \{x(k) > f_a^{-1}(y(k-1))\}, \text{ Ouput on Ascending Function} \\ D_z &= \{sign(y_d(k)) = 0\}, \quad \text{Ouput Inbetween Functions} \\ D_n &= \{sign(y_d(k)) = -1\}\{x(k) < f_d^{-1}(y(k-1))\}, \text{ Ouput on Descending Function} \end{aligned} \tag{4.22}$$

This represents a complete partition in that $P(D_p) + P(D_z) + P(D_n) = 1$ Now we define the following sign difference compound event:

$$A = \{((y(k) > 0) \text{ and } (\hat{x}(k) < C)) \text{ or } ((y(k) < 0) \text{ and } (\hat{x}(k) > C))\} \tag{4.23}$$

What we would like to be monotonic θ with is:

$$P(A, D_p) + P(A, D_n) = P(A \mid D_p)P(D_p) + P(A \mid D_n)P(D_n) \tag{4.24}$$

The partition $D = [D_p, D_z, D_n]$ depends on:

1. The true but unknown impulse response *h* that determines joint probability of pairs $[x(k-1), x(k)]$ of intermediate samples. In general, samples in these pairs are not independent because of (4.15).
2. The variance of the i.i.d. input samples $u(k)$.
3. The shape of the ascending and descending functions

Thus, the sample by sample probability of events in partition *D* are impossible to characterize without a priori knownledge of the above three items. Also the probability

of events D_p, D_z, D_n changes every sample because they depend on the output $y(k-1)$. The non-zero $P(D_z)$ has the effect of randomly zeroing $y_d(k)$ in (4.6) and nullifying the contribution to (4.7) of $\phi(k)$ occupying a sign difference region based on $\theta = \angle\left(h, \hat{h}\right)$.

Another factor that greatly confounds the convergence question is that different values of *h* result in different covariance between pairs of intermediate samples. Thus a general proof of convergence is not possible for this approach.

Noise immunity enhancement

All of the preceeding analysis has assumed that noise term $v(k) = 0$ in Figure 26. In this case, (4.5) works well for indicating when output $y(k)$ is on the ascending or descending function. However, adding non-zero noise to the output confuses the detection mechanism of (4.5) because $y_d(k) = y(k) - y(k-1)$ will likely be non-zero even if $y(k)$ is between the ascending and descending functions. With added noise, the detection mechanism of $y_d(k)$ will be invalid as almost every output point will be indicated on one of the two functions.

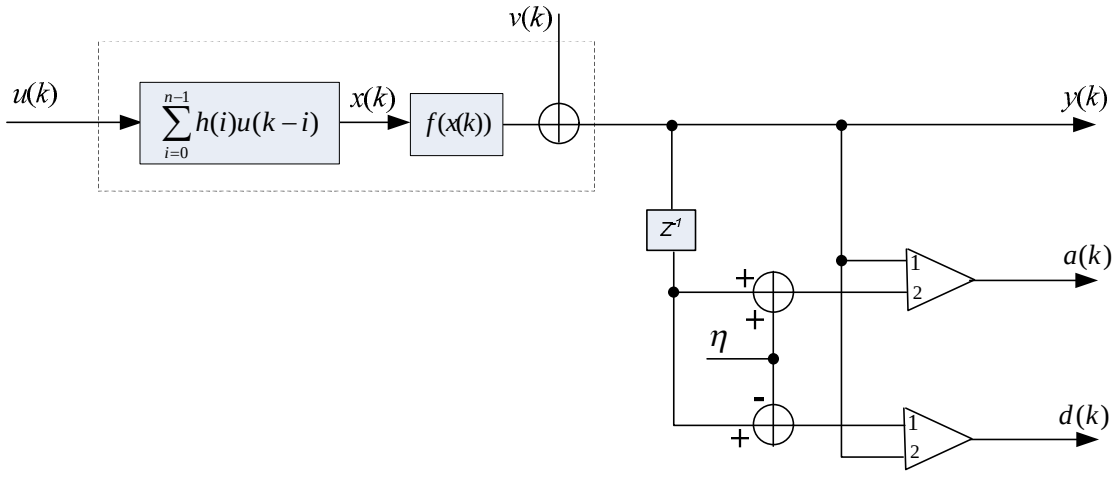

Figure 28: Improved ascending/descending function detection

To improve estimation performance, we modify the ascending/descending function detection as shown in Figure 28.

$$\begin{array}{lcll} y(k) > y(k-1)+\eta & \Rightarrow & a(k)=1, d(k)=0 & \Rightarrow \quad y(k)= f_a(x(k)) \\ \left|y(k)-y(k-1)\right| < \eta & \Rightarrow & a(k)=0, d(k)=0 & \\ y(k) < y(k-1)-\eta & \Rightarrow & a(k)=0, d(k)=1 & \Rightarrow \quad y(k)= f_d(x(k)) \end{array} \tag{4.25}$$

Thus $\pm\eta$ sets a "deadzone" to mitigate the effects of output noise. We modify (4.6) as:

$$e(k)=\begin{cases} sign\big(y(k)\big)-sign\big(\phi^T(k)\hat{h}-C\big) & a(k)=1, d(k)=0 \\ 0 & a(k)=0, d(k)=0 \\ sign\big(y(k)\big)-sign\big(\phi^T(k)\hat{h}+C\big) & a(k)=0, d(k)=1 \end{cases} \tag{4.26}$$

Note that the circuit of Figure 28 is designed to preclude the condition $a(k)=1, b(k)=1$. In the above, η gives the $a(k)=1$ or $d(k)=1$ decisions noise immunity.

Simulation testing

To demonstrate the performance of our algorithm, we provide two numerical simulations. Simulation A estimates a 9th order FIR filter:

$$\begin{aligned} A(z) &= 0.265+0.556z^{-1}+0.523z^{-2}+0.419z^{-3}+0.301z^{-4} \\ &+0.205z^{-5}+0.136z^{-6}+0.088z^{-7}+0.056z^{-8}+0.035z^{-9} \end{aligned} \tag{4.27}$$

The true and estimated frequency responses are plotted as the dotted and solid lines, respectively, in Figure 30. Simulation B estimates an 8th order FIR filter:

$$B(z)=0.764+0.448z^{-2}-0.413z^{-4}-0.091z^{-6}+0.190z^{-8} \tag{4.28}$$

The true and estimated frequency responses are plotted as the dotted and solid lines, respectively, in Figure 31.

The backlash function, plotted in Figure 29, satisfies Assumption 4.1 with X-axis intersection points ± 1. Figure 29 was generated by simulation. First a set of 10000

backlash input/output points $\left[x(k), y(k), y_d(k)\right]$ was collected from Simulation A. Then the outputs that were not on the ascending or descending function were transfered to the origin so that the plot area betwwen the two functions was not filled in.

The input $u(k)$ is Gaussian with variance $\sigma^2 = 2$. Uncorrelated Gaussian noise is added to the output to produce SNR of 10dB, 20dB and 30dB. A genetic algorithm (GA), similar to that described in Chapter 3 was used to search for the true FIR coefficients. The number of 'parents' was 64 and the number of iterations was set to 200. The GA is a zero-order organized search algorithm that solves the following minimization problem:

$$\hat{h} = \underset{\|\hat{h}\|=1}{\arg\min} \frac{1}{N} \sum_{k=1}^{N} e(k)^2 \tag{4.29}$$

With $e(k)$ defined by (4.25) and (4.26). To show the improvement obtained by these modified error equations, we set noise threshold $\eta = 0$ and $\eta = 2\sigma$, where σ is the standard deviation of the input samples.

Note that the GA is not necessarily optimum and has not been proven to converge in every case. The results presented here are the averages of 4 Monte-Carlo simulations. The FIR means squared coefficient error is defined as $\text{MSE} = \left\|\hat{h} - h\right\|$. This demonstrates the effectiveness of the identification algorithm. However, we should emphasize that the uniqueness of the estimate $\hat{h}$ is achieved as sample record size $N \to \infty$. For finite *N*, a slight variation in $\hat{h}$ may not result in a change in the number of $\phi(k) \in S_1$ or $\phi(k) \in S_3$ for $k = 1, 2, ..., N$. For these simulations, *N* is set to 10000, 20000, 40000 and 80000 samples.

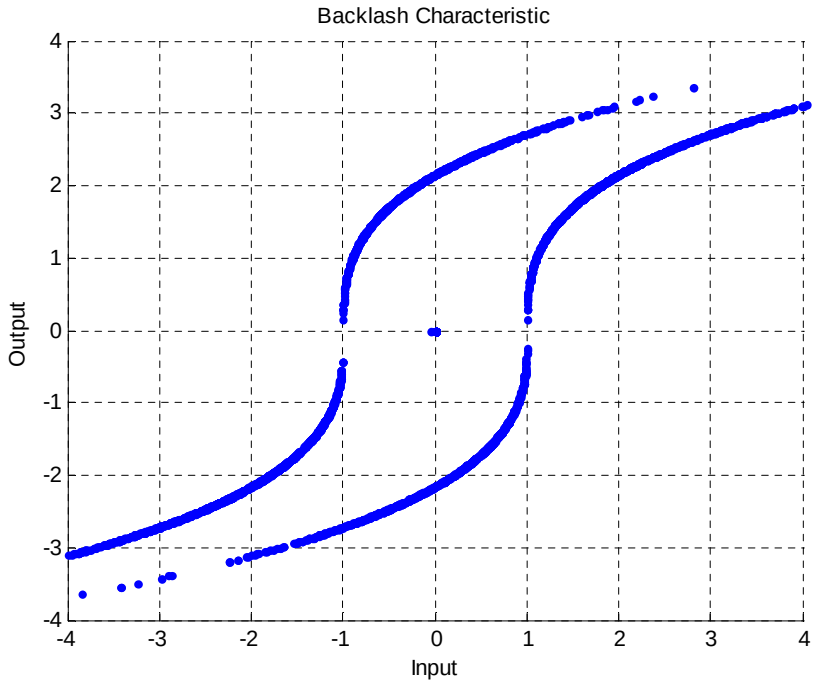

Figure 29: Backlash function used in simulations A and B

Simulation A results are shown in Table 10 and Table 11. Table 10 shows the expected decrease in MSE as *N* and/or SNR are increased. Also, as the noise threshold is increased, the MSE decreases by a factor of 2 in most cases. Table 11 illustrates how the noise interferes with the ascending/descending function decision. With the noise threshold set to zero, non-zero added output noise causes the two point output difference in (4.25) to always be non-zero so that the ascending function is indicated for about 50% of samples and the descending function is chosen for the other 50%. This is clearly invalid and setting $\eta = 2\sigma$ alleviates this problem. Note that this setting has not been shown to be optimum; there may be a different setting that produces even better results. Figure 30 shows the frequency domain estimation performance for SNR=10, *N*=10000

and $\eta = 2\sigma$. Instead of plotting impulse response estimate $\hat{h}$ directly on top of true impulse response *h*, Figure 30 compares the equivalent frequency responses. This approach better reveals the actual estimation performance because very slight impulse response inaccuracies can lead to large changes in the zeros of the system function. Parts of the spectral response that depend on these zeros can be greatly affected. Note that the horizontal scale of Figure 30 is in radians per sample = $2\pi f_{in}/F_s$, where F_s is the sampling rate and f_{in} is the input frequency.

While Simulation A estimated a lowpass filter, Simulation B shows an alternate estimation for a bandstop filter. Results are shown in Table 12, Table 13 and Figure 31. All the Simulation A comments above apply directly to Simulation B.

Compare Table 1 in Chapter 2 and the results presented here. From Table 13 consider the case where *N*=80000, SNR = 20dB and noise threshold is 2σ. The total number of ascending and descending function output points are 31498 and the MSE is 0.0177. Compare this with Table 1 where *N* = 35000, SNR = 20dB and resulting MSE = 0.0211. The MSE results are close. Although the input distributions and the linear parts are different, a reasonable explanation for the similar MSE results is that the quadrant scheme of Chapter 2 was based on a priori knowledge of a single point on a single function nonlinearity and the algorithm presented here is based on a priori knowledge of a single point on each of the functions in a bi-functional memory nonlinearity.

This chapter has shown that the FIR linear part of a Wiener system with backlash can be identified by comparing the output polarity of the unknown system with that of an adjustable known system. For proof of identifiability, a Gaussian random input is shown to be sufficient. A detailed discussion of convergence is offered.

N	Noise Threshold	SNR = 10dB		SNR = 20 dB		SNR = 30 dB	
		MSE	CPU(min)	MSE	CPU(min)	MSE	CPU(min)
10000	0	0.0620	6.2	0.0664	8.3	0.0561	4.8
	2σ	0.0317	4.1	0.0242	4.17	0.0245	6.06
20000	0	0.0393	14.4	0.0312	16.2	0.0364	9.4
	2σ	0.0191	7.9	0.0202	8.00	0.0177	11.80
40000	0	0.0425	27.6	0.0332	25.4	0.0316	18.8
	2σ	0.0190	15.9	0.0140	16.2	0.0133	22.32
80000	0	0.0339	59.7	0.0288	41.3	0.0211	41.9
	2σ	0.0163	35.6	0.0148	47.8	0.0134	61.13

Table 10: Simulation A, FIR backlash identification performance

N	Noise Threshold	SNR = 10dB		SNR = 20 dB		SNR = 30 dB	
		Asc	Des	Asc	Des	Asc	Des
10000	0	4990	5010	4973	5027	5007	4993
	2σ	1028	1011	1275	1284	1577	1581
20000	0	10039	9961	10003	9997	9959	10041
	2σ	2011	2024	2550	2565	3222	3202
40000	0	20016	19984	20057	19943	20022	19978
	2σ	3970	4014	5069	5146	6367	6364
80000	0	40011	39989	39976	40024	39994	40006
	2σ	8158	8172	10263	10242	12805	12691

Table 11: Simulation A backlash ascending/descending statistics

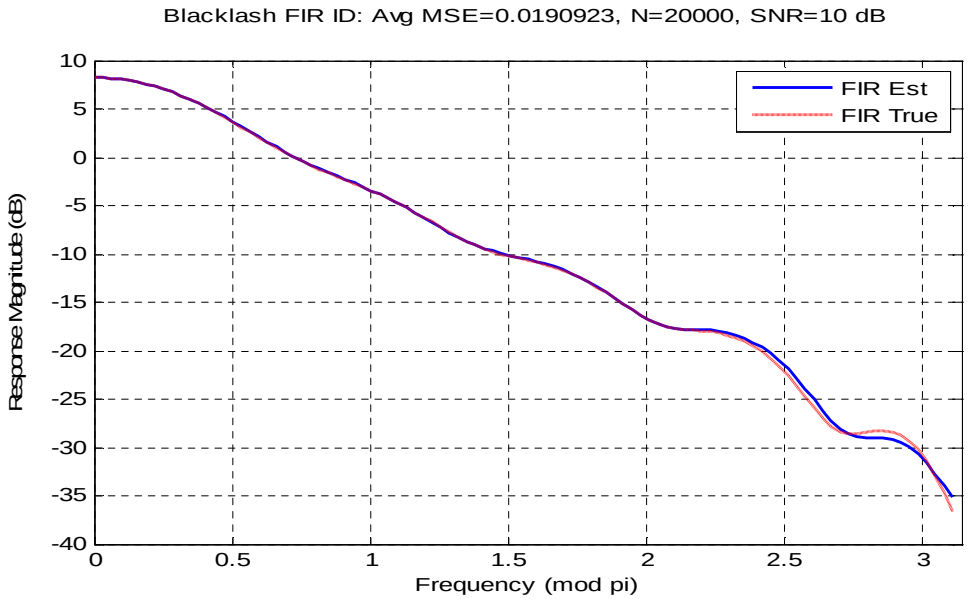

Figure 30: Simulation A, FIR backlash frequency response matching

N	Noise Threshold	SNR = 10dB		SNR = 20 dB		SNR = 30 dB	
		MSE	CPU(min)	MSE	CPU(min)	MSE	CPU(min)
10000	0	0.0633	5.1	0.0616	6.2	0.0635	4.9
	2σ	0.0320	4.3	0.0304	4.5	0.0267	4.7
20000	0	0.0527	9.6	0.0491	14.8	0.0547	9.6
	2σ	0.0351	8.3	0.0250	8.6	0.0223	8.8
40000	0	0.0495	25.6	0.0497	32.6	0.0496	18.8
	2σ	0.0338	16.8	0.0194	17.5	0.0212	17.9
80000	0	0.0491	56.4	0.0498	51.3	0.0451	43.0
	2σ	0.0235	37.4	0.0177	39.3	**0.0185**	**46.7**

Table 12: Simulation B, FIR backlash identification performance

N	Noise Threshold	SNR = 10dB		SNR = 20 dB		SNR = 30 dB	
		Asc	Des	Asc	Des	Asc	Des
10000	0	4967	5033	4997	5003	4986	5014
	2σ	1595	1583	1968	1981	2214	2227
20000	0	10021	9979	9962	10038	10002	9998
	2σ	3157	3168	3947	3966	4416	4423
40000	0	19993	20007	19999	20001	20059	19941
	2σ	6302	6302	7893	7945	8982	8928
80000	0	39972	40028	39956	40044	39953	40047
	2σ	12736	12726	15737	15761	**17794**	**17828**

Table 13: Simulation B backlash ascending/descending statistics

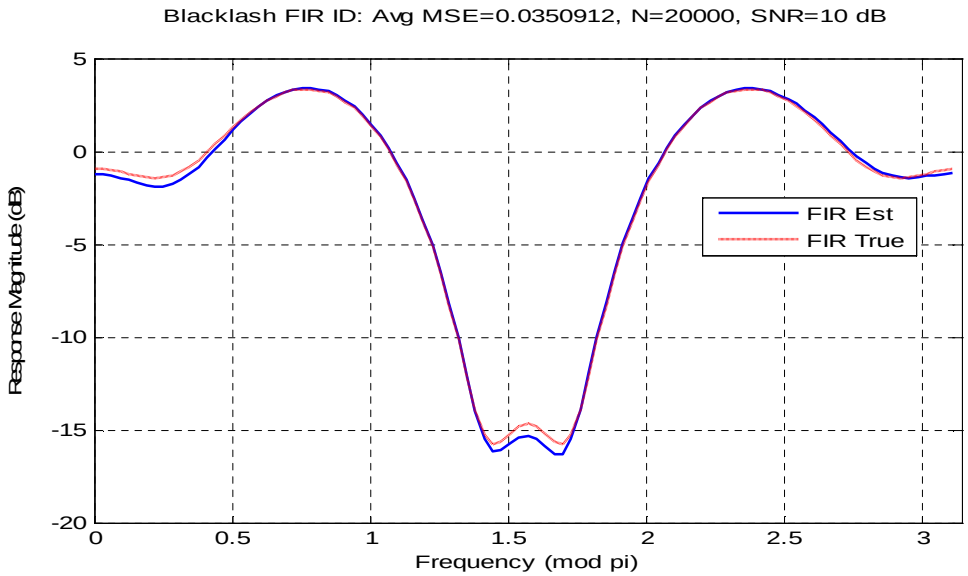

Figure 31: Simulation B, FIR backlash frequency response matching

CHAPTER 5
CONCLUSION

This thesis has shown that, given certain very minimal a priori information on the nonlinearity, both the FIR and IIR linear parts of a Wiener system are identifiable without a Gaussian distributed input in all cases except the memory nonlineaerity. The unknown nonlinearity is not necessarily invertible and need not be parameterized in any way.

The focus has been on the study of the least amount of a priori information needed on the nonlinearity to identify the linear system. As shown, very little information is actually needed although intuition suggests that the algorithms will converge more quickly if more information is available. The following algorithms were developed and tested:

1. Quadrant a priori information
2. Single point a priori information
3. Locally monotonic a priori information

For each algorithm, identifiability and in some cases convergence proofs were provided for various combinations of Wiener system FIR and IIR linear blcoks and memory and non-memory nonlinear blocks. The effect of threshold settings on noise performance was discussed and tested at length.

Hopefully, this work will benefit future practitioners of this important field of nonlinear system identification.

APPENDIX

This appendix provides the proof that, for an *N* sample experiment:

$$E\left\{\frac{1}{N}\sum_{k=1}^{N}\left(sign(\phi(k)^T h)-sign(\phi(k)^T \hat{h})\right)^2-4F(\theta)\right\}^2 \to 0 \quad \text{as } N\to\infty$$

Note that the law of large numbers invoked above requires the random samples of the squared error to be i.d.d. Because of the overlap in the FIR shift register for changes in *k* less than *n*, the squared error samples are not necessarily i.d.d.

For $|k-j|\geq n$, $\phi(k)$ and $\phi(j)$ are independent and we have : $F(\theta)=\lim_{N\to\infty}\left(\frac{w}{N}\right)$, here *w* is the sign difference count in the set of *N* samples.

$$\left|E\left(\left(sign(\phi(k)^T h)-sign(\phi(k)^T \hat{h})\right)^2-4F(\theta)\right)^2\right|$$
$$=\left|E\left(2-2sign(\phi(k)^T h)sign(\phi(k)^T \hat{h})-4F(\theta)\right)E\left(2-2sign(\phi(j)^T h)sign(\phi(j)^T \hat{h})-4F(\theta)\right)\right|$$
$$=\left|\lim_{N\to\infty}\left(2-2\left(\frac{N-2w}{N}\right)-4\left(\frac{w}{N}\right)\right)\lim_{N\to\infty}\left(2-2\left(\frac{N-2w}{N}\right)-4\left(\frac{w}{N}\right)\right)\right|=0$$

We find that for *k=j:*

$$\left|E\left(\left(sign(\phi(k)^T h)-sign(\phi(k)^T \hat{h})\right)^2-4F(\theta)\right)^2\right|$$
$$=\left|E\left(\left[2-2sign(\phi(k)^T h)sign(\phi(k)^T \hat{h})-4F(\theta)\right]\left[2-2sign(\phi(j)^T h)sign(\phi(j)^T \hat{h})-4F(\theta)\right]\right)\right|$$
$$=\left|E\begin{Bmatrix}4-4sign(\phi(j)^T h)sign(\phi(j)^T \hat{h})-8F(\theta)-4sign(\phi(k)^T h)sign(\phi(k)^T \hat{h})\\+4sign(\phi(k)^T h)sign(\phi(k)^T \hat{h})sign(\phi(j)^T h)sign(\phi(j)^T \hat{h})\\+8F(\theta)sign(\phi(k)^T h)sign(\phi(k)^T \hat{h})-8F(\theta)\\+8F(\theta)sign(\phi(j)^T h)sign(\phi(j)^T \hat{h})+16F(\theta)^2\end{Bmatrix}\right|$$

$$= 4 - 4 + 8F(\theta) - 8F(\theta) - 4 + 8F(\theta) + 4 + 8F(\theta) - 16F(\theta)^2$$
$$-8F(\theta) + 8F(\theta) - 16F(\theta)^2 + 16F(\theta)^2 = 16F(\theta) - 16F(\theta)^2$$

Finally, for $|k - j| < n$, we claim that:

$$\left| E\left\{ \left(sign(\phi(k)^T h) - sign(\phi(k)^T \hat{h}) \right)^2 - 4F(\theta) \right\}^2 \right| = \bar{c}(k, j)$$

For some constant c where $0 \le \bar{c}(k, j) \le c < \infty$. The proof proceeds as follows:

$$\left| E\left\{ \frac{1}{N} \sum_{k=1}^{N} \left(\left(sign(\phi(k)^T h) - sign(\phi(k)^T \hat{h}) \right)^2 - 4F(\theta) \right) \right\}^2 \right|$$
$$= \left| \begin{array}{l} \dfrac{1}{N} \displaystyle\sum_{k=1}^{N} \dfrac{\mathbf{E}([(sign(\phi^T(k)h) - sign(\phi^T(k)\hat{h}))^2 - 4F(\theta)])^2}{N} \\ + \dfrac{\mathbf{E}((sign(\phi^T(k)h) - sign(\phi^T(k)\hat{h}))^2 - 4F(\theta))}{N} \\ \times \displaystyle\sum_{0<|k-j|\le n-1} ((sign(\phi^T(j)h) - sign(\phi^T(j)\hat{h}))^2 - 4F(\theta)) \end{array} \right|$$
$$\le \frac{1}{N} \sum_{k=1}^{N} \frac{(16F(\theta)(1 - F(\theta)) + 2(n-1)c)}{N} = \frac{(16F(\theta)(1 - F(\theta)) + 2(n-1)c)}{N}$$
$$\frac{(16F(\theta)(1 - F(\theta)) + 2(n-1)c)}{N} \to 0 \text{ as } N \to \infty$$

Therefore:

$$\lim_{N \to \infty} \left[E\left\{ \frac{1}{N} \sum_{k=1}^{N} \left(sign(\phi(k)^T h) - sign(\phi(k)^T \hat{h}) \right)^2 - 4F(\theta) \right\}^2 \right] = 0$$

This implies, in probability:

$$\lim_{N \to \infty} \left[\frac{1}{N} \sum_{k=1}^{N} \left(sign(\phi(k)^T h) - sign(\phi(k)^T \hat{h}) \right)^2 \right] = 4F(\theta)$$

REFERENCES

[1] M. Abe and M Kawamata. Comparison of the Convergence of IIR Evolutionary Digital Filters and Other Adaptive Digital Filters on a Multiple-Peak Surface. *Proceedings of the Thirty-First Asilomar Conference on Signals, Systems \& Computers*, 2: 1674-1678, 1997

[2] E. W. Bai. A blind approach to the Hammerstein-Wiener model identification. *Automatica*, 38: 967-979, 2002

[3] E. W. Bai. Identification of linear systems with hard input nonlinearities of known structure. *Automatica*, 38: 853-860, 2002

[4] E. W. Bai and J. Reyland. Towards identification of Wiener systems with the least amount of a priori information on the nonlinearity. *Automatica*, 44: 910-919, 2008.

[5] E. W. Bai and J. Reyland. Towards identification of Wiener systems with the least amount of a priori information: IIR cases. *Automatica*, 45: 956-964, 2009.

[6] S. Benedetto, E. Biglieri and R. Daffara. Modeling and Performance Evaluation of Nonlinear Satellite Links, A Volterra Series Approach. *IEEE Transactions on Aerospace and Electronic Systems.* 15(4): 494-501, 1979

[7] S. A. Billings and S. Y. Fakhouri. Identification of a class of nonlinear systems using correlation analysis. *Proceedings of the IEE*, 125(7): 691-697, 1978

[8] A. Bjorck. *Numerical methods for least squares problems*. SIAM, Philadelphia, PA, 1996.

[9] V. Cerone, D. Piga and D. Regrunto. Parameters bounds evaluation for linear systems with output backlash. *Proceedings of the Fifteenth IFAC Symposium on System Identification*. pages 575-580, Saint-Malo, France, 2009

[10] V. Cerone and D. Regrunto, D. Bounding the Parameters of Linear Systems with Input Backlash. *IEEE Transactions on Automatic Control*, 52(3): 531-536, 2007

[11] R. Dong, Q. Tan and Y. Tan. Recursive Identification Algorithm for Dynamic Systems with Output Backlash and its Convergence. *International Journal of Applied Math and Computer Science*. 19(4): 631-638, 2009

[12] M. Enqvist and L. Ljung. Linear Approximations of nonlinear FIR systems for separable input process. *Automatica*. 41: 459-473, 2005

[13] J. Fan and I. Gijbels. *Local Polynomial Modeling and Its Applications*. Chapman

& Hall/CRC, New York, 2003

[14] F. Giri, Y. Rochdi, F. Z. Chaoui and A. Brouri. Identification of Hammerstein Systems in the Presence of Hysteresis-backlash and hysteresis-relay Nonlinearities. *Automatica*, 44(3): 767-775, 2008

[15] F. Giri, Y. Rochdi, J. B. Gning and F. Z. Chaoui. Identification of Block Oriented Systems in the Presence of Nonparametric Input Nonlinearities of the Switch and Blacklash Type. 2009

[16] D. E. Goldberg. *The Design of Innovation*. Kluwer Academic Publishers, New York, NY, 2002

[17] G. H. Golub and C. Van Loan. *Matrix Computation*. The John Hopkins University Press, Baltimore, MD, 1996

[18] J. C. Gomez, A. Jutan and E. Baeyens. Wiener Model Identification and Predictive Control of a pH Neutralization Process. *IEE Proceedings*, 151(3): 329-338, 2004

[19] W. Greblicki. Nonparametric identification of Wiener Systems. *IEEE Transactions on Information Theory*. 38(5): 1487-1493, 1992

[20] M. W. Hauser. Principles of Oversampling A/D Conversion. *Journal of the Audio Engineering Society*. 39(1/2): 3-26, 1991

[21] M. H. Hayes. *Statistical Digital Signal Processing and Modeling.* John Wiley & Sons, New York, NY, 1996

[22] X. Hu and H.F. Chen. Strong consistence of recursive identification for Wiener systems. *Automatica*, 41 (11): 1905-1916, 2005

[23] C. Johnson and T. Szulc. Further lower bounds for the smallest singular values. *Linear algebra and its applications*, 272(1-3): 169-179, 1998

[24] A. Juditsky, H. Hjalmarsson, A. Benveniste, B. Delyon, L. Ljung, J. Sjoberg and Q. Zhang. Nonlinear Black-box Models in System Identification: Mathematical Foundations. *Automatica*, 12(31): 1725-1750, 1995

[25] A. Y. Kibangou, G. Favier and M.. Hassani. Semi-blind receiver for the Fiber-Wireless Uplink Channel. *Proceedings of the 44th IEEE Conference on Decision and Control*. 8168-8173, 2005

[26] L. Ljung. *System Identification, Theory for the User*. Prentice-Hall, Englewood Cliffs, NJ, 1987

[27] M. Loeve. *Probability Theory I.* Springer-Verlag, New York, NY, 1977

[28] A. V. Oppenheim and R. W. Schafer. *Discrete-Time Signal Processing*. Prentice Hall, Englewood Cliffs, New Jersey, 1989

[29] A. Papoulis. *Probability, Random Variables and Stochastic Processes*. McGraw-Hill, New York, NY, 1984

[30] J Reyland and E.W. Bai. Wiener System Identification: Backlash Nonlinearity. To be submitted.

[31] M. A. Shoukat Choudhury, N. F. Thornhill and S. L. Shah. Modeling Valve Stiction. *Control Engineering Practice.* 13(5): 641-658, 2005

[32] J. Sjoberg, Q. Zhang, L. Ljung, A. Benveniste, B. Delyon, P. Glorennec, H. Hjalmarsson and A. Juditsky. Nonlinear Black-box Modeling in System Identification: a Unified Overview. *Automatica*. 31(12): 1691-1724, 1995

[33] G. Strang. *Linear Algebra and its Applications.* Saunders College Publishing, Fort Worth, TX, 1988

[34] L. Sun, W. Liu and A. Sano, A. Identification of a dynamical system with input nonlinearity. *IEE Proceedings on Control Theory and Applications*, 146(1): 41-51, 1999

[35] J. Voros. Modeling and identification of systems with backlash. *Automatica,* 46(2): 369-374, 2010

[36] J. Voros. Parameter identification of Wiener systems with discontinuous nonlinearities. *Systems and Control Letters,* 44(5):363-372,2001.

[37] D. Westwick and M. Verhaegen. Identifying MIMO Wiener systems using subspace model identification method. *Signal Processing*, 52(?): 235-258, 1996

[38] N. Wiener. *Nonlinear Problems in Random Theory*. The Technology Press, John Wiley and Sons, New York, NY, 1958

[39] T. Wigren. Adaptive filtering using quantized output measurements. *IEEE Transactions on Signal Processing*, 46(12): 3423-3426, 1998

[40] T. Wigren. Circle criteria in recursive identification. *IEEE Transactions on Automatic Control*, 42(7): 975-979, 1997

[41] Q. Zhang, A. Iouditski and L. Ljung. Identification of Wiener System with Monotonic Nonlinearity. *14th IFAC Symposium on System Identification*. pages 166-171, Newcastle, Australia, 2006

[42] D. Zwillinger. *CRC Standard Mathematical Tables and Formulae*. Chapman & Hall/CRC, London, 2003